In-situ non-destructive evaluation process monitoring for CFRP manufacturing

Miesen, Nick

DOI
10.4233/uuid:2126edcb-7c7d-4195-a270-74e41526cfdb

Publication date
2018

Document Version
Final published version

Citation (APA)
Miesen, N. (2018). *In-situ non-destructive evaluation process monitoring for CFRP manufacturing*. [Dissertation (TU Delft), Delft University of Technology]. https://doi.org/10.4233/uuid:2126edcb-7c7d-4195-a270-74e41526cfdb

In-situ non-destructive evaluation process monitoring for CFRP manufacturing

Dissertation

for the purpose of obtaining the degree of doctor
at Delft University of Technology
by the authority of the Rector Magnificus
prof.dr.ir. T.H.J.J. van der Hagen
chair of the Board for Doctorates
to be defended publicly on
Friday 2 November 2018 at 10:00

by

Nick MIESEN
Master of Science in Physics and Astronomy,
University of Amsterdam, the Netherlands
born in Maastricht, the Netherlands

This dissertation has been approved by the promotors.

Composition of the doctoral committee:

Rector Magnificus,	chairperson
Prof. Dr. Ir. R. Benedictus	Delft University of Technology, promotor
Dr. R. M. Groves	Delft University of Technology, copromotor
Ir. J. Sinke	Delft University of Technology, copromotor

Independent members:

Prof. C.A. Dransfeld	Delft University of Technology
Prof. Y. Mizutani	Tokyo Institute ofTechnology
Prof Dr. Ir. R.P.B.J. Dollevoet	Delft University of Technology
Dr. M. Waas	AkzoNobel Chemicals

TU Delft Delft University of Technology

ISBN: 978-94-6380-032-7

Cover design and printing by ProefschriftMaken | www.proefschriftmaken.nl
An electronic version of this dissertation is available | repository.tudelft.nl

Ἓν οἶδα ὅτι οὐδὲν οἶδα

‘The only true wisdom is in knowing you know nothing.’

–

Socrates

Summary

Carbon fibre reinforced plastics (CFRPs) are increasingly used in the aerospace industry because they offer lightweight construction and design flexibility. As sustainability becomes more important in business and to consumers, these materials help vehicles use less fuel and become more durable. The aerospace industry started the development of CFRP materials in the 1970's, after which were also introduced in other industries, such as marine and automotive, leading to higher volumes of CFRP materials in subsequent years. This thesis is focussed on prepreg CFRP manufacturing and the detection of specific production flaws found in an industry survey. During the CFRP prepreg manufacturing process, raw CFRP layers are stacked during the layup phase and then cured to reach the component's design mechanical and geometric specifications. To assure the right quality of the end product, the product is tested for flaws in the non-destructive evaluation (NDE) phase. The criticality of any detected flaw needs to be evaluated and if required reworked or rejected. This research presents an industry survey of typical CFRP manufacturing flaws and evaluates possible NDE technologies to detect these flaws in-situ in the manufacturing process. Analysis is performed by literature review and experimental tests. NDE process monitoring system should decrease the number of rejected and repaired products and increase the efficiency of the manufacturing process. Three NDE techniques were investigated in depth in this thesis to make a detailed design of a monitoring system: Lamb waves, laser displacement sensing and fibre optic sensors. This thesis concludes that the two latter technologies are promising for industrialization to improve the CFRP manufacturing process.

The costs of production flaws in the CFRP manufacturing process are normally hidden in the cost structure of the end product. To address this the research also investigated the financial impact of rework and rejection of products in a CFRP manufacturing process and the estimated financial benefits of implementing an NDE process monitoring system. Overall, this research shows that the potential to detect flaws in-situ, the impact of rework and rejection and the financial feasibility of implementing a novel NDE process monitoring system will increase the efficiency and effectiveness of the CFRP manufacturing process.

Samenvatting

Koolstofvezelversterkte kunststoffen worden steeds meer gebruikt in de luchtvaartindustrie, omdat ze lichtgewicht constructie en flexibiliteit in het ontwerp bieden. Naarmate duurzaamheid belangrijker wordt in het bedrijfsleven en voor consumenten, helpen deze materialen voertuigen minder brandstof te gebruiken en duurzamer te worden. Sinds de lucht- en ruimtevaartindustrie in de jaren '70 begon met de ontwikkeling van deze kunststofmaterialen, werden deze later ook geïntroduceerd in andere industrieën, zoals de scheepvaart en de auto-industrie, Dit leidde in de daaropvolgende jaren tot hogere productie volumes. De focus van deze thesis ligt op prepreg koolstofvezelversterkte kunststoffen, omdat er uit onderzoek blijkt dat er in de industrie specifieke fouten bestaan. Tijdens het productieproces wordt het kunststofvezel material laagje voor laagje opgebouwd tijdens de lay-upfase en tijdens de cure fase uitgehard om het gewenste eindproduct te bereiken. Om de juiste kwaliteit van het eindproduct te verzekeren, is een non-destructieve evaluatie (NDE) nodig om de producten op fouten te testen. Elke gedetecteerde fout moet worden geëvalueerd en indien mogelijk gerepareerd worden, anders wordt het product weggegooid. Dit onderzoek presenteert een industrie-enquête met typische fabricagefouten en onderzoekt verschillende NDE-technologieën om deze fouten tijdens het productieproces te detecteren. Een NDE procesbewakingssysteem zal het aantal afgewezen en gerepareerde producten verminderen en de efficiëntie van het productieproces verhogen. Drie technieken werden in detail onderzocht: Lamb waves, laser detectie en optische vezelsensoren. De laatste twee technologieën zijn veelbelovend voor industrialisatie om het productieproces te verbeteren.

De kosten van deze productiefouten in het productieproces zijn normaliter verborgen in de kostenstructuur van het eindproduct. Dit onderzoek kijkt ook naar de financiële impact van reparatie en afwijzing van producten in een productieproces. Dit onderzoek toont succesvol het potentieel aan om fouten tijdens het productie proces van kunstvezelmaterialen te detecteren, de impact van reparatie en afwijzing en de financiële haalbaarheid van een nieuw NDE procescontrolesysteem om de efficiëntie en effectiviteit van het productieproces te verhogen.

Table of Contents

List of Figures

List of Tables

List of Abbreviations

ACCEM	Advanced Composite Cost Estimating Manual
A/D	Analogue Digital
AIC	Akaike Information Criterion
C-scan	Ultrasonic Plan View Imaging
CAD	Computer Aided Design
CCD	Charged-Coupled Device
CFRP	Carbon Fibre Reinforced Plastic
eFPI	Extrinsic Fabry-Pérot Interferometer
FBG	Fibre Bragg Grating
FC	Ferrule Connector
FAW	Fibre Areal Weight
FOS	Fibre Optic Sensing
IQR	Interquartile Range
IR	Infrared
LDS	Laser Displacement Sensing
MOS-FET	Metal-Oxide Semiconductor Field-Effect Transistor
NCR	Non-Conformity Report
NDE	Non-Destructive Evaluation
NDT	Non-Destructive Testing
PZT	Piezoelectric Transducer
RF	Radio Frequency
RTM	Resin Transfer Moulding
SHM	Structural Health Monitoring
SNR	Signal-to-Noise Ratio
TC	Thermocouple
TRL	Technology Readiness Level
UV	Ultraviolet

List of Symbols

A_n	Antisymmetric Lamb wave mode n
C_T	Temperature coefficient
I	Intensity
I_0	Source amplitude
I_d	Amplitude at distance d
N_λ	Spectral radiance of the surface
$N_{\lambda, b}$	Black body radiance at wavelength λ (b for blackbody)
P	Pressure
P_0	Uncalibrated pressure measurement
P_1	Calibrated pressure measurement
S_n	Symmetric Lamb wave mode n
T	Temperature
X_n	Vacuum bag rip at location n
c	Speed of light
c_L	Longitudinal mode velocity
c_P	Phase velocity
c_T	Transverse mode velocity
d	Distance
d_{decay}	Attenuation length
h	Thickness of plate
k	Wave number
m	Integer
n	Number of wave mode
n_{eff}	Effective refractive index
Δ	Difference
Λ	Grating period
α	Attenuation coefficient
ε	Emissivity (p.40) or Axial strain (p.43)
λ	Wavelength
λ_B	Bragg wavelength
μ	Visibility
ω	Circular wave frequency
ϕ	Random phase angle

Preface

This dissertation introduces several current trends that are hot topics to address efficiencies and effectiveness in manufacturing.

Ford started to increase the flow in its production at the beginning of the 20th century [1], further automation, or the third industrial revolution, ramped up production after World War 2. The use of control loops to measure and control production lines was introduced and therefore more in-line measurements were installed. A higher level of standardization and simplified products allow a higher level of automation. Where industries have low volume products, more manual work is expected and therefore more variation in the quality of the product is expected.

Lean Six Sigma is a method to remove the variation in processes through root cause analysis and statistics [2, 3]. Among others, Motorola, Toyota and GE have developed this methodology in the past decades to optimize their production by identifying and removing waste from their processes [1]. Waste can be categorized into transporting, inventory, motion, waiting, overprocessing, overproduction and defects. The Six Sigma component refers to decreasing the variance in the processes by the use of statistics and aims to decrease the number of flaws to 3.4 defects per million opportunities. The production of Carbon Fibre Reinforced Plastics is diverse with relatively low volumes, which makes a quantitative approach less suitable to remove manufacturing flaws. More standardization in parts could help to reduce flaws during manufacturing.

Currently, the fourth industrial revolution has started, where industries move to more cyber-physical systems [4, 5]. This fourth revolution is also called Industry 4.0 or Internet of Things. Because of the availability of more types of sensors and computing power becoming more affordable, online analytics makes it possible for machines to be interconnected and to not only control the production but also to predict future production or maintenance [6, 7]. Where the next step of prediction is prescriptive, the machine will not only indicate a future state, but also the actions that have to be taken. With more in-line sensing and the need for industries to become more efficient and effective, the development of preventive Non-Destructive Evaluation systems is necessary. This system should be able to detect flaws during manufacturing and also to remove these flaws, especially in industries with high quality standards, like aerospace.

1
Introduction

1.1 Aerospace Composites

Carbon fibre reinforced plastics (CFRPs) are increasingly used in the aerospace industry because they offer lightweight construction and design flexibility [8-10]. As sustainability becomes more important in business and to consumers, these materials help vehicles use less fuel and become more durable. The aerospace industry started the development of CFRP materials in the 1970's [11], after which were also introduced in other industries, such as marine and automotive [12], leading to higher volumes of CFRP materials in the subsequent years [13, 14].

The boundaries of this research start at the end of the chemical production process of carbon fibres and ends at the assembly of the cured CFRP products. The focus is to detect flaws (and ideally removed) before assembly of the manufactured CFRP part. This viewpoint is not widely researched.

CFRP material consists of a matrix of resin and reinforcing carbon fibres. A standard CFRP production process is as follows. Raw materials consisting of pre-impregnated (prepreg) layers (see Figure 1.1) are received at the production facility and if not required for immediate production are stored in a freezer. The production starts by preparing and cutting the prepreg material at room temperature.

Figure 1.1 CFRP prepreg roll with layers separated by foil, together with an example of a cut part (© Zoltek Toray Group).

CFRP manufacturing is the middle part of the production process of composite structures from chemicals to physical assembly. A typical CFRP manufacturing process consists of several phases: stacking the material layer by layer using manual or automated layup, then controlled curing under pressure and high temperature to consolidate the CFRP prepreg and the resin matrix to meet final

design specifications [3]. The final stage of part CFRP manufacturing is non-destructive evaluation (NDE), which, as it occurs at the end of the manufacturing process, only controls the quality of the end product [8-10].

During the layup phase, an automatic tape layer machine or worker stacks the CFRP layers according to the design specifications. During the layup of CFRP, the correct number, position and orientation of layers must be controlled [15]. An automated CFRP tape layer (see Figure 1.2) can automatically lay prepreg tape to the prescribed design specification and is used for large smoothly curved CFRP panels. A machine will lay CFRP tape onto a mould in a set sequence, while an operator is still necessary to control the machine. During hand layup (see Figure 1.3), the CFRP layers are cut to prescribed sizes and manually stacked in the correct order, location and fibre orientation. If needed, the worker applies pressure to the stack. A manual layup is typically used for smaller parts or parts with high complexity.

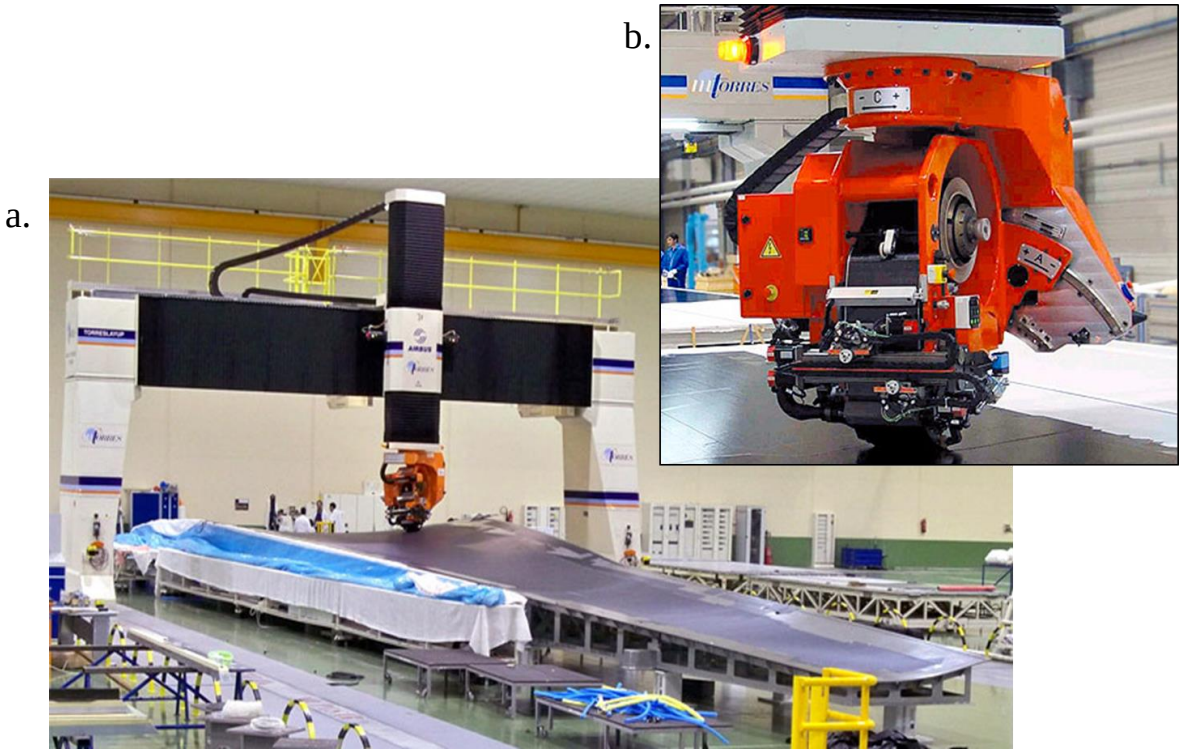

Figure 1.2 An automatic tape layer machine. This example is the TORRESLAYUP by MTorres, used by aircraft manufacturers such as Airbus and Boeing. The lower left image (a) shows the tape layer manufacturing a wing part and the upper right (b) image shows a close up of the tape layer head (© MTorres).

Figure 1.3 An example of hand layup, where workers apply CFRP layers to a mould. (© Lee Aerospace)

In the curing phase, the product is cured under specified conditions, such as time, temperature and pressure, to enable chemical reactions to proceed to determine the properties of the end product. CFRP products can be cured with different methods, such as curing at room temperature [16] or by an autoclave [8]. An alternative manufacturing method is resin transfer moulding (RTM) [17]. During curing, the temperature and pressure in time must be controlled to ensure the correct material properties [18].

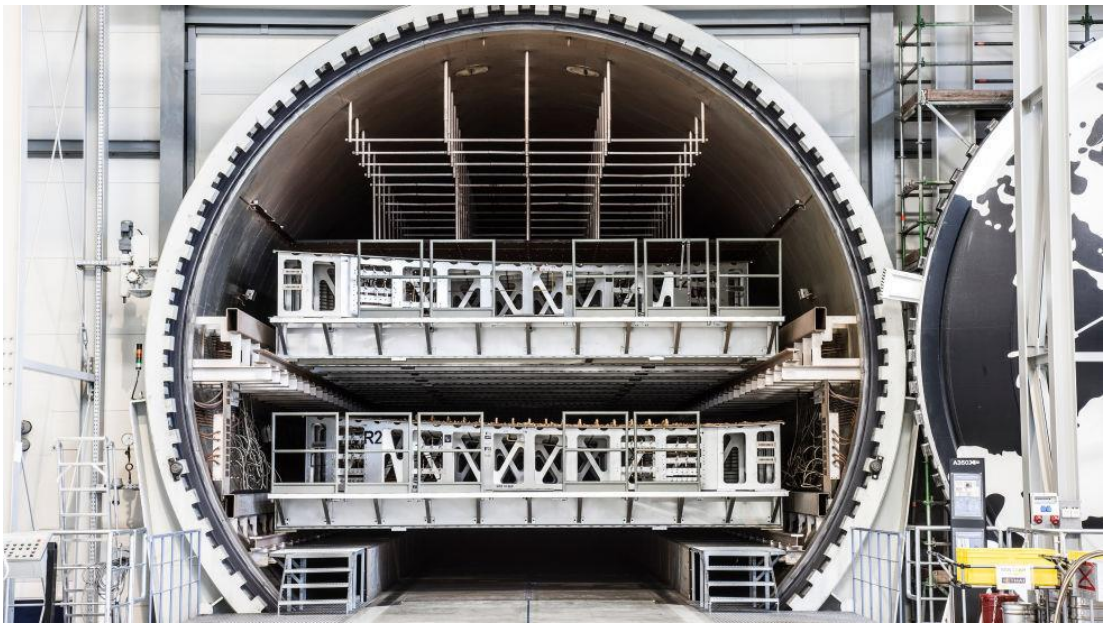

Figure 1.4 An autoclave at the Airbus Stade facility, this autoclave can take up to two wing shells simultaneously (© Werner Bartsch).

During final inspections, the CFRP products are inspected with NDE techniques for deviations from their original design specifications, such as geometric

deviations and the presence of flaws. The detection of the sizes and locations of flaws in the laminate is input for the assessment of the quality of the end product. Any detected flaws need to be assessed and if necessary the part is reworked if possible, otherwise it will be rejected. The maximum allowable diameter of a delamination in commercial aviation is commonly a circular flaw in the order of 12.5 mm diameter [8].

Quality control in the production of CFRP [8-10] starts with physical testing of the raw materials at the fibre production facility and then is performed at the subsequent composite production facilities. Current quality control focuses only on production process control and not on actual flaw detection in CFRP material. Any deviation from the design specifications after production decreases the level of product performance, reduces manufacturing efficiency and increases the costs of CFRP production through rejection, rework and additional quality assurance as will be demonstrated in this thesis. The manufacturing process of CFRP materials is costly due to the high cost of raw materials, skilled staff and high industry quality standards, which may lead to rework and rejection of the final product.

1.2 Flaws in CFRP Production

To identify which flaws occur during the production of CFRP in industry, the author conducted a market survey in 2011 at several Tier 1 European aerospace manufacturers. Large and small CFRP producing companies were consulted to provide information on their production and especially on which production flaws occur during layup and curing. The companies have asked to remain anonymous as a condition for publishing the results of the survey.

Table 1.1 shows an overview of the reported flaws that occur during layup and curing and a concise description of those flaws. The consultation was performed in two rounds; first, four companies were consulted for their CFRP production related flaws. The results of this round were listed and a fifth company was asked to review the list of flaws and failures and to add its top three flaws that occur in the layup and curing phases.

The survey found that the reported flaws are mostly in the layup and curing phases which are in direct control of these manufacturers. These flaws are related to geometric, temperature or pressure related deviations from manufacturing specifications. The survey shows that the industry has many flaws in the manufacturing phase and this gives the opportunity for improvement in process

monitoring and cost efficiency. This forms the basis of definition of the research objectives in section 1.4.

Table 1.1 Results of the market survey with a brief description of the flaw or failure (■: occurs at the corresponding company).

	Flaw/failure	Company 1	Company 2	Company 3	Company 4	Company 5	Brief description of flaw or failure
Layup phase	Fibre bridging/wrinkling		■			■	The layers are not correctly placed and form wrinkles, which cause local accumulation of material
	Incorrect overlap		■			■	The layers are not correctly placed and overlap, which cause local accumulation of material
	Incorrect fibre orientation			■			The directions of the fibres are incorrect, which causes deviations from the design specifications in terms of material strength
	Unremoved foil	■	■	■	■	■	Foil is not correctly removed from the layer and can cause local debonding of the layers and foreign material in the structure
	Incorrect number of layers	■		■	■		Too many or too few layers, which causes deviations from the design specifications
	Anomalies enclosed			■	■		Foreign objects are enclosed which can cause local debonding of the layers
Curing phase	Incorrect vacuum bagging				■		If the material is incorrectly packed, gradients in pressure can occur during the cure cycle
	Vacuum leakage		■		■		If the material is incorrectly sealed or has the incorrect pressure cycle, gradients in pressure can occur during the cure cycle
	Incorrect autoclave charge	■					Setting an incorrect cycle for the autoclave will cause deviations from the material specifications
	Temperature incorrect	■	■		■		Setting an incorrect temperature cycle as part of the autoclave cycle will cause deviations from the material specifications
	Pressure incorrect			■	■	■	Setting an incorrect pressure cycle as part of the autoclave cycle will cause deviations from the material specifications

1.3 Research Objectives

The objective of this research is to investigate the possibility of using an in-situ NDE monitoring system to detect manufacturing flaws during the layup and/or curing phases of CFRP manufacturing. A successful NDE system would be able to detect flaws listed in Table 1.1 to enable the manufacturing process to be modified in real-time, for example by adapting during the autoclave curing cycle. The novelty is that this is the most detailed study of the use of in-situ NDE to detect flaws during layup and curing. A successful process monitoring system is only able to detect and localize deviations in the manufacturing process, but not *prevent* the flaws. Counter-measures are needed to remove or prevent the flaw from occurring once the flaw is detected. This trend would lead to the introduction of preventive NDE in CFRP production, allowing flaws to be detected and removed in real-time during the manufacturing process. The composite manufacturing industry has confirmed that the detection and localization of flaws during production is valuable; therefore, the focus of this research will be on the first step: the detection of flaws during manufacturing. The novel in-situ process monitoring system will contribute to the manufacturing process by:

1. Monitoring critical parameters during the CFRP manufacturing process.
2. Giving feedback as input to customized process cure cycles to reduce the occurrence of flaws.

1.4 Methodology

A range of NDE techniques will first be evaluated in Chapter 2 based on their ability to detect the flaws, listed in Table 1.1. The preliminary evaluation will identify potential sensing techniques that will be further investigated. In Chapters 3 and 4 discuss the proof-of-concept and the laboratory demonstration of Lamb waves in CFRP prepreg as a process monitoring system during the layup phase. Chapter 5 discusses laser displacement sensing (LDS) as a potential process monitoring technology for flaw detection during the layup process. Chapter 6 discusses fibre optic sensing (FOS) techniques to monitor the curing process in-situ in the autoclave cycle. Chapter 7 will show the industrial value of implementing a novel process monitoring system, by modelling the costs for rejection and rework in CFRP manufacturing. In other financial models in composite manufacturing the cost of rejection and rework were never explicitly taken into account, by taking these into account, it will show the true financial costs. Chapter 8 concludes with the results of the research, and future work is presented in Chapter 9.

2

Selection of Non-Destructive Evaluation Techniques

2.1 Introduction

To be effective, an in-situ NDE process monitoring system must be able to track quality parameters and detect one or more of the flaws listed in Table 1.1.

This chapter will focus on the evaluation and selection of NDE techniques for preventative NDE based on a literature review of previous research. The selection of NDE technologies is based on their ability to monitor critical parameters related to the production flaws in CFRP prepreg manufacturing shown in Table 1.1. During the layup phase, the NDE technique should be able to measure geometrical deviations in CFRP prepreg positioning without harming the material or the manufacturing process. During the curing phase, the NDE technique should be able to measure the temperature and/or pressure without negative effects on the material or production process.

The current procedure in industry is to assess the quality of the end product before it is assembled. Five existing NDE techniques were selected by the author in 2011 to be assessed for the in-situ process monitoring system. The selection was based on the experience and availability of techniques at the Delft University of Technology and their detection ability. In line with the trend for more automation, measurement techniques that are independent of human judgement are preferred over visual control and subjective assessment. Based on this procedure the following NDE method and techniques were selected for preliminary evaluation:

- Ultrasonic C-scan
- Ultrasonic Lamb waves
- Laser displacement sensing
- Shearography
- Thermography
- Fibre Optic Sensing:
    - Fibre Bragg grating
    - Fabry-Pérot interferometers

This chapter will introduce and evaluate each technique by literature review of its sensitivity, accuracy, speed and relevant applications of the NDE technique in relation to flaw detection in CFRP prepreg.

The selection criteria are presented in Section 2.2 and Sections 2.3 to 2.8 present an overview of relevant NDE techniques. The assessment is made in Section 2.9 and the discussion and selection are presented in Section 2.10. Section 2.11 presents relevant developments since 2012. Section 2.12 concludes by presenting

which NDE technologies show potential for further research for NDE process monitoring systems.

2.2 Selection Criteria

The following criteria were used to rank and choose the most suitable technique for further development. The following criteria have been selected, as explained below:

- Effect on the structural integrity of the CFRP component
- Performance of the technique in detecting flaws during the layup phase
- Performance of the technique in detecting flaws in the curing phase
- Speed of detection
- Maturity of the technique in current aerospace composite material manufacturing.

The effect of the technique on the structural integrity of the CFRP prepreg is a prerequisite, as the quality of the product must be guaranteed during production. The ability to detect production flaws during layup or curing is of next importance. The speed of detection and maturity of the technique are of lower importance as it is expected that these will be improved through the development of the technique. However, a faster detection speed and higher maturity in a composite production process will increase the practical use of the system and cost efficiency. The term maturity is assessed by techniques that are widely applied during composite production processes. The following sections will describe the selected NDE techniques in more detail.

2.3 Ultrasonic C-scan

Ultrasonic C-scan is widely used for NDE in the aerospace industry [19]. Ultrasonic waves with frequencies above 20 kHz are transmitted through the sample are scattered or reflected from regions with a difference in acoustic impedance [20]. Flaws are identified by differences in impedance, such as differences in density, thickness or discontinuities from surrounding material.

This section reviews C-scan techniques for the inspection of CFRP material. All C-scan methods probe the specimen point-by-point; therefore, this technique is time consuming and the minimal detectable flaw size (inspection density) is a trade-off with the detection speed. A typical custom build ultrasonic C-scan at Delft University scans at 400 mm per second with a minimal grid of 0.1 mm length and 0.25 mm width. Automated C-scan is used for larger structures and the signal is coupled the material through a couplant due to high attenuation with, for

example, glycerine, water [9] or air [21]. The focus of this section is on the different variants of the technique and how they could be applied to the NDE of prepreg layers. The following researchers use different coupling techniques of C-scan to detect flaws in CFRP. In 2001, Bastianini et al. [22] used ultrasonics in pulsed echo configuration to test CFRP and used the first echo peak to localize and characterize bonding flaws. Subsequently, Berketis et al. [23] compared water-coupled and air-coupled ultrasonics to detect impact damage in CFRP. In 2004, Imielińska et al. [24] demonstrated the ultrasonic air-coupled C-scan method to detect impact damage in CFRP. They concluded that the air-coupled method gave better results than the water-coupled method. Laser ultrasonics [25] has also been investigated for non-contact inspection of CFRP.

2.4 Guided Waves

Guided ultrasonic waves are discussed in this section. Through thickness guided waves, such as Lamb waves [26], are usually investigated for structural health monitoring (SHM) [27]. Lamb waves [28] are one type of guided waves that can be introduced in materials and can be applied for density measurements [29]. Lamb waves are excited and detectable by piezoelectric sensors [30]. The Lamb wave technique uses waves that propagate in thin solid media and has been successfully used for damage detection, such as cracks, in structures made of metals or composites [29]. Thursby et al. [31-33] and Takeda et al. [34, 35] used fibre Bragg grating (FBG) sensors, in addition to piezoelectric transducer (PZT) sensors, to detect Lamb waves in cured CFRP materials to locate flaws.

A Lamb wave is a superposition of transverse and longitudinal components. Equations (2.1) give the phase velocity dispersion curves (velocity as a function of frequency) for symmetric and antisymmetric modes respectively [28].

$$\frac{\tan(qh)}{\tan(ph)} = \frac{4k^2qp}{(k^2-q^2)^2} \quad \text{and} \quad \frac{\tan(qh)}{\tan(ph)} = \frac{(k^2-q^2)^2}{4k^2qp}, \tag{2.1}$$

where

$$p^2 = \frac{\omega^2}{c_L^2} - k^2, \quad q^2 = \frac{\omega^2}{c_T^2} - k^2, \quad k = \frac{\omega}{c_p}, \tag{2.2}$$

and wave $\omega, h, k, c_L, c_T, c_p$ are the circular wave frequency, thickness of the plate, number, velocities of the longitudinal and transverse modes and phase velocity, respectively. See Figure 2.1 for a schematic overview of both modes.

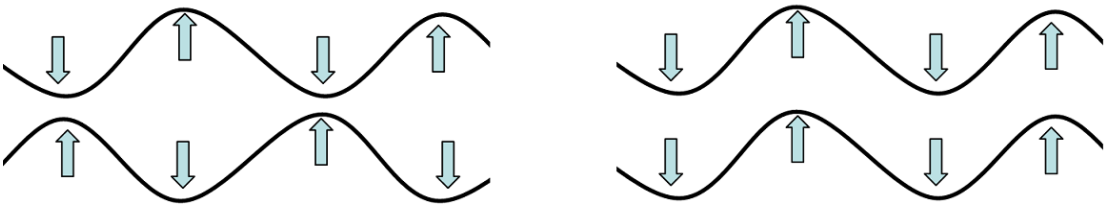

Figure 2.1 Left image represents the zero-mode symmetric Lamb wave (S_0) and the right image the antisymmetric Lamb wave (A_0).

Equations (2.1) and (2.2) can be solved for the phase velocity as a function of the frequency to generate the dispersion curves. Examples of these dispersion curves are modelled and shown in Figure 2.2.

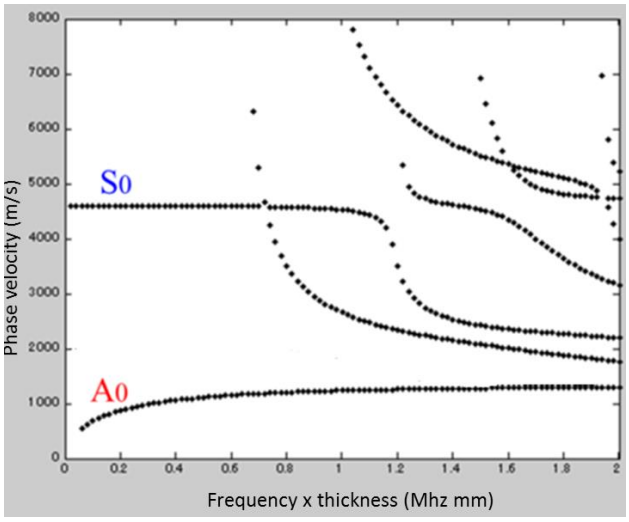

Figure 2.2 An example of the dispersion curve of a $[0]_8$ CFRP layup. The antisymmetric (A_n) and symmetric (S_n) zero order are plotted, including some higher modes.

Typical flaws, like debonding, will cause a local density difference and therefore a different local stiffness. As Su et al. [28] showed, equations (2.1) and (2.2) are linked to Young's modulus, which is a measure of stiffness in the material and determines the characteristics of waves propagating through the material. The velocity and attenuation of the Lamb waves are altered due to a changed Young's

modulus and, with the use of velocity changes in the dispersion curve, flaws can be detected. The minimum detectable flaw size is directly related to half the wavelength ($\lambda/2$), as was shown by Holnicki-Szulc and Soares [36]. Aerospace applications of Lamb waves include the development of smart structures for delamination detection in CFRP [37].

2.5 Laser Displacement Sensing

Laser displacement sensing (LDS) are a less conventional NDE technique in the aerospace industry for flaw detection, but this technique is used for many other industrial applications [38]. In-situ process monitoring of CFRP manufacturing with a confocal laser system was demonstrated by Liu et al. [39]. The laser could measure 10 nm deviations through reflection measurements, by a combination of the laser distance technique with scanning position information from linear encoders. Related work to control CFRP production focused more on the automated control of the (tape) layer process. Schmitt et al. [15, 40-42] also identified the negative influence of manual layup in the production of CFRP. Their research succeeded in contour scanning of the CFRP specimen and detecting out-of-plane flaws. Other research on laser distance sensing on CFRP material was performed by Faidi et al. at GE Global Research Center [43]. Faidi investigated an in-line inspection system to improve the automated production of CFRP wind turbine blade spar caps.

LDS are based on the time of flight of the laser signal. A two-dimensional (2-D) laser line is projected onto and reflected from the measurement target and the received signal is processed to obtain the distance:

$$d = \frac{c \cdot \Delta t}{2}, \tag{2.3}$$

where d is the distance to the object, c the speed of light and Δt the time of flight. The limiting factor for the precision is the interrogation speed [38]. The detection of a typical CFRP layer with a thickness of 160 µm would need a minimum interrogation speed of 0.3 ps for the sampling frequency to be three times the detection frequency. Flaw detection with this technique is based on geometrical deviations from design specifications.

2.6 Shearography

The principle of shearography is the correlation of shearograms recorded before and after mechanically or thermally loading the specimen. Laser light from two

sheared images is optically mixed in an interferometer to form an interferogram [44, 45].

Chen and Hung [46] showed the potential of shearography as an inspection method for large areas of all types of materials, including CFRP laminates. Shearography was developed to detect flaws at the surface or subsurface of specimens, such as bond lines, core crush and delaminations. Flaw sizes to 10 mm can be detected with this methodology in aerospace parts [47]. Commercially available aerospace applications include the NDE inspection of composite parts [48] and load monitoring of CFRP pressurized tanks or rotor blades [49].

The basic optical setup is shown in Figure 2.3. The shearogram recorded before deforming of the object is represented by [50]:

$$I = I_0(1+\mu\cos\phi), \tag{2.4}$$

where I is the intensity distribution of the fringe pattern received at the image plane of the CCD, I_0 the peak intensity of the fringes, μ the visibility and ϕ the random phase angle.

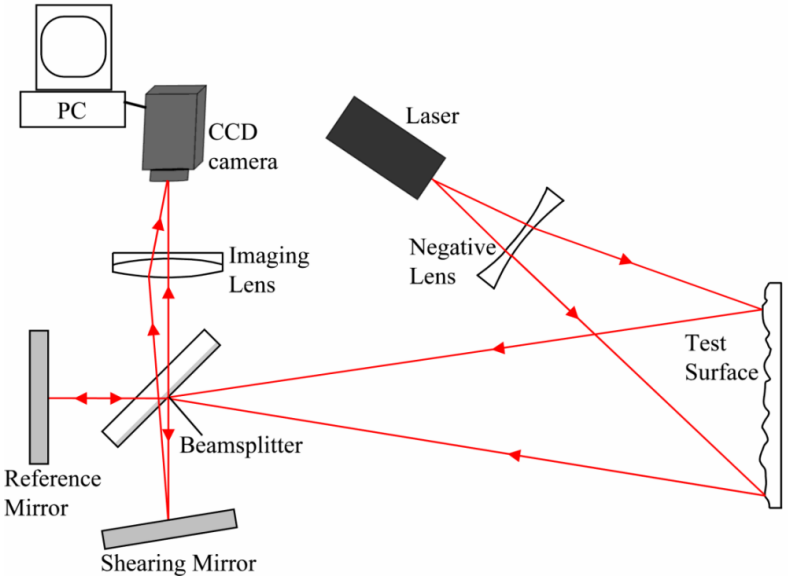

Figure 2.3 A schematic overview of a shearography setup [45].

After deformation of the object, a second shearogram is recorded, I':

$$I' = I_0(1+\mu\cos(\phi+\Delta)), \tag{2.5}$$

where Δ is the phase change due to the deformation. The pixel by pixel intensity difference is represented by I_d:

$$I_d = 2I_0\left[\mu \sin\left(\phi + \frac{\Delta}{2}\right)\sin\left(\frac{\Delta}{2}\right)\right]. \tag{2.6}$$

The measurement principle is based on the different surface deformation response of material with flaws [44]. The global deformation of the object surface is typically constant or slowly varying in the shearing direction. At the damage location, a fringe pattern with a 'butterfly' shape appears for a point damage, resulting from a nonlinear deformation due to loading. This change in the fringe pattern is caused only by flaws and these can be detected by analysis of the fringe patterns [51].

2.7 Thermography

Dissipation of heat from CFRP can be monitored with infrared (IR) devices. Thermography detects differences in surface temperature that can indicate flaws, such as cracks, which show different heat dissipations on or near the surface of the specimen. Thermography can be used in either passive or active modes [52]. Passive thermography measures the thermal dissipation of the specimen without introducing heat. This method can be used for measurements of objects as they stabilize to the environmental temperature or that cool down or heat up in operation, such as an engine. In active thermography, the object is heated to increase the thermal contrasts of the specimen. Several methods are used actively to heat the test specimen, such as pulse or lock-in thermography [52]. Aerospace applications include structural inspections of propellers, motor case tubes, wind turbine blades and others [53]. This technique can detect delaminations, large voids and some foreign objects included in CFRP [46]. The technique of infrared thermography can be very sensitive, as Bates et al. [54] demonstrated in measurements of barely visible impact damage (diameter of 0.315 mm) in CFRP. Many others have demonstrated the potential of infrared thermography to detect flaws in different types of composite materials. Halabe et al. [55] showed the use of thermography to detect delaminations in glass fibre reinforced polymers. Another example of the widespread use of thermography is thermo-acoustic fatigue detection for aircraft [56].

For passive and active thermography, the heat dissipation can be measured with contact sensors (e.g. thermocouples or fibre optic sensors) [57] or non-contact thermal imaging [58]. The spectral radiance of the surface of the specimen is:

$$N_\lambda = \varepsilon N_{\lambda,b}(\lambda, T) \quad (Wm^{-2}sr^{-1}\mu m^{-1}) \tag{2.7}$$

where ε is the emissivity, $N_{\lambda,b}$ is the black body radiance, λ its wavelength and T the body temperature [52]. The measurement principle is based on the characteristic dissipation of the material and its composition. Any cracks or debonding in the CFRP will show a discontinuity in the thermal gradient of the specimen. This discontinuity is measured and the flaw can be indirectly identified. The measurements are more complex for materials with different emissivities, as these appear as different temperatures in the thermographic images.

2.8 Fibre Optic Sensors

This section discusses two typical fibre optic sensors: FBG and extrinsic Fabry-Pérot interferometer (eFPI) sensors. The evaluation of these optical sensors will focus on the detection of temperature and pressure, although more applications are possible (e.g. strain measurements) [59, 60]. This will not only impact the structural integrity of the product but will also impact the production speed. These sensors have several advantages compared with electrical sensors, including small size and good immunity to electromagnetic interference [30]. Research in cure monitoring with FOS has focused on simultaneous sensing with FBG and eFPI sensors [61, 62], residual stress measurements [63-65] and applications in RTM [63, 66, 67]. A brief description of the relevant research in optical sensing of temperature and pressure in an autoclave environment is given below.

Kang et al. [61, 62] developed a hybrid sensing system combining FBG sensors with eFPI sensors. The temperature measurements were derived from the FBG signal, while the strain was derived from the eFPI signal. Other related work has been performed by Leng et al. [68], who performed cure monitoring with FBG and eFPI sensors and successfully detected delamination in CFRP material. They used a heat-press instead of an autoclave and they did not monitor pressure. Wang et al. [69] later used a hybrid FBP/eFPI sensor to measure temperature and pressure simultaneously. In this work the FBG was maintained in a strain-free condition, acting as a temperature sensor and providing data to compensate the eFPI. The results show a low temperature-dependence error of 2.8 Pa/°C with a pressure resolution of 37 nm/Pa. These developed sensors were, however, not

tested in the extreme environment of an autoclave under high temperature and pressure. Several variations on this concept have been researched to adapt the sensor to different environmental conditions [70]. Xu et al. designed an eFPI sensor with a resolution of 34.5 Pa and a measurement range from 35 kPa to 69 MPa, which can operate at temperatures up to 250 °C [70]. Aref et al. [71] made improvements to the eFPI sensor to increase the temperature sensitivity by using a metal housing in the sensor. Iannuzzi et al. [72] developed a fibre tip sensor by carving a cantilever beam at the fibre tip. The sensing principle is comparable to the reflective membrane; however, the cantilever replaced the membrane at the fibre tip. Qi et al. [73] investigated the response to thermal curing and mechanical loading of an FBG in a CFRP. The specimen was cured at high temperature (177 °C) and high pressure (630 kPa) inside an autoclave. The FOS have a possible resolution of 0.5% at 20 MPa pressure [74] and of 0.001 °C for temperature [75] measurements. No research has been published on local pressure measurements during an autoclave cure cycle of CFRP material before this research.

2.8.a Extrinsic Fabry-Pérot Interferometer

An eFPI is a passive optical sensor, which is able to measure strain, temperature and pressure at the tip of a fibre [76]. The concept is based on placing a membrane on the end of the fibre tip to form a Fabry-Pérot cavity (see Figure 2.4).

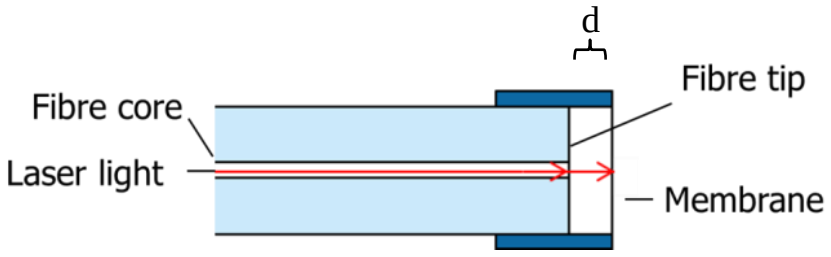

Figure 2.4 Schematic representation of a fibre tip with an eFPI sensor, where d is the distance to the membrane creating a cavity.

Light reflecting from the fibre tip interferes with the reflection from the membrane at the interferometer to give an interference signal sensitive to the cavity length, *d*. To measure the absolute cavity length, two-wavelength interferometry [77] is used:

$$d = \frac{m\lambda_1\lambda_2}{2(\lambda_1 - \lambda_2)} \tag{2.8}$$

where d is the cavity length, λ_1 and λ_2 are optical wavelengths $2m\pi$ out of phase, and m is an integer. The measuring principle is based on the calibration of Δd to changes in the cavity distance due to the variable, in this case, the pressure. The membrane reacts to changes in the external pressure, while the fibre tip remains stable [76]. A higher external pressure will cause the membrane to bend inwards, decreasing the cavity length, which changes the interferometric signal. Another application of the sensor is to react to temperature changes, the membrane experiences external pressure due to higher temperatures. This means that the eFPI sensor is sensitive to both temperature and pressure and compensation is needed for accurate pressure measurements in an autoclave.

2.8.b Fibre Bragg Gratings

FBGs are passive fibre optic sensors, which are sensitive to strain and temperature change. An FBG sensor is a longitudinal periodic variation in the index of refraction of the core in an optical fibre. FBGs are made by exposing the fibre core to high power ultraviolet light through a mask creating a grating pattern or a fixed refractive index modulation. The grating pitch or the spacing of the variation determines the reflected Bragg wavelength. An FBG sensor acts as a reflective band-pass filter in reflection and as a band-stop filter in transmission (see Figure 2.5).

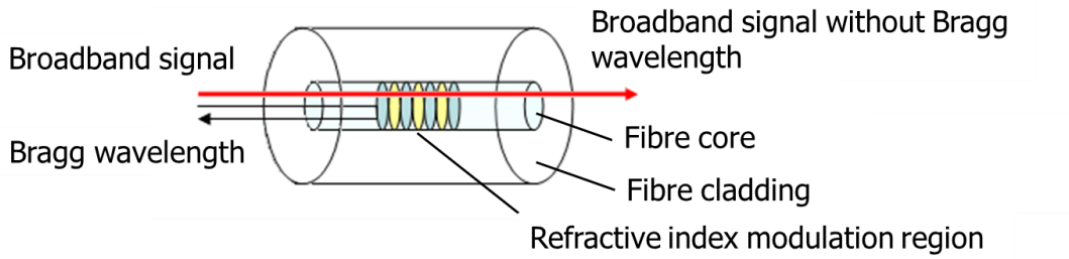

Figure 2.5 Schematic representation of an FBG.

The reflected wavelength, the Bragg condition, can be expressed as [78]:

$$\lambda_B = 2n_{eff}\Lambda\,, \tag{2.9}$$

where λ_B is the reflected Bragg wavelength, n_{eff} is the effective refractive index of the grating and Λ is the grating period. Varying mechanical and environmental conditions, such as changes in strain and temperature, cause both the index of refraction and the optical spacing in the grating to change. This causes a shift in

the reflected wavelength. The Bragg grating wavelength shift due to temperature or strain changes, $\Delta\lambda_B$ is [78]:

$$\Delta\lambda_B = \frac{\partial\lambda_B}{\partial\varepsilon}\Delta\varepsilon + \frac{\partial\lambda_B}{\partial T}\Delta T\,, \tag{2.10}$$

where ε is the axial strain along the optical fibre axis and T is the temperature. A single length of optical fibre may contain multiple FBGs, and wavelength-division or time-division multiplexing may be used to separate the signals at the interrogator [30]. The interrogator measures the change in reflected or transmitted wavelength from an individual FBG and converts it to a change in strain or temperature.

As equation (2.10) shows, the FBG sensitivity has a strain and a temperature component. The temperature coefficient of an FBG is typically very low and to amplify the temperature sensitivity of an FBG, it can be bonded to a material with a higher temperature coefficient, such as metals, to utilize the strain response for temperature sensitivity [79].

2.9 Assessment

The C-scan contact probe method requires a medium for ultrasonic coupling and the specimen needs to be fixed in the C-scan instrument. Air coupled C-scan does not use any coupling medium but has 120 dB more amplitude loss due to acoustical mismatch compared with water-coupled C-scan [21]. Using air-coupled C-scan would, therefore, need 10^{12} more coupling power for the same results as water-coupled C-scan. Air coupled C-scan could potentially detect flaws in the layup phase, as it can distinguish different densities in specimens; however, it would be of no use in measuring temperature or pressure parameters during the cure cycle. Although the C-scan method is mature and widely used in aerospace production facilities, it slowly scans each layer for flaws and would affect production time.

LDS is a non-contact non-destructive measuring technique. This technique can measure the dominant production flaws during the layup, but it is unsuitable to measure pressure or temperature in the curing phase. Measurements are performed in less than a second and the laser displacement technique is used in many production industries, but is less integrated into aerospace manufacturing facilities.

Another option for ultrasonic NDE is Lamb waves. This novel detection technique could be able to detect the production flaws during layup, and Lamb waves can scan a larger surface of the specimen instead of the point-by-point scanning used for C-scan. Most Lamb wave detection methods need contact measurements to couple the signal from the transducer in the material. Recent research in Lamb wave detection techniques includes non-contact measurements, like laser-induced Lamb waves [80].

Shearography would also have a negative effect on CFRP prepreg as the specimen needs to be loaded to detect any flaws. The method would be able to detect flaws near the surface of the specimen [46], which is sufficient for the layup. However, loading, if possible, will make the method unsuited to use in layup, and shearography is unable to measure locally the environmental temperature or pressure during production. This technique would be able to monitor the overall effect of the pressure on the specimen during curing, as this causes fringe patterns. However, shearography could not measure the negative effect of air pockets trapped between the specimen and the mould and especially these local points need pressure monitoring. This technique is widely used in research, but not used in the production of CFRP, except for specialized applications [49].

Active thermography impacts the CFRP prepreg negatively as it would pre-cure the material, increasing the sample's temperature. Passive thermography is based on the dissipation of heat from the specimen; however, it would not be possible if the specimen has the same temperature as its environment. During the curing phase, it could be possible to measure the temperature, but not the pressure.

The FBG and eFPI optical sensors are evaluated based on their ability to measure temperature and pressure. These optical sensors are not suitable to use during the layup phase as these need to be mounted on each layer to measure strains [35]. If these sensors are used to monitor (local) environmental temperature and pressure, then this does not affect the specimen during the curing phase, especially when the sensors are used to monitor the environmental temperature and pressure of the curing instead of the internal materials parameters. The measurement of internal parameters would need surface mounting or embedding of the sensors. Specific local weak points, such as the pressure valve, could be monitored with these fibre optic sensors without mounting them in or on the specimen. Temperature and pressure measurements can be made real-time during the curing phase. These optical sensors are investigated in a broad range of research fields, but the techniques are not fully accepted in general production industry [81, 82].

2.10 Selection and Discussion

A ranking of six different techniques was made according to the following criteria.

Table 2.1 summarizes how each NDE technique is able to detect common production flaws in CFRP and Table 2.2 shows the overall ranking of the selected NDE techniques. A distinction is made between a negative, neutral or positive impact on the criteria by each NDE technique.

The primary criterion, effect on the material, is negatively influenced by C-scan, thermography and shearography in the layup phase. These three techniques will be less qualified to monitor the CFRP prepreg. Of the remaining three techniques, fibre optic sensors and LDS show clear advantages for a potential in-situ monitoring system in the layup phase and are positively assessed as an in-situ monitoring system. Lamb waves qualify as a potential third method over the three disqualified techniques because they affect the specimen less negatively. However, Lamb waves will need more development in the understanding of its use for CFRP prepreg.

Table 2.1 The possibility of the NDE techniques to detect (+) or not detect (–) a common production flaw.

	C-scan	Lamb waves	Laser distance	Shearography	Thermography	FBG and eFPI
Enclosures or embedded anomalies	+	+	+	+	+	–
Incorrect number of layers	+	+	+	–	–	–
Pressure measurements during curing	–	–	–	–	–	+
Temperature measurements during curing	–	–	–	–	+	+

Table 2.2 Ranking of the NDE techniques by a positive (+), neutral (0) or negative (–) score on the selected criteria.

	C-scan	Lamb waves	Laser distance	Shearography	Thermography	FBG and eFPI
Effect on prepreg material	–	0	+	–	–	0
Performance of the technique during layup	+	+	+	0	0	0
Performance of the technique during curing	–	–	–	–	0	+
Speed of detection	–	+	0	+	+	+
Maturity	+	–	0	0	+	0

This leads to the following NDE techniques being selected as most promising for in-situ monitoring techniques:

- Lamb waves during the layup phase
- Laser distance sensing during the layup phase
- Optical sensors (FBG and eFPI) during the curing phase

These three NDE techniques show the highest potential as in-situ process monitoring techniques. A technology readiness analysis in the next section will show the developments needed for these techniques to evolve into an in-situ process monitoring system.

A challenge of the three promising NDE techniques is in the use for CFRP prepreg monitoring and in the development of an in-situ process monitoring system. CFRP prepreg has different properties than cured CFRP, such as the viscoplastic properties. On the other hand, a suitable NDE techniques should not interfere with the current production process.

Lamb waves, LDS and fibre optic sensors were evaluated in this thesis as promising NDE techniques. In respect to previous research, there is no research done in the area of flaw detection in CFRP prepreg material. Therefore, a technology readiness analysis is necessary to assess the current level of the

selected NDE techniques compared with the necessary in-situ production monitoring system requirements. Not only the physical working principles of the techniques need validation for this application but also practical implementation issues for production environments need consideration.

Lamb waves can detect typical flaws in cured CFRP, which have comparable types and sizes to the flaws present in CFRP prepreg. This method needs at least one transducer to couple the signal in the material and one receiver to retrieve the propagated Lamb wave from the material. Depending on the attenuation and size of the CFRP prepreg, more transducers and receivers may be needed. Ideally, this should be done without physical contact, but this will depend on the signal loss of the coupled signal and the attenuation in the material. The major technical challenges are

- High attenuation in the prepreg material and the anisotropic internal distribution of CFRP prepreg causing higher complexity in the signal compared to cured CFRP.
- Lamb waves are complex signals and to distinguish all components in the signals demands more research. Current research focuses on other types of material and this provides no reference research.
- The interface of the layers of the prepreg affects the transfer of Lamb waves and their propagation is affected by the thickness of the prepreg laminate [28]. More layers will cause higher amplitudes, assuming that the layers have an interaction with each other.

A single LDS can detect geometrical deviation without contact or interfering with the manufacturing process. However, a standalone LDS technique will not bring sufficient data to detect any flaws during production, unless the geometrical measurements are coupled with numerical steering data to locate the coordinates of the measurement. The combined coordinates and geometrical height measurements need to be evaluated against product designs, such as CAD drawings, to assess the quality during production. Deviations from the design must be marked as flaws and, if necessary, production needs to be stopped. The in-situ monitoring system could detect the flaws and can trigger the process to stop. The following step would be another process to remove and resolve the detected flaw. Although several laser distance sensing systems are available, several technical challenges remain before industrializing this concept. A proof-of-concept research must indicate if this technique is feasible to use as an in-situ CFRP production monitoring system. Foreseen technical challenges are

- How to integrate the system in real-time into the production process? Can the system operate independently from the workers or tape layers to monitor the quality in-situ during layup? As an example, this means that the system needs to correct for any dynamic vibrations due to the layup process.
- Once the detection during the production of composite laminates is possible, how will the feedback of the monitoring system be integrated to remove the flaw?

The FOS systems always need at least one fibre with one or more optical sensors to measure critical parameters, with an interrogator to process the measurements. If environmental variables (e.g. temperature or pressure) need to be measured, contact with the CFRP part is not necessary. The first step in the research with fibre optic sensors is to demonstrate the ability to detect flaws related to temperature and pressure in an autoclave environment. As these sensors are emerging techniques and few standards are available, the practical use of these sensors can be an issue. Currently, there are different interrogation techniques for FBG and eFPI measurements available but a combined interrogation system for both sensors is not commercially available. This increases the complexity of measurements, but hybrid measurement systems are currently being researched [61, 69]. Several technical challenges are

- How to integrate the sensors during the curing (e.g. autoclave) without affecting the curing process?
- Besides this challenge, linking the signals from the optical sensors to actual flaws will be another issue. For example, the FBG sensor is also sensitive to strain and this measurement sensitivity needs to be excluded.
- Finally, when flaws can be detected successfully, how does the measurement feedback alter the production process? Completely stopping the curing process will harm the structural integrity of the product, so other measures need to be developed to remove and resolve the actual flaws.

These three NDE techniques need further research to understand the specific issues for the new application and to mature the technique into an in-situ process monitoring system. In addition to solving the technical issues of implementing these promising techniques, the practical use in an actual production environment is a future step. Any new system should interfere little or not at all with the production process. The system also needs to be automated, as this tool should provide immediate feedback on the quality. This feedback loop should be fast, as any detected flaw must be removed immediately before the production of CFRP continues.

Although production companies have installed quality assurance techniques, such as visual control, autonomous detection systems can improve the production process. The three promising techniques need more development to adapt to the industrial production environment and to CFRP prepreg. As laser displacement and optical sensing are not dependent on the material characteristics of CFRP prepreg, the next steps in research after proof-of-concept will focus on the gaps towards industrialization. As laser displacement measurements need to be combined with hand or automatic tape laying processes, vibrations of the tape laying process will cause additional errors in measurements. While optical sensors can measure pressure and temperature, the challenge is to measure at the right places during the curing phase without altering the curing process. For both techniques, the issue arises of flaw removal after detection. How can a production flaw be removed without impacting the structural integrity during layup or cure? Together with production facilities, the impact of interrupting the layup process or curing cycle needs to be further investigated.

For the detection of flaws with Lamb waves in CFRP prepreg, more fundamental issues need to be investigated before addressing industrialization gaps. Material characteristics, such as Young's modulus and Poisson's ratio, of CFRP prepreg, differ from those of cured CFRP.

2.11 Recent Developments in Relevant Research

The previous sections in the chapter were based on a literature review started in 2011 and are complemented in this section with relevant research studied at the time of writing the thesis.

Lamb waves have only been investigated in cured CFRP to determine material characteristics [83] or to localize damage [84, 85]. This technology is still under investigation, without focus to use this technology in CFRP prepreg. Hudson et al. [86] demonstrated an online guided wave system for in-process cure monitoring using high-temperature PZT sensors. The research demonstrates successful results after the point of vitrification of the CFRP material. Laser displacement technology is increasingly under investigation to be integrated into the manufacturing process [87] but is more focused on layer placement and not on flaw detection [88]. Shearography has no published developments in CFRP prepreg but is increasingly investigated as an NDE technology for CFRP material [89-91]. Thermography has made interesting advances in flaw detection in CFRP prepreg layups [92-95]. Specifically, Shepard et al., who could detect foil of a quarter inch squared (about 161 mm^2) between layers 3 and 4 in CFRP prepreg at

a distance of 16 feet (about 4.9 m). Shepard also addressed the difficulty of flaw detection, as CFRP prepreg cannot be contaminated with contact or immersive NDE and has high attenuation to ultrasound. This research does note limitations due to the prepreg state of the CFRP material, such as the penetration depth of a maximum of five layers, but provides no impact of active thermography on the prepreg part. Relevant FBG made advances in cure monitoring by focusing on residual stress and temperature measurements during the cure cycle [96-99] but none during the autoclave cycle. Relevant research in eFPI concentrates mostly on the further development of the sensor or the integration with FBG sensors [100-102]. Related research on cure monitoring with other measurement technologies was presented by Torres et al. [103], who used tunnelling junction sensors to monitor temperature locally at each curing state.

At the time of scoping of this research, Eddy currents did not show potential for in-line monitoring, but in the meantime, Eddy currents have developed rapidly and have become an established NDE method to test CFRP parts. Through analysis of conductivity and permeability, they test for material discontinuities or inclusions [104, 105]. A primary magnetic field is generated by an alternating current in the excitation coil. When the excitation coil is placed near a conductive specimen, Eddy currents within that specimen are generated. The Eddy-current flow generates a secondary magnetic field, opposed to the primary, which can be detected by a receiving coil. Excitation current, electrical conductivity and magnetic permeability indicate the material characteristics [106, 107].

These recent developments were not taken into account during the evaluation and choice of NDE techniques for further investigation. However, some interesting developments will be further discussed in Chapter 9, Future work.

2.12 Conclusions

This chapter has evaluated and assessed several NDE techniques on their ability to detect in-situ production flaws in CFRP. Through the ranking of NDE techniques against several criteria, three were identified as promising in-situ monitoring techniques:

- Lamb waves
- Laser distance sensing
- Fibre optic sensors (i.e. FBG and eFPI sensors)

While flaw detection with Lamb waves will need more fundamental understanding, the other techniques require more practical challenges to be

addressed. Industrialization of these techniques will contribute to detecting production flaws in-situ and improve the efficiency of CFRP production.

Recent external developments are included in the discussion of future work in Chapter 9.

3

Lamb waves Proof-of-Concept

Propagation of Lamb waves in a single layer CFRP prepreg

Adapted from: *Lamb wave detection in prepreg composite materials with fibre Bragg grating sensors; Miesen, N., Mizutani, Y., Groves, R. M., Sinke, J. & Benedictus, R. 2011. In: Proceedings of SPIE–International Society for Optical Engineering. 7981, p. 1–11.*

3.1 Introduction

The research goal of this chapter is to demonstrate the propagation of Lamb waves in CFRP prepreg material. Lamb waves already been used to detect and monitor flaws in cured composite material, see a technical introduction in Section 2.4.

In this chapter, the propagation of Lamb waves will be investigated in unidirectional CFRP prepreg and for its ability to detect flaws. To detect and measure these Lamb waves, FBG sensors, introduced in Section 2.8.b, will be investigated and in parallel, PZT [108] is used for verification measurements of Lamb waves. The major bottleneck is the expected different behaviour of CFRP prepreg material compared with cured CFRP. Both materials are characterized using different sets of variables: prepreg by variables related to processing and viscosity, and cured laminates by their mechanical properties. Therefore, these materials are hard to compare from specifications. A second challenge is measuring Lamb waves with FBG sensors is that the frequencies of Lamb waves are ultrasonic and the interrogation using FBG sensors must reach this interrogation speed. A third challenge in Lamb wave detection with FBGs in prepreg material is the coupling of the sensor with the material. A good quality bond between the material and the sensor is essential for increasing the signal-to-noise ratio (SNR).

The novelty of this research is the proof-of-concept of Lamb wave propagation in CFRP prepreg material and the detection with FBG and PZT sensors.

3.2 Experimental Setup

To measure Lamb waves in CFRP prepreg, experiments were conducted using both FBG and PZT sensors. Both setups are in Figure 3.1 and 3.2. The type of CFRP is the DT120 matrix system with toughened thermoset epoxy from Delta-Preg Spa [109]. This CFRP is used in the experiments as a representative prepreg.

The following experiments were conducted to demonstrate the propagation of Lamb waves in a single layer of CFRP prepreg:

- Lamb wave detection in CFRP prepreg with FBG and PZT sensors.

- Damage detection using Lamb waves in a single CFRP layer.

Figure 3.1 shows the experimental setup used for the FBG measurements. A super luminescent diode (Frankfurt Laser Company, 20 mW, 1520–1580 nm wavelength range at full width half maximum) was used as the light source. Reflection spectra from the FBG sensors were directed via an optical coupler to a scanning Fabry-Pérot interferometer (Micron Optics, Model FFP-TF2) and detector (Micron Optics FFP-C). The FFP-T2 was used initially in scanning mode to detect the FBG reflection; subsequently, the scanning voltage was manually decreased until the interferometer acts as an edge filter [110]. This edge filter monitors the shift in the slope of the FBG reflection. The signal was digitized by an analog/digital (A/D) converter (PICO Technology Model 3224). The interrogation speed is therefore only limited by the A/D converter. Digitized data are fed to the computer and analysed by software developed using LabVIEW (National Instruments) to determine the wave arrival time. The FBG sensor (FOS&S, Bragg wavelength 1530 nm) was attached to the layer of CFRP prepreg specimen (200 mm × 300 mm) using ultrasonic gel (Sonotrace, Sonotech). The attachment was without adhesive, as this would not be suitable to use in the production phase. To generate Lamb waves, an impactor dropped from a height of 35 mm was used. To provide reference measurements, two PZT sensors were used, with PZT 1 on the same side of the layer as the FBG sensor and PZT 2 on the opposite side.

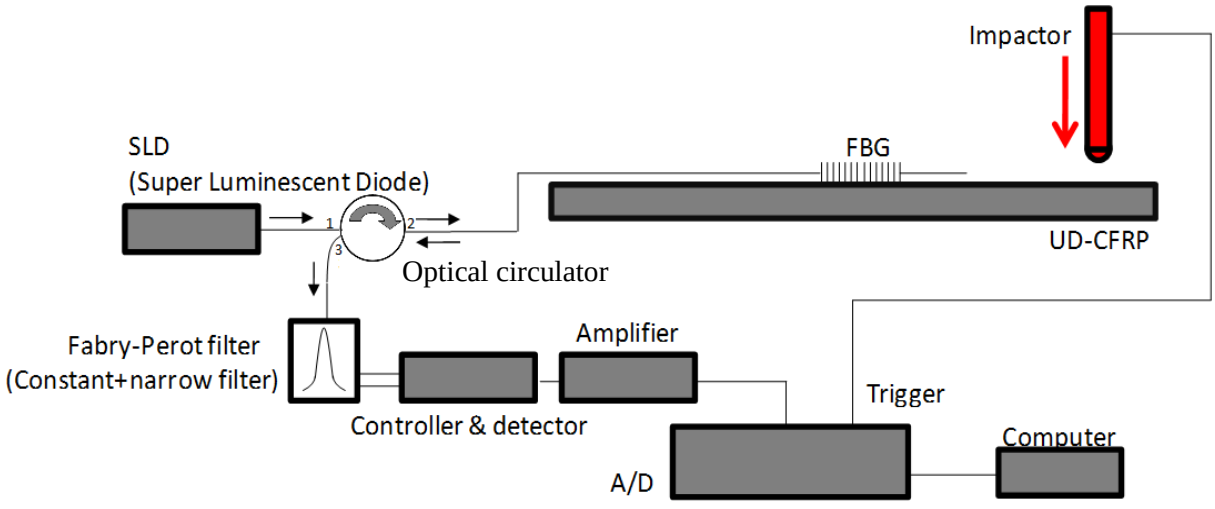

Figure 3.1 Schematic overview of the FBG experimental setup.

Figure 3.2 shows the experimental setup for the validation measurements with PZT sensors (PICO-HF1.2, Physical Acoustics Corporation). An in-house

developed MOS–FET-based pulser [111] was used to excite a Langevin ultrasonic transducer (Honda Electronics HEC-301002) at 51 kHz, in order to generate high powered ultrasonics. The signal from the PZT sensors was amplified using a low-noise wide-band amplifier (NF Electronic Instruments 9913). The same experimental setup was used for the FBG measurements, except that the drop weight was replaced by a transducer and the FBG sensor was replaced by two PZT sensors placed 30 mm and 50 mm along a line from the transducer. Both FBG and PZT sensors were interrogated at 312.5 kHz.

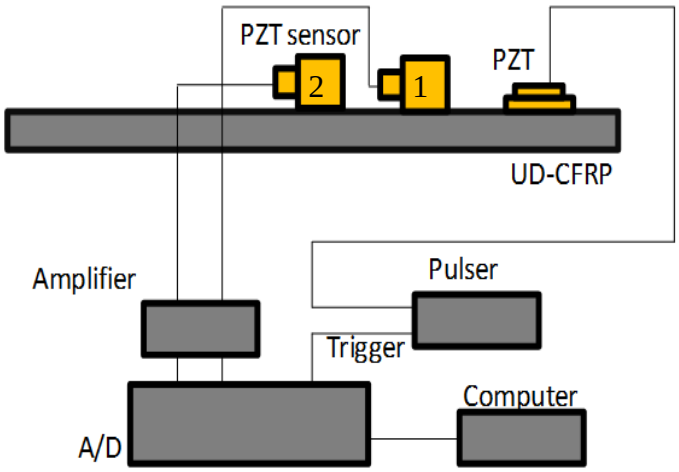

Figure 3.2 Schematic overview of the PZT experimental setup.

The algorithm to determine the arrival time of the first wave at the measurement point was developed according to the Akaike Information Criterion (AIC) [112].

3.3 Results

The results of the impact measurements are shown in Figure 3.3 and 3.4.

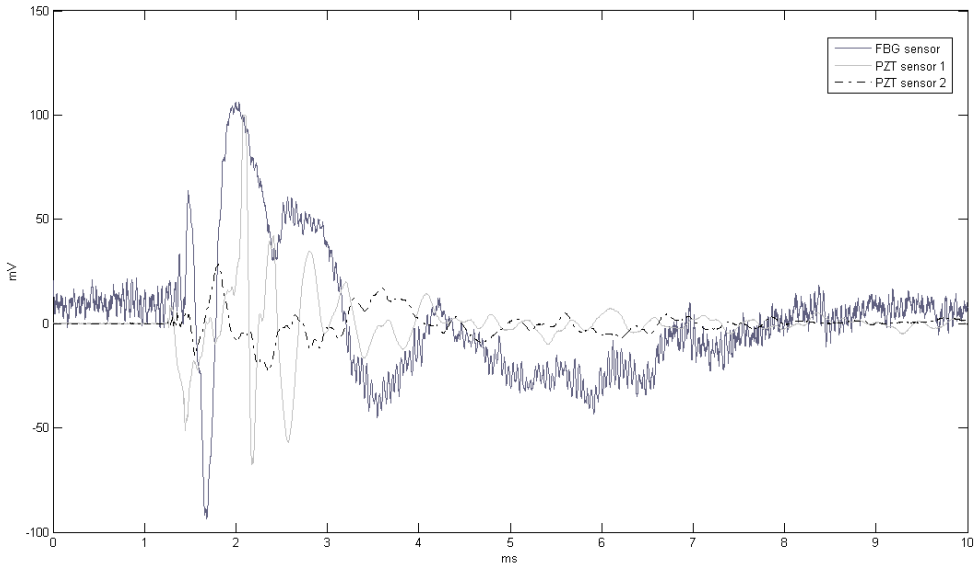

Figure 3.3 Example FBG measurement in the 0° orientation in a single CFRP prepreg layer.

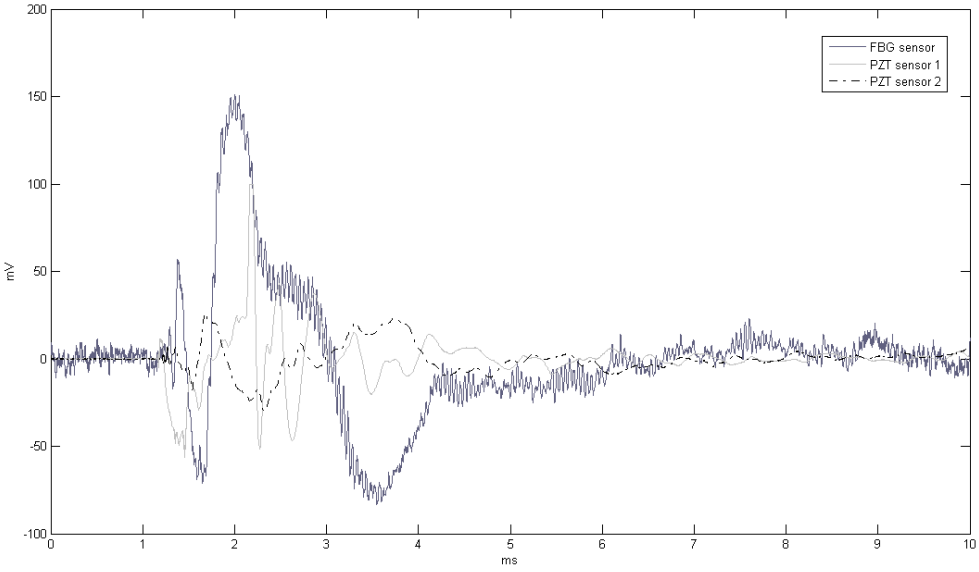

Figure 3.4 Other example FBG measurements at 0° orientation in a single CFRP prepreg layer.

In Figure 3.3, because the arrival of high frequency components, the Lamb waves are in A_0 mode. The frequency of Lamb waves detected by the FBG sensor is

lower than that detected by the PZT sensors. Comparable results from duplicate measurements are seen in Figure 3.4.In these experiments, the PZT sensors at 30 mm and 50 mm were used to determine the velocity of the Lamb wave in a CFRP prepreg layer.

This experiment investigated the potential of Lamb wave velocity measurements as a qualitative tool in the production process of composite materials. After determining the velocity in an undamaged layer of CFRP prepreg, cracks (10 mm) were introduced at 40 mm (between the PZT sensors) from the transducer perpendicular to the Lamb wave propagation. The transducer was aligned with the PZT sensors using a mould. Two orthogonal orientations of the carbon fibres were investigated to determine the velocity because of the dependence of the velocity on the fibre orientation, as shown in Figure 3.5.

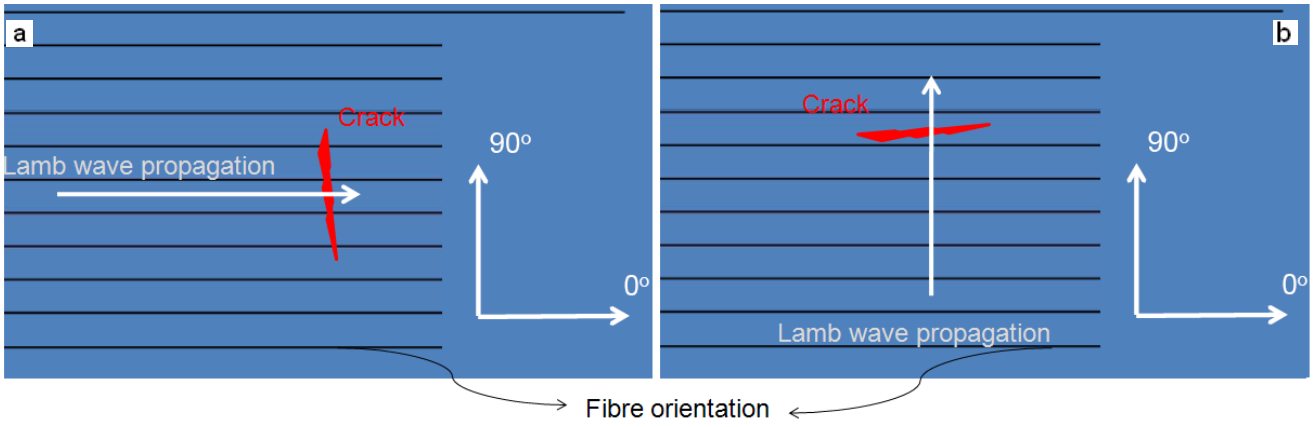

Figure 3.5 (a) The Lamb wave propagates parallel to the fibres in the 0° orientation with the crack at 90° to the wave propagation. (b) The Lamb wave propagates perpendicular to the fibres in the 90° orientation with the crack at 0° to the wave propagation

The original velocity in the 0° orientation of the first arriving frequency is 7100 m/s (standard deviation of 400 m/s). After introducing a flaw at 40 mm the velocity of the Lamb wave decreases to an average velocity of 2000 m/s (standard deviation of 340 m/s).

To improve the SNR in the measurements, an amplifier was used to increase the signal from the PZT. The error in the measurements was decreased as the AIC software could now determine the time of arrival with more precision. After introducing a flaw at 40 mm from the transducer in the 90° configuration, the

velocity of the Lamb wave decreased significantly from 2400 m/s (standard deviation of 12 m/s) to 900 m/s (standard deviation of 5 m/s).

Not only is the velocity of the Lamb wave of value in the production process, but the wave form itself can contain information on the 'health' of the material. As shown by Zhang et al. for cured composite material, a hole (i.e. a flaw) in the material reflects the Lamb wave and an extra wave group appears compared with the non-flaw situation [113]. In this research, the same phenomenon was detected in CFRP prepreg, which is shown in Figure 3.6. Before a flaw is introduced, the PZT sensor at 30 mm measures three separate wave packets. After introducing a crack of 10 mm at 15 mm from the source, reflection wave packets are measured after approximately 1.5 ms. The amplitude of the signal decreases also significantly after the introduction of the flaw.

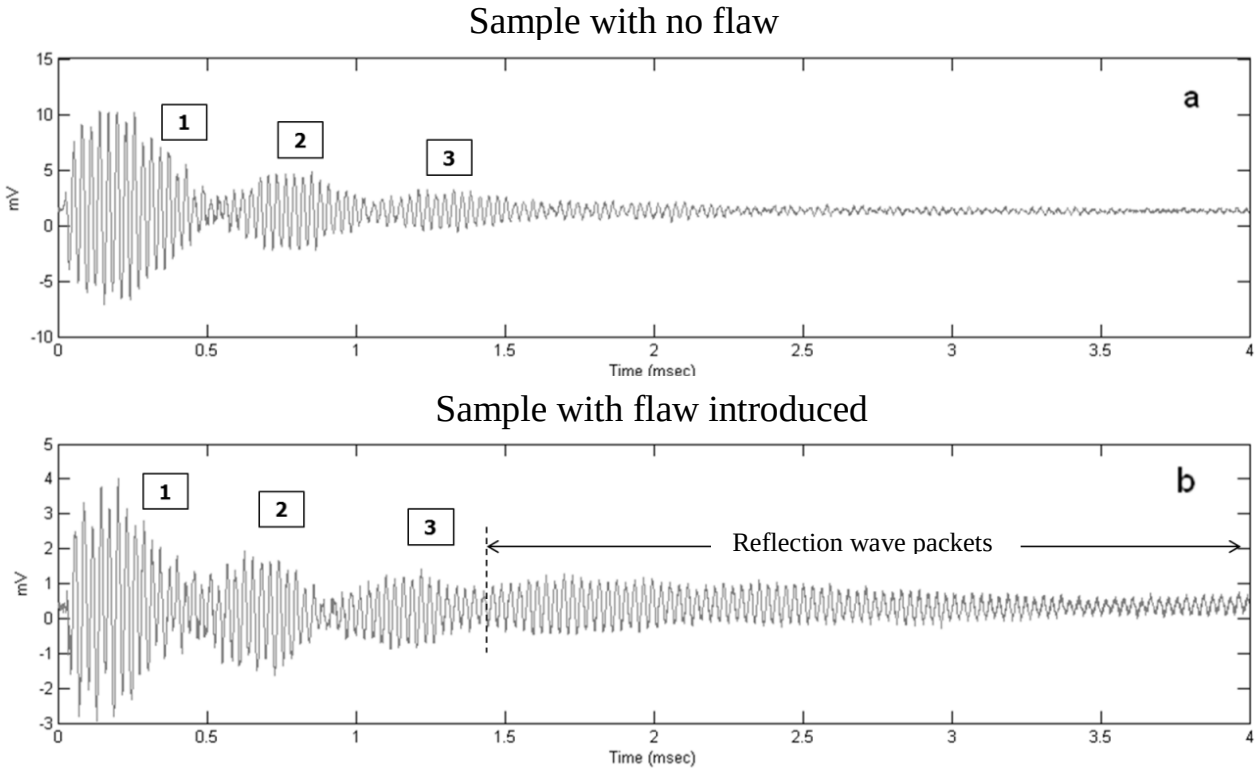

Figure 3.6 Lamb wave measurements at 51 kHz before (a) and after (b) flaw introduction in a single CFRP prepreg layer are shown for the 0° configuration.

The crack produces a reflection of the source signal, which is shown in (b). Note the change in mV scale between (a) and (b).

3.4 Discussion

The transducer that was used in the verification experiments introduced low-amplitude Lamb waves. The combination of the FBG sensors and the bond between the sensors and the prepreg layer needed higher amplitude Lamb waves. Therefore, an impact source of a weight was used to generate high-amplitude Lamb waves, and these were successfully detected by the FBG sensors. Outside the laboratory, the measurement would be easier to perform, as manually tuning an edge filter was time consuming. The bonding of the sensors to the prepreg is also important. The bond of the FBG sensor to the single layer of prepreg was insufficient to transfer the energy from the Lamb waves in the prepreg material to the sensor. A single layer prepreg configuration is also not representative of the industry situation; instead, multiple layers will be stacked. The FBG sensor would, therefore, need to be embedded between two layers of prepreg, and in this case, the bond between the sensor and the prepreg will be enhanced.

The velocity of the Lamb waves was first measured in the verification measurements with PZT sensors. It was demonstrated that Lamb waves can detect a crack in CFRP prepreg in both the 0° and 90° angles of propagation. In the verification measurements, a high variation was measured, but the use of an amplifier decreased the error in the next measurements. The amplifier increased the signal and the AIC algorithm could detect the time of arrival.

More complex layups need to be investigated. In this research, a crack was introduced in a single layer of prepreg. There must also be a better understanding of the behaviour of prepreg composite material. The material properties change over time as the material is subjected to room temperature. The next chapter investigates multiple prepreg layers and a range of typical flaws, which occur during the layup production phase listed in Table 1.1. Furthermore, the detection of a flaw is the first step. Locating and identifying the flaw is a more difficult task.

The FBG sensor measures the same Lamb wave as the PZT sensor on the same side of the prepreg layer. The FBG sensor is sensitive to the negative and the positive strains induced by the Lamb wave. The higher frequencies are detected before the lower frequencies arrive, as the theory for antisymmetrical waves describes. The results presented in this paper demonstrate that the FBG sensors can measure The PZT sensors are currently more sensitive than FBG sensors in

this research and as the goal is to demonstrate the use of Lamb waves in the layup phase, PZT sensors will be used in the following research, presented in Chapter 4.

3.5 Conclusions

This chapter presented these novel aspects

- The measurement of Lamb waves with FBG and PZT sensors in CFRP prepreg, where the Lamb waves were generated by an impactor.
- The velocity of Lamb waves in CFRP prepreg was determined for the 0° and 90° carbon fibre orientations. The velocity of the Lamb wave propagating at 0° is much higher than the velocity of the Lamb wave propagating 90° to the carbon fibres.
- Damage detection in CFRP prepreg using Lamb waves is possible by measuring the Lamb wave velocity or by monitoring the wave form. The velocity drops drastically if a crack is present between the transducer and the receiver. This effect is demonstrated in two perpendicular propagation directions. The Lamb wave is also deformed by the crack, which causes reflection of the original signal.

The initial goal was to prove that an existing NDE method of flaw detection is also applicable in the production phase of the composite material. The first Lamb waves exited in CFRP prepreg and successful detection with FBG and PZT sensors was demonstrated. FBG is currently not suitable to measure Lamb waves in CFRP prepreg, therefore PZT is used in subsequent research presented in Chapter 4.

4

Lamb waves Demonstration

Laboratory demonstration of propagation of Lamb waves in multi-layered CFRP prepreg

Adapted from: *Demonstration of novel Lamb wave detection of flaws during the layup process of composite laminate production; Miesen, N., Sinke, J., Groves, R. M. & Benedictus, R. 2012. Proceedings of the 4th International Symposium on NDT Aerospace. Hanke, R. & Boller, C. (eds.). Berlin, Germany: DGfZP, p. 1–8.*

4.1 Introduction

This chapter investigates the use of Lamb waves (see Section 2.4) in multi-layered CFRP prepreg. This research investigates the relevant material characteristics to assess the Lamb wave technique as an NDE process monitoring system in CFRP prepreg material during layup manufacturing. The propagation of Lamb waves in CFRP prepreg material was successfully demonstrated in a single prepreg layer of CFRP in Chapter 3. Accuracy and attenuation of Lamb waves in CFRP prepreg are critical factors to assess the method as an NDE technique as the attenuation indicates how far the wave will propagate and how many measurement points are needed to cover a certain area. The accuracy and reproducibility need to be investigated to determine the detectable flaw size in CFRP prepreg and the impact of environmental variables, such as temperature, must also be evaluated [114].

Section 4.2 describes the experimental design and setup. Sections 4.3 to 4.7 describe the experiments and their results. The following experiments were performed:

1) Determination of wave propagation velocities
2) Determination of wave propagation attenuation
3) Wave propagation in partially cured CFRP
4) Angular dependence of wave velocity
5) Validation of measurements using a dispersion curve model

Section 4.8 discusses the results and the chapter is concluded in Section 4.9.

4.2 Experimental Design and Setup

The experiments are designed to understand the characteristics of Lamb waves and to demonstrate the feasibility of flaw detection by Lamb waves in multilayered prepreg laminates as an in-situ NDE process monitoring technique.

The samples are $[0]_8$ or $[0]_2$ specimens, where the thickness of the specimens was chosen to have a symmetrical stack of layers and a clear difference in thickness. As a practical size for the sample, 200 mm × 200 mm × 0.16 mm per layer was used and the samples were made of DT120 unidirectional CFRP (Delta-preg),

which is representative of composites found in aerospace manufacturing [109]. Lamb waves were generated in the samples by transducers, by exciting the sample at 51, 139, 227 and 526 kHz. In Chapter 3, 51 kHz was already used and experimentally was found that above 0.5 MHz these frequencies are attenuated.

Figure 4.1 shows the experimental setup used to excite and detect Lamb waves in CFRP prepreg specimens. A single frequency block pulse generated by an Agilent 33220A function generator was amplified by an AR 75A250A RF amplifier to excite Langevin transducers (Honda Electronics) at 51, 139, 227 and 526 kHz. After propagation of the ultrasonic wave through the CFRP prepreg, the signal from the PZT sensor (Physical Acoustics Corporation PICO-HF1.2) was amplified by 6 dB using an in-house developed low-noise wide-band pre-amplifier and measured with a Picoscope 4424 at a sampling rate of 20 MHz. The ultrasonic wave coupling between the transducer and sensors and the CFRP prepreg was enhanced by using ultrasonic gel (Sonotrace). The distance between the sensors was measured and used in the group velocity calculations.

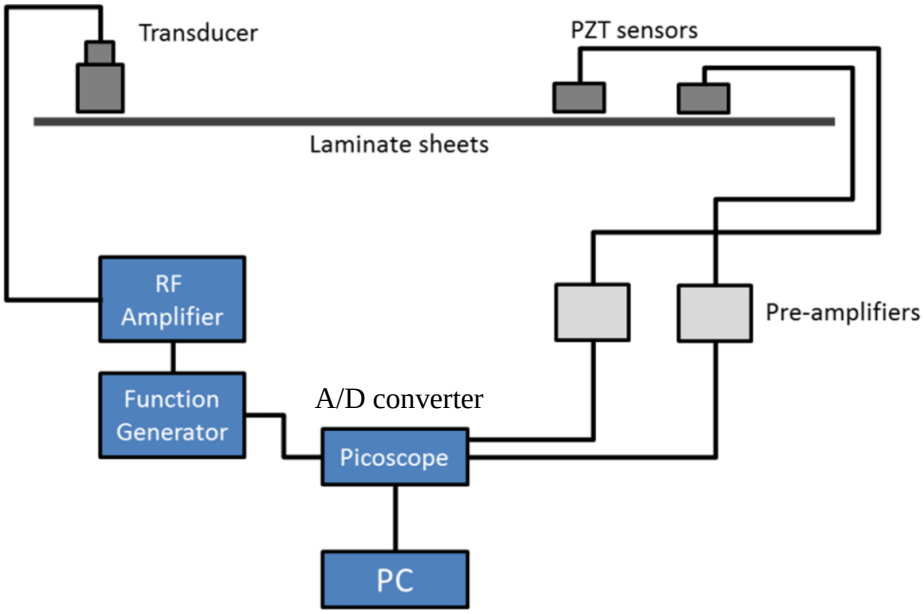

Figure 4.1 Schematic overview of the experimental setup using PZT sensors.

4.3 Determination of Wave Velocities

Group velocity measurements were performed with a $[0]_8$ specimen with four test frequencies. Reproducibility was checked through cross-correlation of the Lamb waves signals.

The Lamb waves were generated at 51, 139, 227 and 526 kHz and were successfully detected at 50 cm from the PZT actuator. The amplified signals are shown in Figure 4.2.

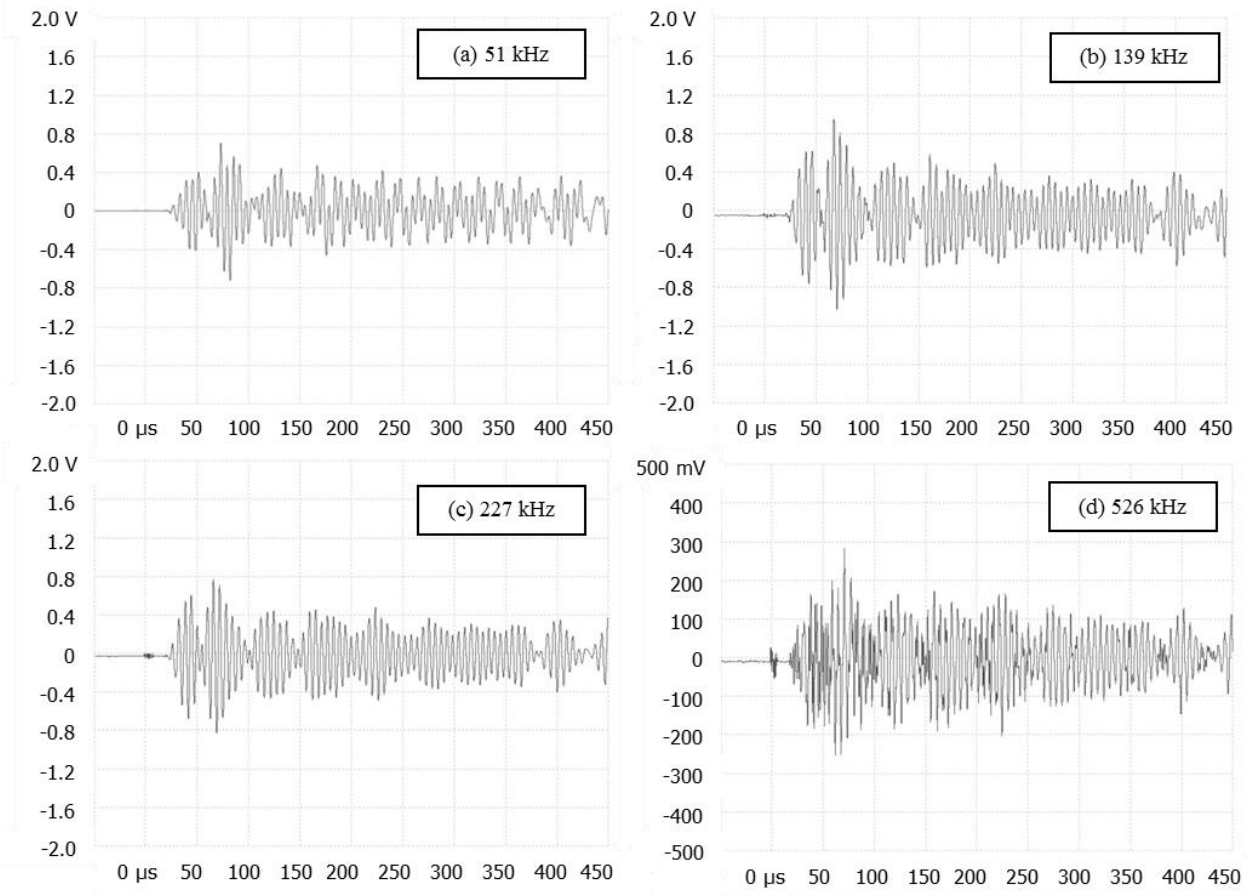

Figure 4.2 The results of the Lamb wave detection in an eight-layer prepreg specimen measured 50 mm from the transducer. Starting in the upper left, the results are shown for (a) 51, (b) 139, (c) 227 and (d) 526 kHz. In (d) there is a significantly lower amplitude measured.

The group velocity was determined by dividing the distance between the source and sensors by the difference in the manually determined time of arrival of the Lamb wave peak at each PZT sensor. The measured amplitudes of 51, 139 and 227 kHz are similar at the receiving amplitude. However, Lamb waves generated at 526 kHz showed higher attenuation (–8.5 dB), although the sensitivity of the receiving PZT sensor is higher (15 dB, shown from the PZT calibration layers) for this frequency, which results in a lower relative amplitude. It is concluded that Lamb waves generated at higher frequencies are more highly damped. Using the calibration data from the PICO-1.2, the signal from the 526 kHz source is actually –23.5 dB more attenuated compared with the lower frequencies. Table 4.1 shows

the calibrated values. In this research, an equal bonding efficiency is assumed between both PZT sensors and the CFRP.

Table 4.1 The measured amplitudes at the PZT, corrected for PZT sensor damping.

Frequency (kHz)	Correction value for sensor damping (dB)	Maximum relative amplitude at receiving PZT (V)
51	–90	0.8
139	–90	1.0
227	–90	0.8
526	–75	0.05

To test the reproducibility of the signal detection, the Lamb waves signals of both receiving PZTs were analysed. The same signal arrives at the second PZT and a high similarity is expected. The *cross-covariance* MATLAB function measures the similarity between two signals taking a shift in time into account; results are shown in Figure 4.3. Using a similar approach, the signals of the first PZT sensors of two different specimens are also checked for their correlation (see Figure 4.4). A coefficient indicates the correlation between the signals, where a coefficient of 1 means exactly the same signal [115]. Signals with a correlation between 0.8 and 0.6 are considered to have a moderate correlation and below 0.6 a poor correlation.

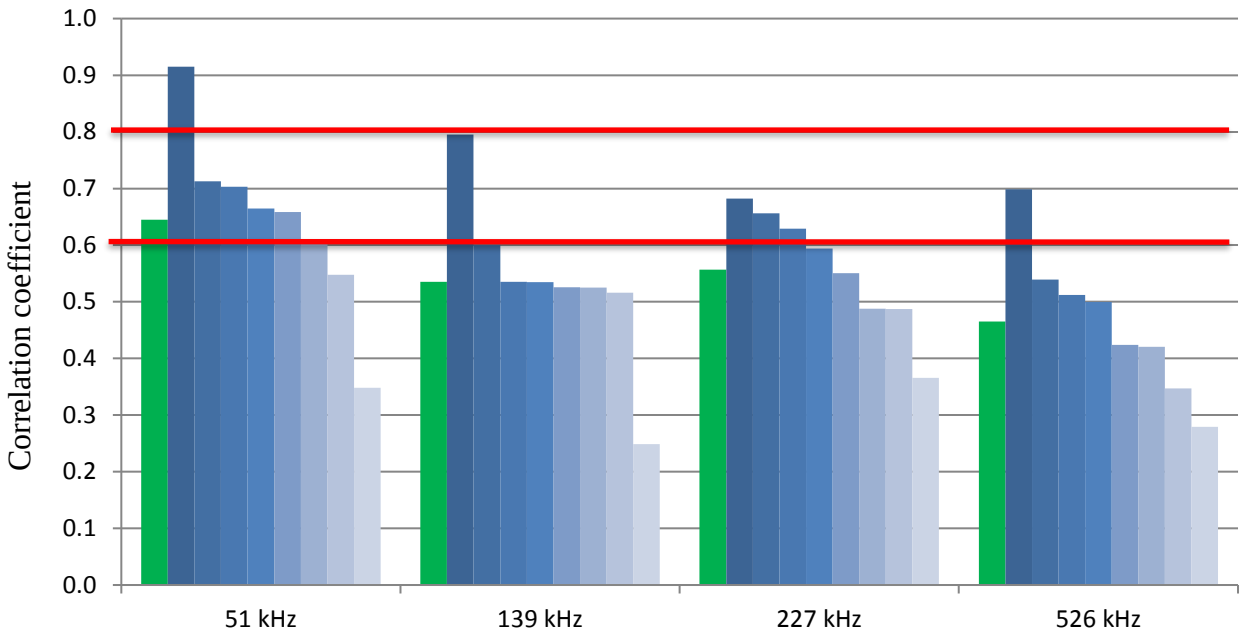

Figure 4.3 The graph shows the correlation coefficients between two measured Lamb waves on the same specimen per frequency from high to low. The green bar shows the average of eight measurements per frequency.

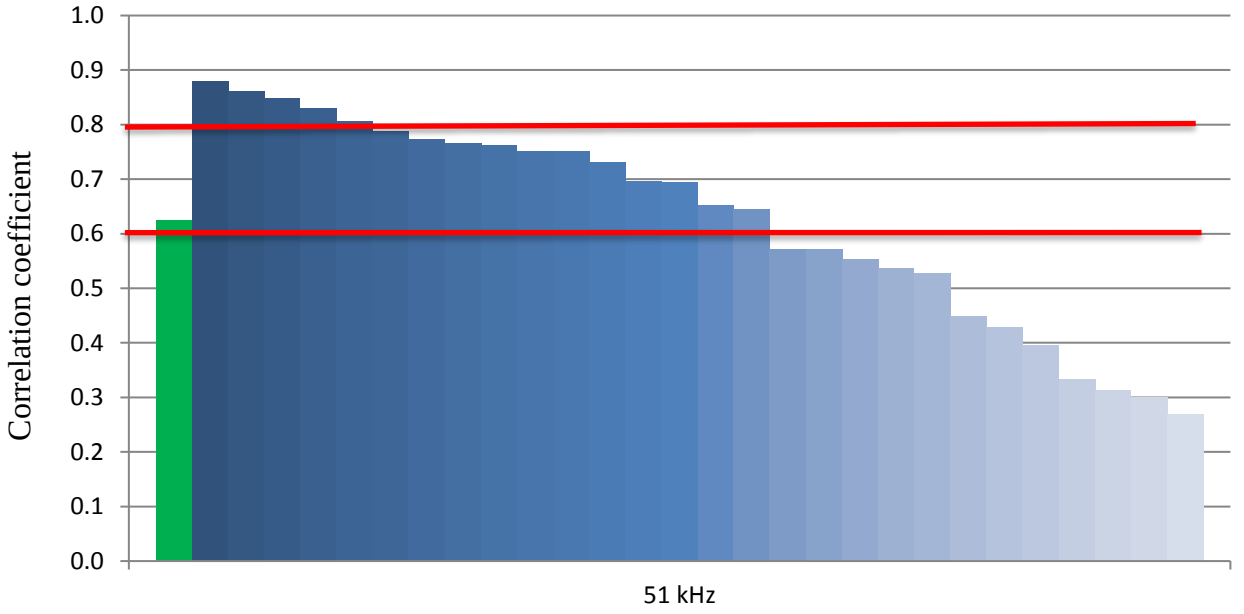

Figure 4.4 The graph shows the correlation coefficients from high to low for 51 kHz. The green bar shows the average of 28 correlation measurements.

4.3.a Determination of Wave Attenuation

Attenuation measurements were performed to determine the attenuation coefficient in CFRP prepreg material. This was calculated through the decay of the amplitude over a measured distance in the CFRP prepreg material. Attenuation measurements were used to calculate attenuation coefficients in CFRP prepreg to estimate the maximum distance of propagation of Lamb waves. The attenuation of Lamb waves was described by Su et al. [116] using natural logarithms and can be expressed as:

$$\mathrm{I}_d = I_0 e^{-\alpha d} \quad or \quad \alpha = \frac{1}{d} \ln\left(\frac{\mathrm{I}_d}{\mathrm{I}_0}\right), \tag{3.1}$$

with propagation distance d, source amplitude I_0, attenuated amplitude at distance I_d and attenuation coefficient α. Geometric damping is ignored as a similar setup is used.The Lamb wave is assumed to be attenuated to 10% of its original signal (I_0) at the attenuation length, d_{decay}, according to:

$$\mathrm{d}_{decay} = \frac{1}{\alpha} \ln\left(0.1\right) \tag{3.2}$$

Attenuation coefficients were calculated using equations (3.1) and (3.2) and are presented in

Table 4.2 for 51 kHz for three different propagation angles. The decay of the Lamb wave amplitudes was measured over distances of 3, 5 and 10 cm. d_{decay} is frequency dependent [117], and the attenuation for the other test frequencies was too high to provide representative values. Attenuation coefficients and distances until decay to 10% of typical cured CFRP samples can be found in Su et al. [116]. Attenuation coefficients in cured CFRP materials for Lamb waves are typically lower, for example 0.0014 mm^{-1} in an eight-ply CFRP sample at 250 kHz.

Table 4.2 This table presents the attenuation coefficients for the S_0-mode Lamb waves in unidirectional CFRP prepreg at 51 kHz with different propagation angles with respect to the carbon fibre orientation.

	Attenuation Coefficient α for 51 kHz (mm^{-1})	**Calculated distance until decay to 10%, d_{decay} (mm)**
0°	0.01	215
45°	0.12	18
90°	>0.25	<10

4.3.b Wave Propagation in Partially Cured CFRP

Other potential variables affecting the propagation of Lamb waves, such as environmental temperature, are investigated for the $[0]_2$ specimens in the similar setup described in the previous sections. The direct environment of the CFRP prepreg laminate is altered to stimulate the self-curing of the resin. Situations with blowing air at room temperature, blowing heated air at 60 °C and self-curing at room temperature were all tested for 240 minutes, with samples measured every 15 minutes.

To assess the Lamb wave technique as a practical NDE technique during manufacturing, environmental effects on the measurements and flaw detections were also investigated.

Table 4.3 presents the variation of group velocity and attenuation measurements caused by environmental effects.

Table 4.3 Environmental effects on group velocity and attenuation of A_0 Lamb waves in CFRP prepreg measured along the carbon fibres (0°).

	Group velocity (m/s)	**Standard deviation (m/s)**	**Attenuation (mm^{-1})**	**Standard deviation (mm^{-1})**
Self-curing at room temperature	2427	16	0.088	0.002
Air at room temperature	2278	38	0.072	0.015
Heated air at 60 °C	2109	8	0.101	0.002

4.3.c Angular Dependence of Wave Velocity

Lamb wave propagation at angles of 0, 30, 60 and 90 degrees relative to the carbon fibre orientation group velocity measurements were used to investigate the angular dependence of the group velocity on the fibre direction in a $[0]_2$ specimen.

Incorrect fibre orientation (i.e. placement of CFRP layer orientation) is related to the material distribution and can affect the propagation of Lamb waves in unidirectional CFRP. To investigate this, group velocity measurements of Lamb waves at 51 kHz were performed on a 20 cm × 20 cm $[0]_2$ specimen (10 measurements per angle) and the results are shown in Figure 4.5.

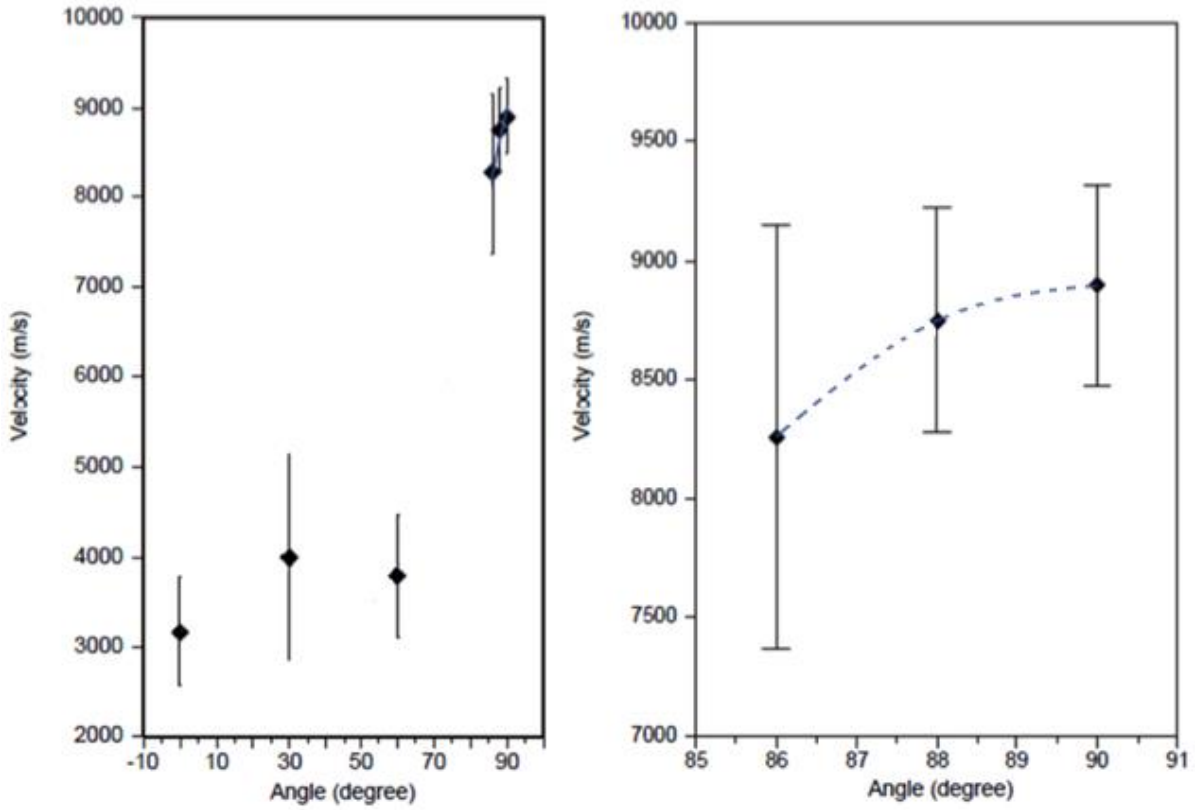

Figure 4.5 Angle dependence of group velocity measurements in CFRP prepreg using a polynomial fit. The 90 degree orientation is perpendicular to the carbon fibre orientation in the specimen. The error bars indicate one standard deviation from the mean.

The average standard deviation for measurements at 86, 88 and 90 degrees is 595 m/s, which provides insufficient accuracy to distinguish a misalignment.

4.3.d Validation of Measurements using a Dispersion Curve Model

Determining Young's modulus and the Poisson ratio experimentally is difficult as the standard approaches use strain and stress to determine these mechanical properties [118, 119]. However, CFRP prepreg is soft and will deform under mechanical stress. In this research a propagation direction along the unidirectional carbon fibres is assumed. Therefor the dispersion model of Barroso-Romero et al. [120] for Lamb waves in an isotropic material was used to obtain Young's modulus and the Poisson ratio. This model is based on solving equations (2.1) and (2.2), as described in detail by Kessler et al. [121]. Group velocity measurements were compared with modelled data to confirm measurements and assumptions.

Iteratively the parameters in the model were adjusted to match the experimental results, estimates of Young's modulus and the Poisson ratio were made. The carbon fibres are the only continuous medium in the CFRP and the resin has low stiffness and is assumed not to transfer the Lamb waves sufficiently.

The measured velocities of the Lamb waves were plotted together with the modelled dispersion curve, using a Young's modulus of 100 GPa and Poisson ratios between 0.1 and 0.3. Young's modulus was iteratively determined at 100 GPa and a Poisson ratio between 0.1 and 0.3 fits the experimental data. The dispersion curves shown in Figure 4.6 were calculated for a $[0]_8$ specimen and for frequency–thickness (*fd*) product values below 1500 kHz mm. Research presented in the previous chapter demonstrated higher attenuations at higher frequencies in CFRP prepreg. Only at an fd above 3 MHz mm is the difference of the Poisson ratio seen in the model, where a higher Poisson ratio causes lower velocities.

The average standard deviation of the group velocity measurements in combination with the dispersion curve were used to estimate the minimum detectable flaw size in CFRP prepreg. The average standard deviation was determined in three separate specimens and 160 m/s corresponds to approximately 0.32 mm in thickness according to the dispersion curve model at 51 kHz for A_0 modes and where an isotropic distribution along the carbon fibre was assumed. Modes were distinguished based on their group velocity and measurements of A_0 modes at 227 and 526 kHz were unusable. Reproducibility was poor from specimen to specimen with the average standard deviation ranging between 7 to 37 m/s. If an SNR of 3 is assumed for reliable flaw detection, flaws within a change in thickness of 0.96 mm or larger could be distinguished. This accuracy proves to be insufficient to detect typical production flaws in CFRP layup manufacturing, as prepreg layers are 160 µm thick and other flaws are even smaller in thickness.

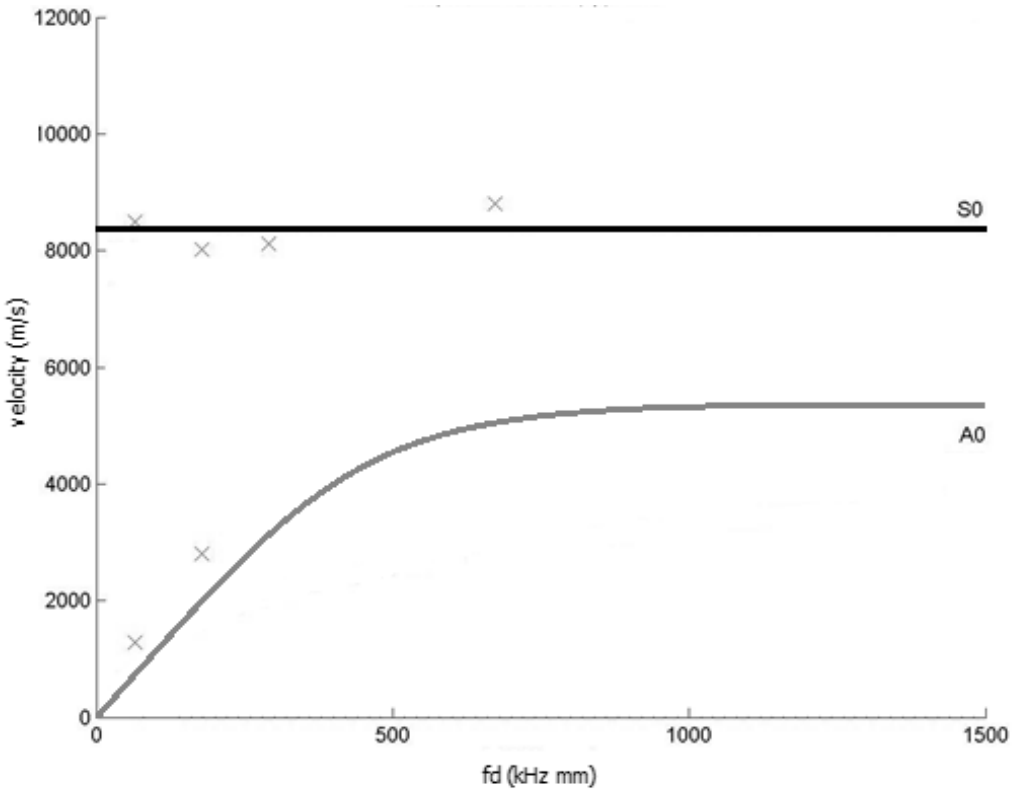

Figure 4.6 Dispersion curve in CFRP prepreg calculated using the model described in [120] and experimental group velocity measurements (X). The model was fitted iteratively to fit the experimental data.

4.4. Discussion

Lamb waves propagate through CFRP prepreg material with minimum attenuation at frequencies between 51 and 227 kHz. Measurements show poor reproducibility and accuracy as shown in Figures 4.3 and 4.4. This complicates the use of Lamb waves in CFRP prepreg. The measurements show an average standard deviation of 160 m/s, which corresponds to approximately 0.32 mm material thickness at 51 kHz for A_0 modes. Higher frequencies are more difficult to measure and have a smaller gradient in the dispersion curve for A_0 modes, which would introduce higher inaccuracies.

High attenuation causes limited area coverage for Lamb waves to propagate through CFRP prepreg. The propagation distance of Lamb waves along the carbon fibre is 215 mm. The signal perpendicular to the carbon fibre propagates less than 10 mm, which agrees with the assumption that Lamb waves propagate along the carbon fibre as experimental data fits the isotropic dispersion model for propagation along the carbon fibres and these values correspond to typical values of carbon fibres [122], so it can be assumed that the Lamb waves propagate

through the carbon fibres themselves. Lamb wave signal analysis shows moderate to poor correlation of the signal in a specimen or between specimens and demonstrates the poor reproducibility. This makes the use of the Lamb wave technique impractical in a manufacturing situation as the coverage of the Lamb wave is only 430 mm by 20 mm (with a centrally placed transducer) in unidirectional CFRP. This means that for each square metre of CFRP material at least 117 measurements would be needed to cover the complete area. If this needs to be done for every layer, the impact on the production time would unacceptable.

An alternative solution could be to embed a large number of transducers and sensors in the mould or layup table, but further research would be needed to study this approach. As attenuation is high in CFRP prepreg, the transfer of the signal between a mould and the specimen is expected to be difficult. The coverage in cross-ply CFRP is expected to be more complex; however, a slightly larger coverage area is expected as the signal will follow both fibre directions.

Table 4.3 showed the impact of several environmental effects on group velocity measurements and attenuation of, which cause self-curing, such as temperature or assisted curing by air. These effects contribute to a larger variation in the accuracy of the measured signals.

The fibre orientation was successfully measured and a significant difference was demonstrated between measurements parallel and perpendicular to the carbon fibres. The accuracy to distinguish the orientation of the fibres is poor, but a misalignment in the order of 10 degrees for 90 degrees orientation can be detected. The determination of fibre orientation and the determination of the degree of self-curing (i.e. time out of the freezer) for CFRP prepreg is a promising concept.

4.5 Conclusion

The propagation of Lamb waves in the CFRP prepreg material was successfully demonstrated with PZT sensors. The mechanical properties of 100 GPa for Young's modulus and a Poisson ratio between 0.1 and 0.3 were estimated by fitting the experimental data to an existing dispersion curve model. The current accuracy of the technique is sufficient to detect 0.32 mm height difference, which is larger than typical flaws found in a manufacturing environment. High attenuation in this type of material causes poor distance coverage and limits the technique to 430 mm parallel and 20 mm perpendicular to the carbon fibres. Measurements in CFRP prepreg material are also influenced by environmental effects, which causes lower accuracy measurements. The results of Lamb wave

measurements in CFRP prepreg show poor reproducibility, poor accuracy and high attenuation due to the material properties of CFRP prepreg. Therefore, the technique is unsuitable to be used as an NDE process monitoring system in CFRP prepreg.

5

Laser displacement sensing

Adapted from: *Laser displacement sensor to monitor the layup process of composite laminate production; Miesen, N., Sinke, J., Groves, R. M. & Benedictus, R. 2013. Proceedings of SPIE 8692. s.n. (ed.). San Diego, CA: SPIE, p. 1–8 (Proceedings of SPIE–International Society for Optical Engineering; vol. 8692)*

and from: *Simulation and detection of flaws in pre-cured CFRP using laser displacement sensing; Miesen, N., Sinke, J., Groves, R. M. & Benedictus, R. 2016. In: International Journal of Advanced Manufacturing Technology. p. 1–9*

5.1 Introduction

Optical techniques are non-contact and familiar techniques in a production environment for measurements in industrial applications [123]. The laser displacement sensor (LDS) is widely used to measure the geometrical dimensions of test specimens. In this technique point or line laser light is projected onto the object and the reflected or scattered signal is processed. LDS has been demonstrated a wide range of applications in industry [38, 124-127], including robotics, autonomous vehicles and anti-collision and proximity sensors. The sensors are also used in industrial manufacturing to monitor the quality in automatic line production, such as a visual inspection sensor system for the automation of laser welding processes in heavy industries. In the aerospace industry, LDS is used for precise measurements of surface flaws and for contour measurements during manufacturing [128]. The objectives of this chapter are to demonstrate the performance of LDS for the detection of typical flaws in the CFRP prepreg layup and to evaluate if LDS is suitable for use as an in-situ NDE technique to detect these typical production flaws in CFRP prepreg.

Section 5.2 describes the working principle of the laser displacement technique and describes the simulated CFRP specimens used in the experiments. Section 5.3 describes the experiments and setups of the proposed research. The results are presented in Section 5.4 and are discussed in Section 5.5. Section 5.6 concludes the research and assesses the suitability of LDS as an in-situ monitoring system for CFRP production.

5.2 Laser Displacement Sensors

LDS with triangulation sensors is based on calibrated detection sensors with a reference laser source, see Figure 5.1 [38, 129] and the theory is described in Section 2.5. The basic principle is to project and receive a laser signal from an

object to determine its distance from the sensor. The setup of the measurement system will make sure that the photodetector is in focus relative to the receiver lens, where the size of the photodetector determines the operating range. The operating range is defined as the minimum and maximum distances to the object from the laser source, as shown in Figure 5.1. Determination of the centre of the received signal on the photodetector is aided by algorithms to minimize the amplitude and position uncertainty due to scattering. Although several algorithms are available, the 'Centre of Mass' algorithm shows the best results [130]. As the size and location of the detector are fixed relative to the laser source, the laser displacement system is calibrated for a certain operating range, which is limited by the size and accuracy of the detection sensor. A limiting factor for size detection is the spot diameter of the laser, beyond which a smaller feature than the laser diameter cannot be resolved.

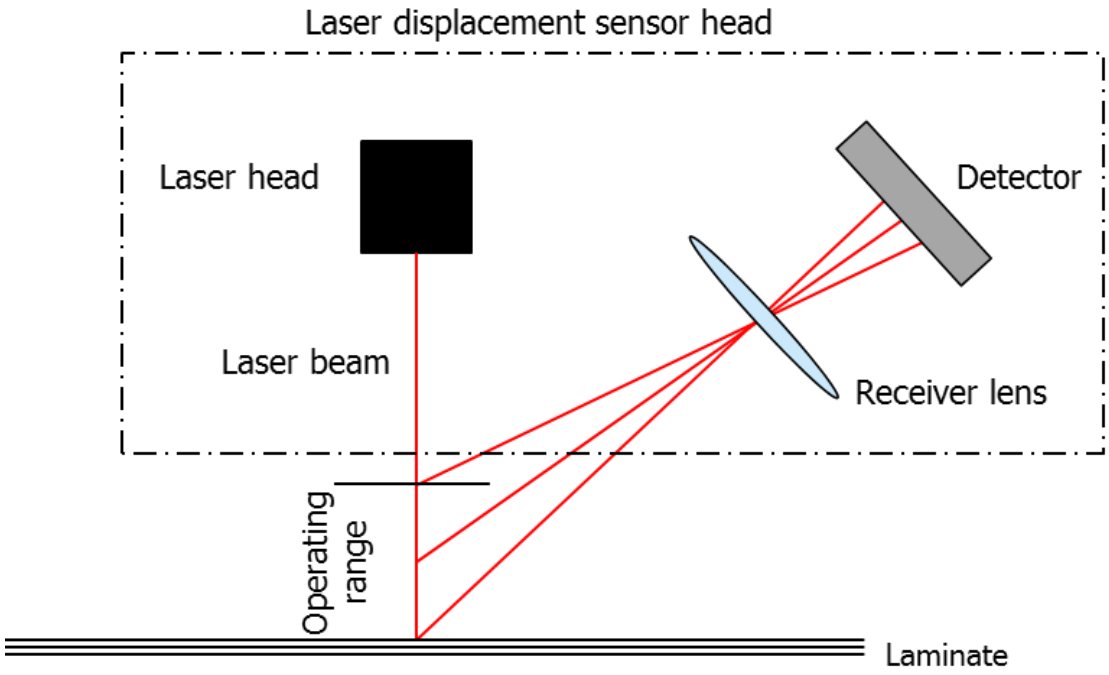

Figure 5.1 A laser head projects laser light onto an object within the operating range and scattered or reflected light is received by a detector to determine the distance from the laser head with triangulation.

This section describes a simulation of the layup and LDS measurements of CFRP prepreg specimens to determine the needed measurement accuracy of the measurement system. During the layup process, each layer of CFRP is stacked according to the design specifications by an automated tape or hand layup. As

every layup process has variance in conditions like the thickness of the layer, Monte-Carlo simulations take this variability into account. These Monte-Carlo simulations take the layup process, material aspects (only those directly affecting measurements), additional measurement errors and production flaws into account. To determine the required accuracy of the measurement system for static measurements, several simulated models were created in MATLAB. As reference material unidirectional carbon fibre layers from DeltaTech DT160 were used, which have a typical thickness of 160 µm (±5 µm) [109]. An additional measurement error expected, according to Schmitt et al. [40], is the scattering of the laser beam between carbon fibres. In the simulated specimens, a maximum scattered path of two times the carbon fibre radius was assumed (0–5 µm). Figure 5.2 shows the different possible light paths, which cause an additional maximum error to the measurement of 5 µm. Note, the fibres will not be distributed as orderly as shown in the schematic graph in a real specimen.

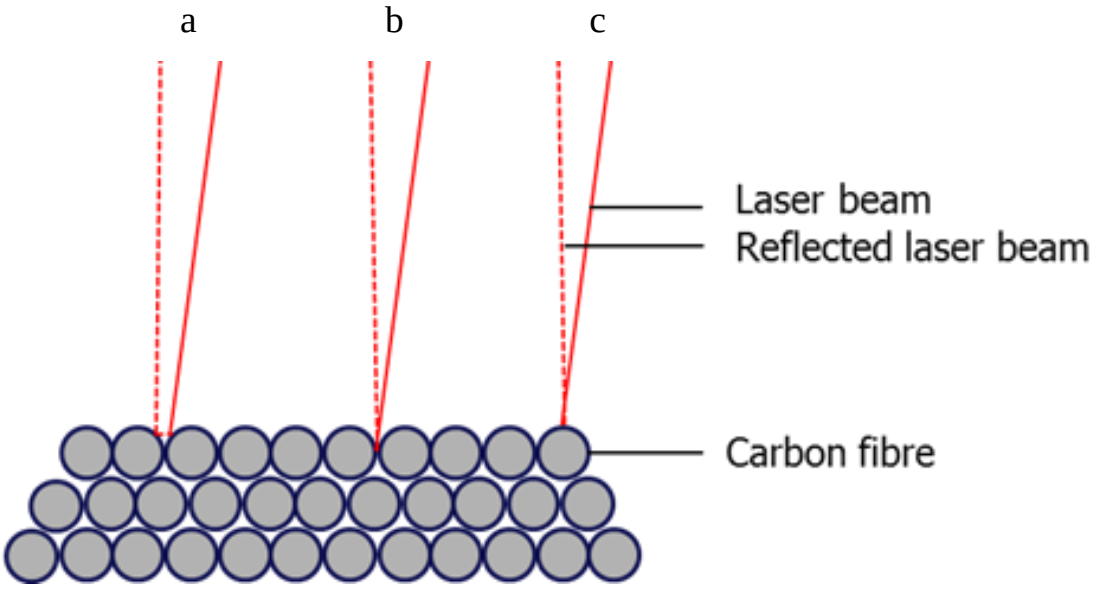

Figure 5.2 Schematic overview of potential measurement errors: (a) multiple-path reflection returning to the laser head, (b) a measurement between two carbon fibres and (c) a reflection from the top of a carbon fibre.

Each layer in the simulated specimen was represented as a matrix A_{nm} and for each layer of CFRP, an error matrix e_{nm} was added to account for the measurement and scatter errors (see matrix 5.1). A total random error of between –5 µm and +10 µm (thickness uncertainty + radius of carbon fibre) was applied perpendicular (*X*-axis) to the carbon fibre axis. In the parallel direction (*Y*-axis) of the carbon fibre, no variations were simulated.

$$\begin{pmatrix} A_{11} & A_{21} & \cdots & A_{n1} \\ A_{12} & A_{22} & \cdots & A_{n2} \\ \vdots & \vdots & \ddots & \vdots \\ A_{1m} & .. & .. & A_{nm} \end{pmatrix} + \begin{pmatrix} e_{11} & e_{21} & \cdots & e_{n1} \\ e_{12} & e_{22} & \cdots & e_{n2} \\ \vdots & \vdots & \ddots & \vdots \\ e_{1m} & .. & .. & e_{nm} \end{pmatrix} \quad (5.1)$$

A practical size of the specimens was chosen as 50 × 150 mm^2 with a resolution of 20 µm in the *X*- and *Y*-axes. As the height of the simulated specimens is critical to measure flaws, the *Z*-axis has a resolution of 1 µm.

Figure 5.3 shows a $[0]_8$ specimen without any production flaws and an average height in the top layer of 1.28 mm. Each layer overlaps by 10 mm to show different layers.

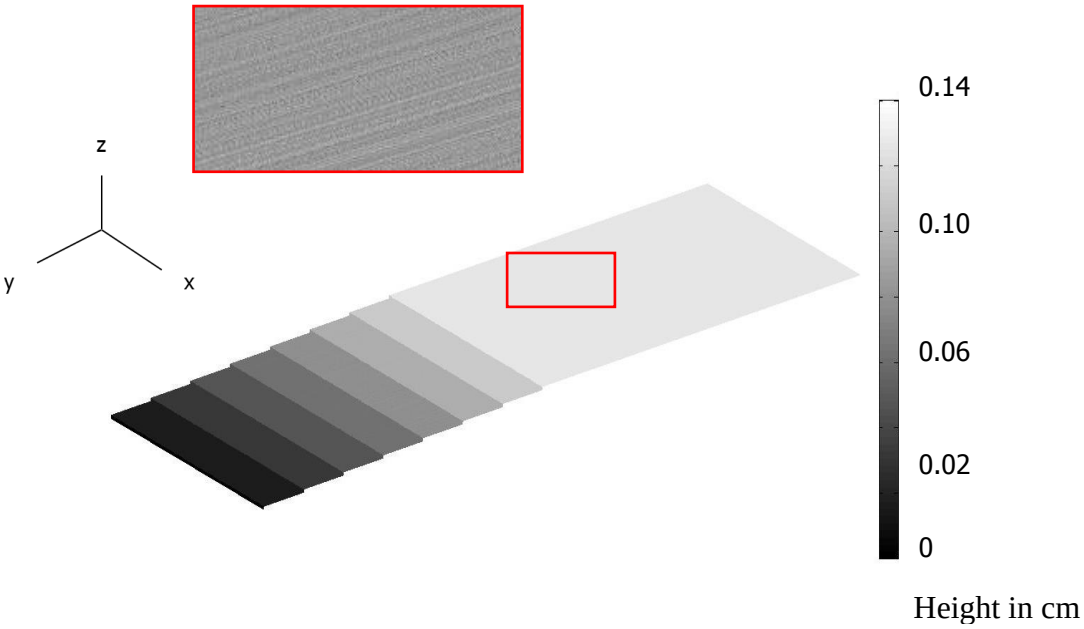

Figure 5.3 $[0]_8$ specimen without any production flaws and an average maximum height of approximately 1.28 mm modelled in MATLAB. In the enlarged red figure, the orientation of the carbon fibres is clearly visible.

Typical production flaws were described in Table 1.1 and the layup flaws are simulated in the following specimens. Figure 5.4 shows a specimen including three typical production flaws: a 50 µm thick foil of 1 × 1 cm^2 embedded underneath the top layer (a), the fourth layer is missing (b) and the first layer with carbon fibres perpendicular to the *X*-axis (c).

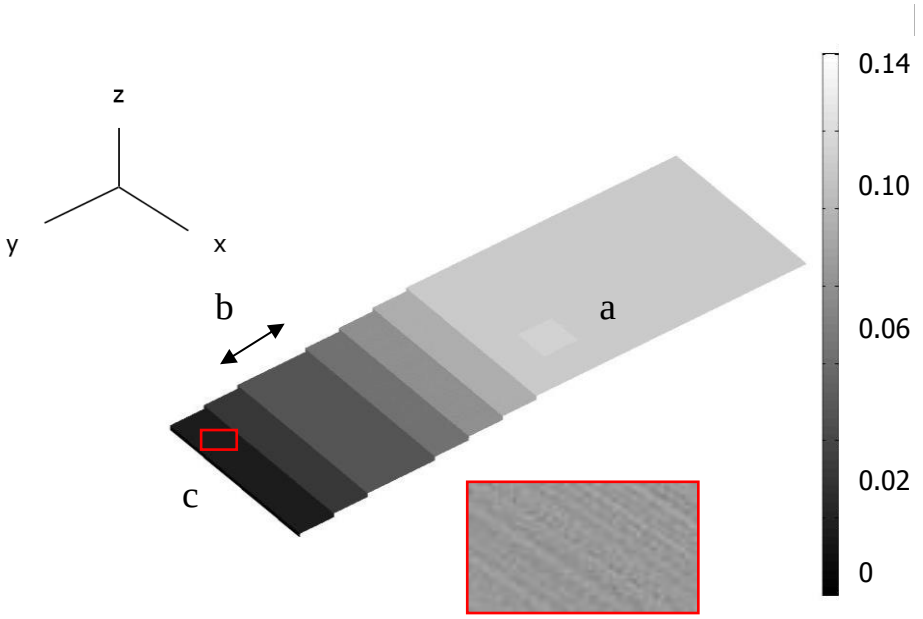

Figure 5.4 $[0]_7$ specimen including typical production flaws of an embedded 50 µm thick foil of 1 cm × 1 cm modelled in MATLAB (a), layer missing (b) and fibres perpendicular to the X-axis (c). In the enlarged region with red border, the orientation of the carbon fibres is clearly visible.

Figure 5.5 shows a specimen with two additional typical flaws: in the top layer, wrinkling is simulated (d) as a simplified stepwise accumulation of the CFRP material simulated of 160 µm in height. This effect causes a strip of missing material at the edges, which will give an incorrect overlap (e).

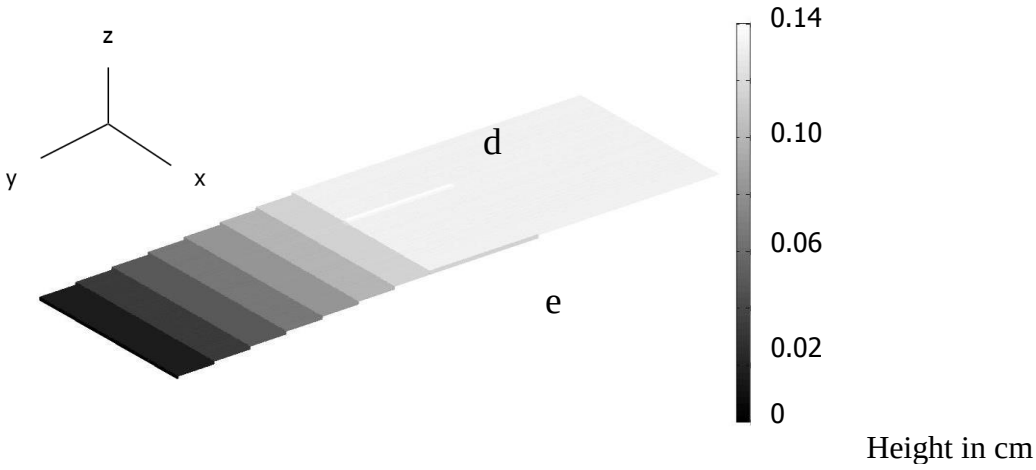

Figure 5.5 [0]8 specimen modelled in MATLAB including a typical production flaw of wrinkling (d) which causes an incorrect overlap at the edge (e).

The models only describe the unidirectional samples in static measurements, in the following experiments the model will be compared with experiments under static conditions.

5.3 Experimental Design

This section describes the experimental setup used to compare the LDS measurement with the simulations. To demonstrate the use of the technique in the production process, several CFRP specimens were manufactured, measured and analysed. The specimens consisted of different types of commonly used materials in CFRP production, unidirectional (160 µm thick) and cross-ply (260 µm thick) CFRP from DeltaTech. The specimens were 150 mm in length and 50 mm in width. The following specimens were prepared for laboratory testing to assess the detectability of the production flaws with LDS:

A. Unidirectional $[0]_8$ sample without flaws
B. Unidirectional $[0]_7$ sample with a missing layer and a piece of enclosed foil of 1 cm^2 and 50 µm in height
C. Unidirectional $[0]_8$ sample with a wrinkle included in the top layer
D. Bidirectional $[45/-45]_7$ sample with a missing layer and enclosed foil of 1 cm^2

During the laboratory tests, the specimens were measured in absolute height to test the LDS technique on typical CFRP materials and typical production flaws.

The laser sensors were chosen based on the results of the simulations and the specifications of the Keyence LJ-V7000 series to detect these typical flaws in production [131]. The specifications of the laser heads are described in Table 5.1 Either the Keyence LJ-V7200 or LJ-V7060 was used in the setup as shown in Figure 5.6. Both types were used to test the needed resolution of the sensor.

Table 5.1 Specifications of Keyence laser heads [131].

		LJ-V7200	**LJ-V7060**
Reference distance		200 mm	60 mm
Measurement range	*Z*-axis	96 mm	16 mm
	X-axis	62 mm	15 mm
Repeatability	*Z*-axis	1 µm	0.4 µm
	X-axis	20 µm	5 µm
Light source output (at 405 nm)		4.8 mW	10 mW
Spot shape and size at reference distance		21 mm × 45 µm	90 mm × 85 µm
Sampling cycle		16 µs (high-speed mode)	

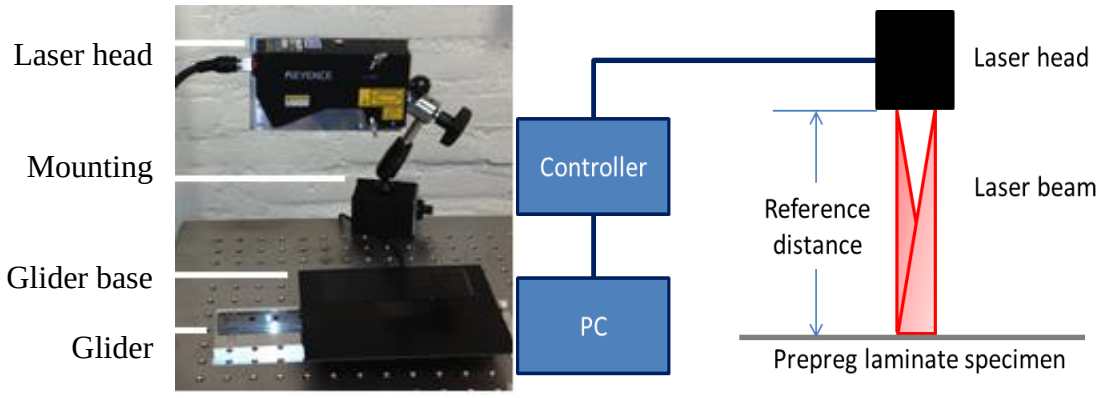

Figure 5.6 Actual (a) and schematic (b) overview of the experimental setup using the laser displacement sensor.

To construct a 3-D image, a horizontal laser line was used instead of a spot. The laser line was projected on the object via a cylindrical lens and can reconstruct a 2-D measurement profile. The sensor head was placed above the test specimen at the reference distance. The specimen was moved manually on a calibrated glider (9.5 mm in height), where the laser measurement is calibrated to trigger every 100 µm on the glider. The measurements of the laser head were registered via a controller, which is connected to a PC.

Analysis of the errors introduced during measurements indicated which factors need attention during the industrialization of the technique [132]. Besides the scattering (0–5 µm) due to the material characteristics and thickness variation (±5 µm), which are included in the simulation, other contributing errors are expected in an industrial environment. According to the manufacturer's specifications, the error introduced by the LDS will be the combined error from the sensor and the algorithm. The specified error is ±0.4 µm or ±1 µm in the *Z*-axis, respectively for LJ-V7060 and LJ-V7200. Absorption can be another error, but this will only have an influence on the intensity and detectability of the reflected signal and has no influence on the distance measurements. The last source of error will be external influences in an industrial environment, such as vibrations. To assess the influence and the allowable limit of vibrations in the measurement system, an experimental setup was used to simulate the dynamic tape laying process. Figure 5.7 shows the setup designed to simulate dynamic measurements with the laser displacement sensor. The laser head (LJ-V7060) was fixed above the specimen. While each layer was pressed on the specimen by a 1.6 kg roller, the laminate specimen was moved through the laser beam for consecutive measurements. The measurements

started from the origin of the specimen and each layer was measured and registered in relative height to the last layer. The speed of the LJ-V7060 is theoretically 100 µm per 16 µs or 6.25 m per minute.

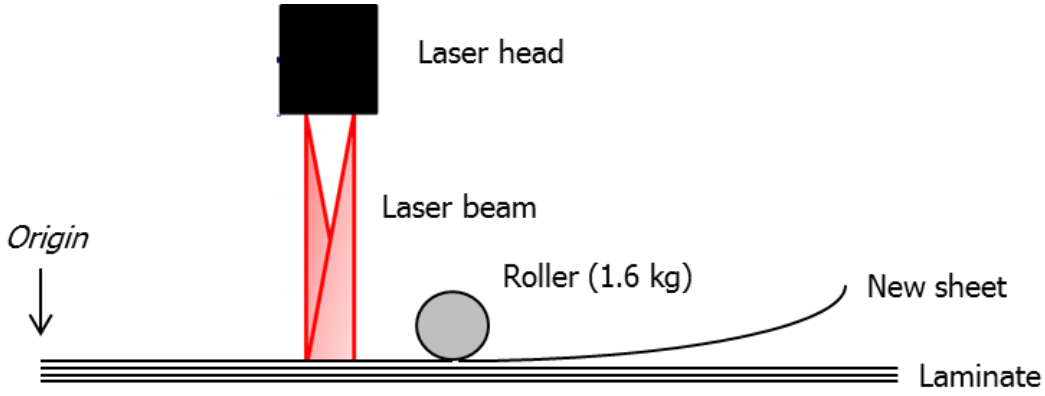

Figure 5.7 Experimental setup for the dynamic measurements.

5.4 Results

This section will discuss the results from the static and dynamic measurements.

5.4.a Static Measurements

In specimen A; eight layers of the laminate were measured by LDS. The results are shown in Figure 5.8 (a) and a cross-section is shown in Figure 5.9 (a). The specimen had a nominal height of 1.2 mm at the top layer and a size of 150 × 50 mm^2. The measured standard deviation was 15 µm for LJ-V7200 and 9 µm for LJ-V7060 for a 160 µm layer, which gives an SNR of 10.7 and 17.8 respectively. The SNR is calculated as the mean divided by the standard deviation of the measurements.

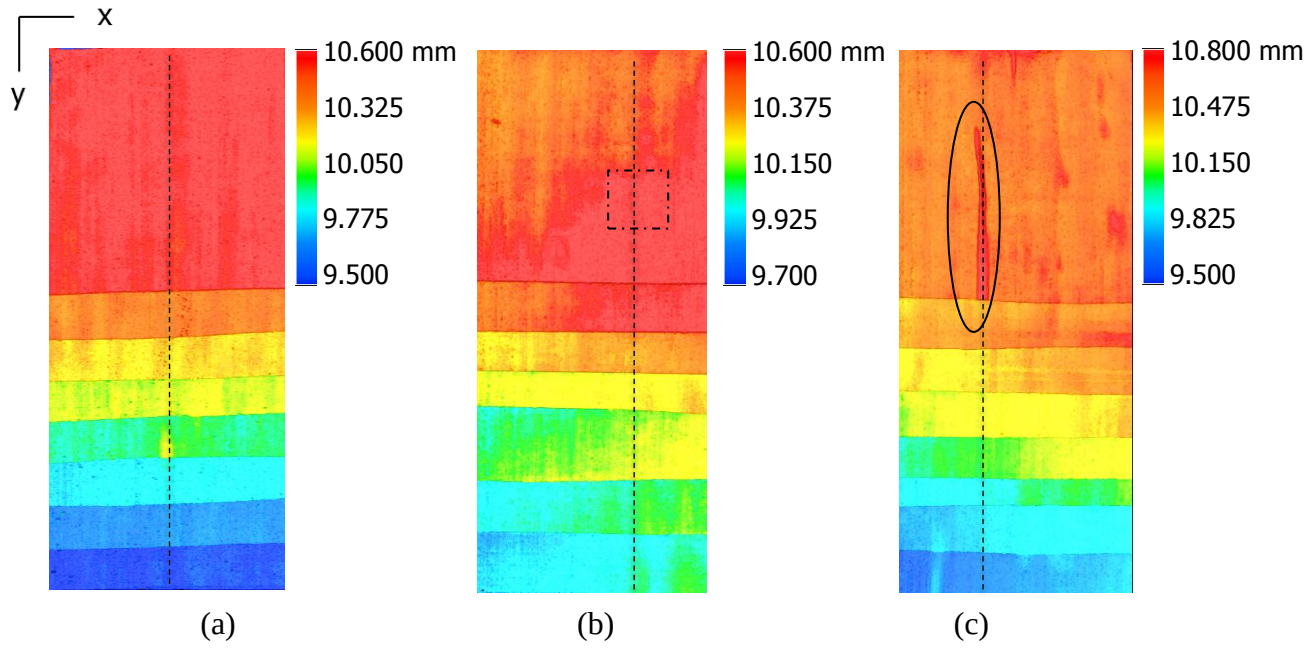

Figure 5.8 (a) Measurement of flawless $[0]_8$ specimen A. (b) and (c) measurements of embedded flaws in specimens B and C. The vertical dotted shows the cross section presented in Figure 5.9.

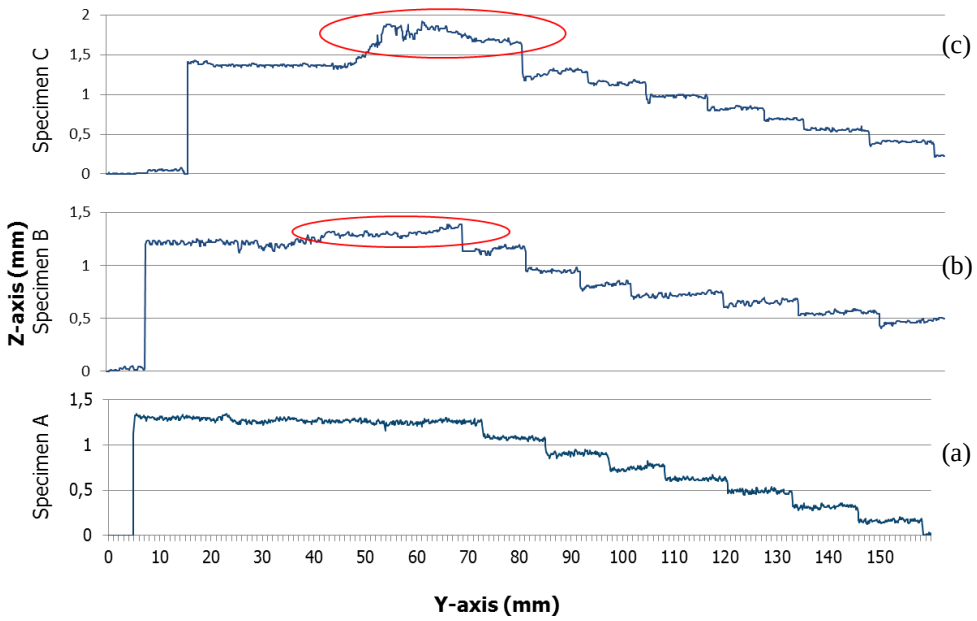

Figure 5.9 Cross sections (a), (b) and (c) of measurements with LJ-V7200 of specimens A, B and C, respectively. The red circles indicate the included foil and the wrinkle.

Specimens B and C include flaws and are measured to demonstrate the detectability of embedded flaws. The results are shown in Figure 5.8 (b) and (c),

respectively, and the cross sections in Figure 5.9 (b) and (c). In specimen B, enclosed foil of 1 cm^2 of 50 µm in height was included beneath the top layer, which is indicated with a dotted square in Figure 5.8 (b). The enclosed foil causes a larger delamination towards the lower right edge of the layer and is clearly detected. The fourth layer is missing in specimen B and results in a lower total height of the specimen of 1.0 mm and a clear deviation from the design specification. The incorrect fibre orientation in the first layer cannot be reliably detected, as the fibre radius is below the standard deviation of the measurement system. In specimen C, a wrinkle was introduced in the top layer and causes a maximum height of 1.8 mm in the top layer.

Figure 5.10 shows the actual surface of a layer of CFRP as imaged by an electron microscope.

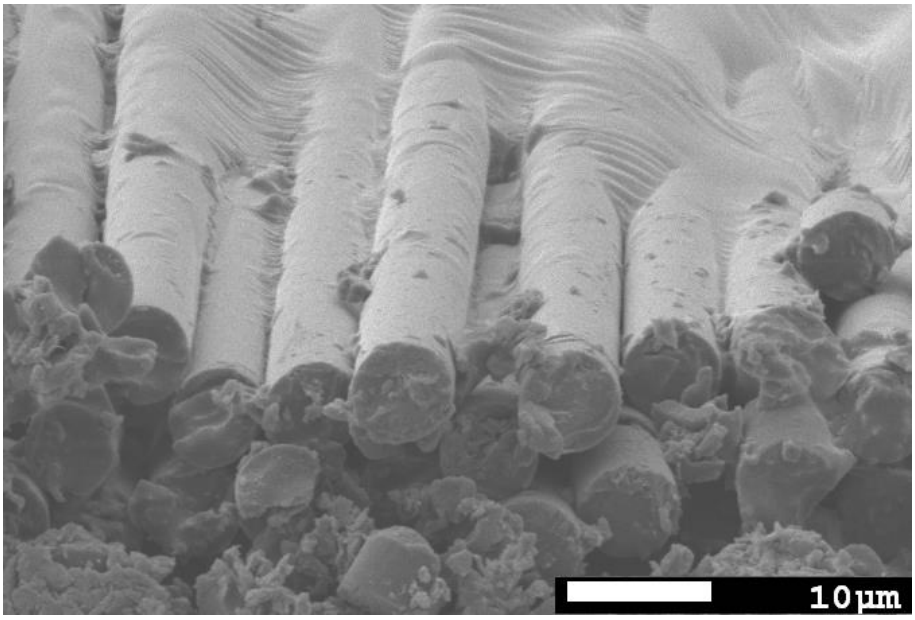

Figure 5.10 shows the actual surface of a layer of CFRP prepreg. The measurement was made by an electron microscope (Jeol, JSM-840A at the Delft University of Technology).

Table 5.2 and Figure 5.11 show the results of the measurements on specimen D, a bidirectional CFRP laminate of 260 µm thick layers. An enclosed piece of foil is included in the top layer and layer 6 is missing.

Table 5.2 shows the average absolute and relative values of the measurements on specimen D, including the flaw. Each layer is clearly distinguished and the flaw

in the top layer is successfully detected. Figure 5.11 (b) shows the results of the LJ-V7200 and (a) the result of the LJ-V7060. The latter shows a higher resolution but has a limited width of the measurement of 16 mm. In Figure 5.11 (c) the enclosed foil (202 µm thick) is directly visible in the detailed colour map.

Table 5.2 Data from measurements from the bidirectional CFRP.

	Absolute height (µm)	Relative height (µm)
Layer 1	2501	277
Layer 2	2778	273
Layer 3	3101	260
Layer 4	3361	237
Layer 5	3598	264
Layer 7	3862	262
Layer 8	4124	261
Flaw	4364	202

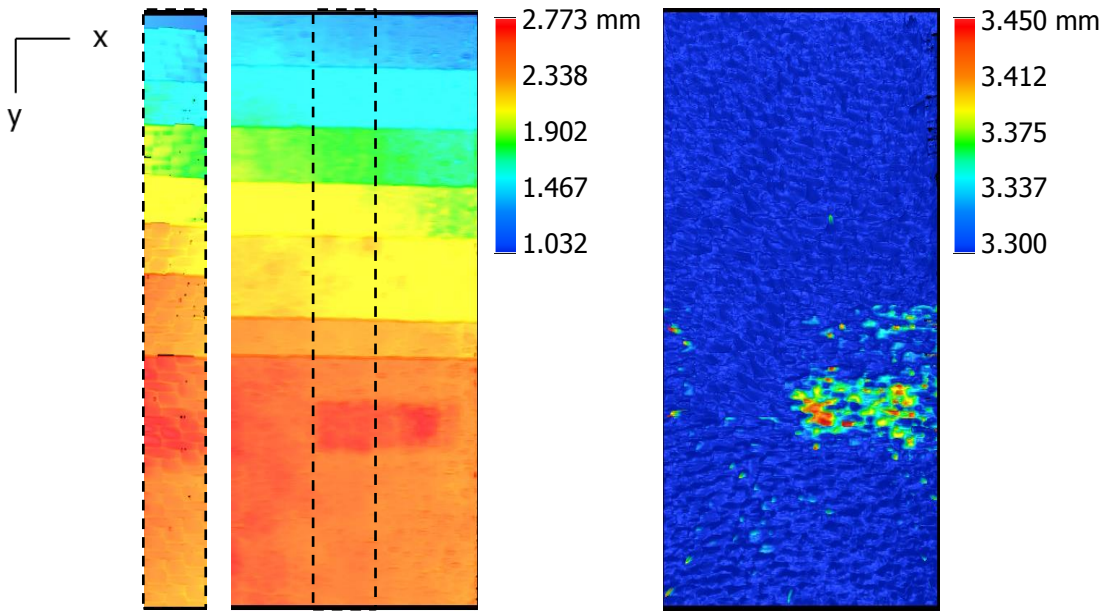

Figure 5.11 Results of measurements of specimen D, bidirectional CFRP, with LJ-V7060 (a) and LJ-V7200 (b) and (c).

5.4.b Dynamic Measurements

The dynamic measurements were performed with the LJ-V7060 using the setup shown in Figure 5.7. A tape layup process was simulated, and the results are shown in Figure 5.12 and Figure 5.13 and in Table 5.3. A 1 cm wide unidirectional CFRP tape was rolled down using a 1.6 kg roller and each layer was measured in height in-situ before stacking the next layer. The specimen and the laser head start each new layer at the calibrated origin. Each layer was separately measured and the height of each layer was determined by relating the value of the new layer to the previously measured value. A calibration measurement was made to remove any angle or height dependencies of the specimen or laser head. The embedded foil was successfully detected underneath the fifth layer. The flaw is 260 µm in absolute height and is significantly 100 µm higher than the surrounding values of layer 5. The enclosed foil of approximately 1 cm^2 can be clearly seen in Figure 5.12 and can be clearly distinguished during the dynamic measurements. Figure 5.13 shows a box plot of each layer, where the data of each layer are represented. The included foil is detected through the identifying significant outliers from the measurement points in layer 5. The outliers are identified as measurement points

outside the upper or lower part of the box plot. The total standard deviation varied between 16 and 29 µm, as vibrations by moving the specimen add to the measurement errors. The last layer has a higher standard deviation of 75 µm due to the included foil and this is actually another indicator of deviations compared with the previous layers with a lower standard deviation.

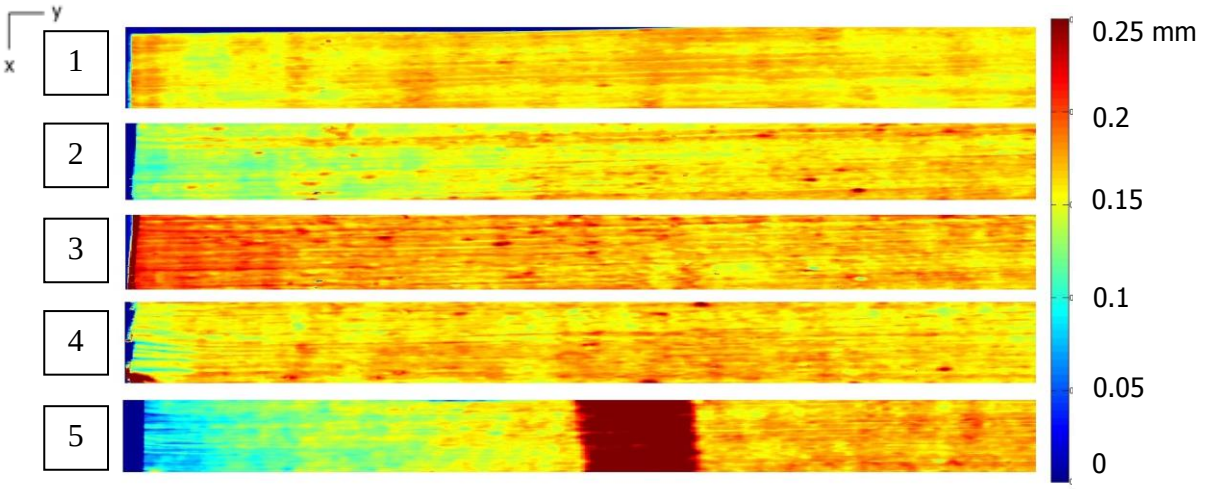

Figure 5.12 Results from the simulation of the tape layup process of unidirectional CFRP, first layer on top of the image.

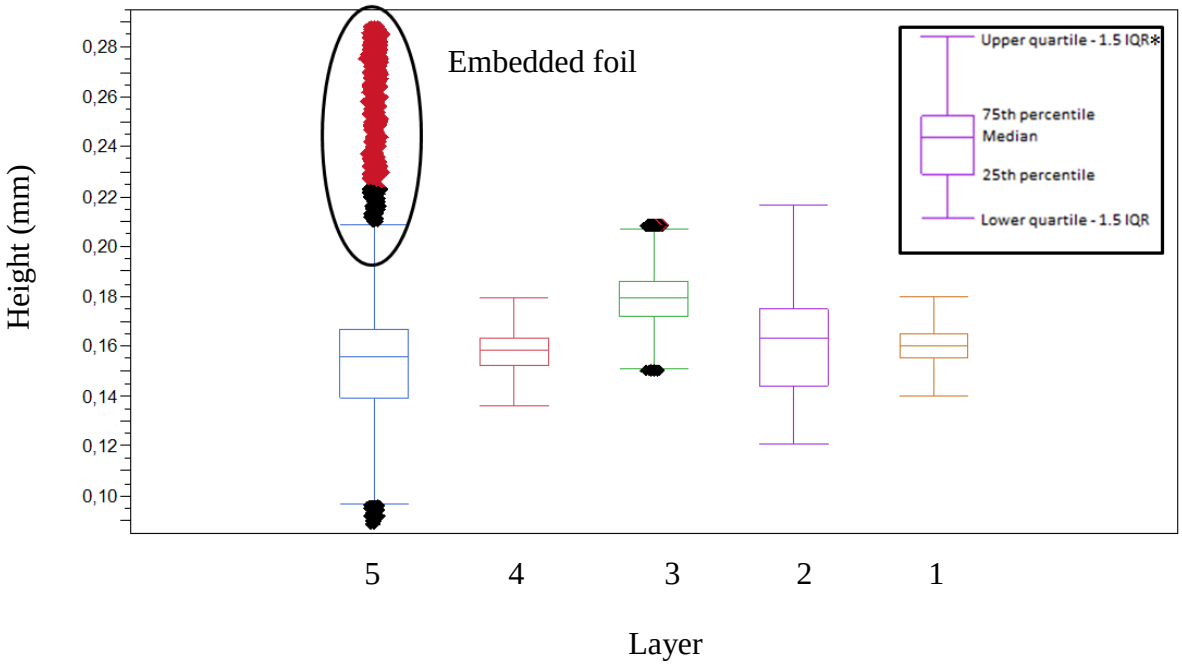

Figure 5.13 Box plot diagram of the dynamic measurement data from the unidirectional CFRP. The outliers in layer 5 indicate the presence of the embedded foil. (Interquartile Range (IQR) = 75th percentile – 25th percentile.)*

Table 5.3 Data of dynamic measurement data from the unidirectional CFRP

	Relative height (µm)	Standard Deviation (µm)
Layer 1	164	15.9
Layer 2	178	28.6
Layer 3	173	28.6
Layer 4	163	29.0
Layer 5	155	75.2

5.5 Discussion

This research demonstrates the potential of the LDS technique to detect production flaws that can be distinguish by height differences in-situ during layup of composite materials. The Keyence LJ-V7200 and LJ-V7060 sensors were able to detect typical flaws that occur during the production of the layup of CFRP. The best accuracy was attained with the LJ-V7060, which resulted in 9 µm standard deviation on a layer of 160 µm in height. The minimum detectable flaw was 27 µm in height at SNR = 3.

In specimen B, the embedded piece of foil is indirectly detectable through debonding of the top layer in the lower left corner and the missing layer, which results in a lower height of the specimen and a geometrical deviation at the missing fourth layer. In specimen C, a wrinkle was introduced in the top layer and caused local height deviations. All flaws thicker than 27 µm in height are significantly detectable and the system can detect the following typical flaws in a static setup:

- Enclosed foil; in this research simulated with 50 µm thick foil
- Missing layer or incorrect overlap; in this research represented as a flaw of 160 µm
- Wrinkling; in this research simulated with 200 µm height

Incorrect fibre orientation in the layers cannot be clearly detected, as the flaw is smaller than the standard deviation. However, this problem does not exist for tape laying machines, as these use unidirectional CFRP and the orientation of the tape laying direction can be monitored by the operational steering. Incorrect fibre orientation occurs in hand layup processes, where layers are placed by workers. The LDS technique may be able indirectly to detect the orientation by measuring the scattering of the laser light from the height differences of the carbon fibres. Tape laying production uses unidirectional CFRP, but hand layup production also uses other types of material, like bidirectional CFRP.

Table 5.2 and Figure 5.11 show the results of measurements of 200 µm thick bidirectional CFRP, specimen D. Because of the woven structure of bidirectional CFRP, the standard deviation is larger (~17 to 53 µm). However, the foil used for this material is also thicker (200 µm). The result is shown in Figure 5.11 (c) by a scaled image, which shows 1 cm^2 embedded foil.

The above-discussed measurements are all static measurements of the specimens with several layers of CFRP. In real-time production, the product is dynamically built up layer by layer, where each layer should be measured and analysed compared with the previous layer to monitor the production. In the laboratory measurements, the absolute height of the specimen was measured to detect any geometrical deviations. As a typical tape layer machine lays 30 metres per minute [133] and the laser head operates at 64 kHz, measurements can be made every 0.5 mm to keep up with the machine. This is sufficiently below the allowable flaw size of 12.5 mm in commercial aviation [8]. However, aerospace industries are already investigating smaller flaw detection in the range of 6 mm to 3 mm.

The foreseen development of the LDS system as an in-situ NDE system is provided in Figure 5.14 according to Technology Readiness Levels (TRLs) [134]. The presented research brings the concept to TRL 4, where all relevant flaws are detected in a laboratory environment. The next step is to validate the economic feasibility to implement LDS in an industrial environment, before demonstrating this in the actual production environment. At TRL 7, separate prototypes for the hand layup and automated tape laying processes need to be developed, as these have other environmental characteristics. After successful prototyping, LDS can be qualified and installed as an in-situ NDE system.

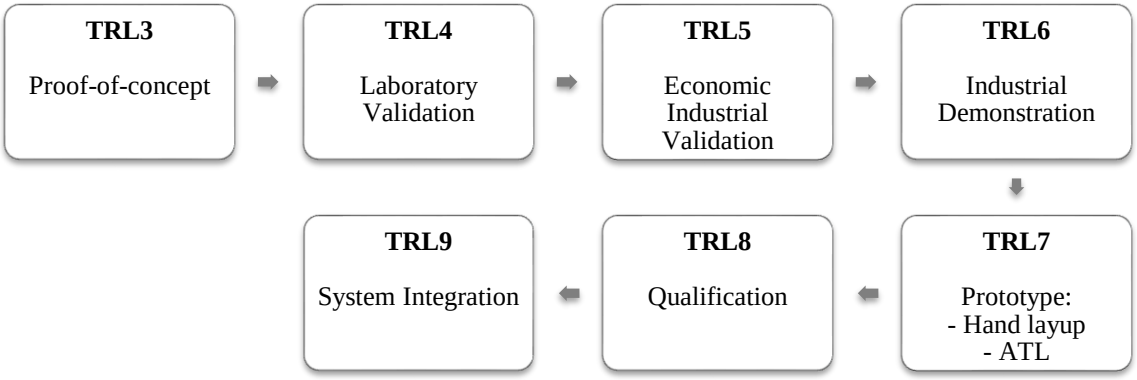

Figure 5.14 The technical roadmap of the further development of LDS as an in-situ NDE system in the TRLs.

Several disadvantages of the systems need attention during further industrialization. For example, small air bubbles can be detected as geometrical deviations but will be removed during the curing phase. These air bubbles have a different structure than enclosed foil. An air bubble has a spherical geometry compared with a rectangular geometry of enclosed foil. However, these air bubbles must not trigger any monitoring system as a false flaw detection system. Another disadvantage of the system is the limited width of the laser signal, although for a tape layer this is not an issue as CFRP tape is typically smaller in width than the laser signals [135]. For hand layup products, this does not apply, as in hand layup large sheets are stacked. This implies several laser heads would be needed to cover the complete width of the product or a mountable laser head fixed on the layup roller. These solutions will cause higher costs or more vibrations, respectively. Additional illumination with a near-UV light source will not impact the specimen through chemical curing or heating of the CFRP. Mascioni et al. [136] have demonstrated the needed illumination times to cure a

typical epoxy resin in prepreg with UV light and the added heat by the LDS light source is negligible.

The described flaws are all geometrical deviations from design specifications, so the candidate in-situ production monitoring system must be capable of measuring these during operations. By moving the laser source or the measured object, a 3-D profile is constructed, but during the industrialization of the in-situ measurement system, these geometrical measurements must be coupled to the original CAD design specifications and the numerical steering of the tape laying process. The dynamic measurements showed an increased standard deviation of 16 to 29 µm due to vibrations in the setup. In calibration measurements at the manufacturer, a vibration error of 7 µm is measured. Any additional vibrations from an industrial environment must be below the allowable standard deviation limit. This limit could be be calculated by using the K-means sampling method [137]. The K-means sampling method and the possible 25 measurement points to detect a flaw of 12.5 mm or larger show a maximum allowable standard deviation of 42 µm to distinguish 210 µm from 160 µm (i.e. the difference between a layer of CFRP and a layer with 50 µm foil embedded). To significantly detect a flaw of 50 µm, amplitude vibration levels lower than 33 µm are accepted or need to be above 64 kHz (i.e. interrogation speed) to be filtered out.

5.6 Conclusion

This research has investigated the suitability of the LDS technique as an in-situ monitoring system for CFRP materials. The technique can detect typical flaws from the production environment, such as enclosed foils, missing layers and wrinkles in the specimen. The technique can be used for unidirectional and bidirectional CFRP materials and is applicable for static measurements of specimens as well as for dynamic measurements, comparable to tape laying machines.

Future research needs to focus on how to integrate the system real-time into the production process and whether the system can operate independently from the workers or tape layers to monitor the quality in-situ during layup. After successful in-situ detection of production flaws, follow-up research needs to address how to remove the embedded flaw during the production without damaging the product.

Acknowledgement

The author likes to acknowledge Keyence for the loan of laser displacement sensors to demonstrate the proof of principle of the approach.

6
Fibre optic Sensors

Adapted from: *Local fibre optic pressure and temperature sensing for autoclave monitoring in CFRP manufacturing; Miesen, N., Warnink, M., Sinke, J., Groves, R. M. & Benedictus, R. 2018: International Journal of Advanced Manufacturing Technology (To be submitted for review).*

6.1 Introduction

This research will investigate Fibre Optic Sensor (FOS) techniques to monitor local temperature and pressure deviations during the curing phase of CFRP manufacturing. The novelty of this research is the simultaneous in-situ measurements of local temperature and pressure with optical sensors on a CFRP part during curing in an autoclave. The techniques investigated have the potential to provide a CFRP manufacturer with real-time information on the location of the flaws presented in Table 1.1 and to investigate customized counter-measures to remove flaws during the curing cycle. This will reduce the flaws in the cure cycle and improve the efficiency of the manufacturing process. Currently, manufacturers see most value in the in-situ detection of flaws to decrease the time of NDE.

Section 6.2 of this chapter discusses the manufacturing process of CFRP in more detail, the technical background of the fibre optic sensors and a review of related research in cure monitoring. Section 6.3 provides the experimental design and the results. These are discussed in Section 6.4 and the paper is concluded in Section 6.5.

6.2 Background

6.2.a Quality of Manufactured CFRP

Curing at an elevated temperature in an autoclave is needed to consolidate and solidify CFRP prepreg with a resin matrix [138]. In the curing process, pressure and vacuum are applied in the autoclave to remove any trapped gases from the layup or curing reactions [139]. During the curing cycle, the temperature will gradually increase to prevent large exothermic reactions that might damage the material [140]. Constant temperature is reached for thin laminates approximately 30 minutes into the cycle, while thicker laminates will take more time depending on the product specifications. The constant temperature regime is designed to evenly distribute the viscous resin and supports the chemical reaction. Constant pressure supresses the size of remaining voids and supports the consolidation of the stack. At the end of the steady state regime, the temperature and pressure are brought back to ambient conditions in a controlled way. Heat-up and cool-down

rates in a CFRP manufacturing facility are regulated to ensure homogeneous and/or efficient curing of the part. As pressure and temperature are critical variables for product quality, vacuum level, autoclave temperature and autoclave pressure are critical curing cycle parameters. Pressure and vacuum are normally monitored globally by the autoclave system sensors and thermocouples are used to track temperatures at critical points. However, pressure or vacuum is currently not locally measured and local pressure deviations can lead to voids or porosity [141]. A new process monitoring system is needed to track these critical variables to detect in-situ manufacturing flaws, see Table 1.1.

6.2.b Fibre Optic Sensing Theory

A novel CFRP cure monitoring sensing system should be able to measure in-situ and locally the part's temperature and pressure. Fibre Optics Sensing technologies are emerging as an important tool for SHM because of their sensitivity and multiplexing capability [142] and have further potential for the process currently available, however currently only a few have reached an industrial application level:

- Low coherent interferometric sensors
- eFPIs
- Rayleigh distributed sensors
- Raman distributed sensors
- Brillouin distributed sensors
- FBGs

From these technologies, two were selected for further investigation. FBGs, which are the most mature grating-based sensors, are most commonly used to measure temperature and strain [143]. eFPIs are a mature technology for pressure sensing with optical fibres [142]. The theoretical background on the working principles of the FBG and eFPI sensors was described in Section 2.8.

In summary, FOS technologies should be further investigated for three reasons:

1. Sensing capability; FOS are able to measure both temperature (FBG) [144] and pressure (eFPI) [145].
2. Sensor characteristics; FOS are lightweight and have a small size [30], which makes them practical to build into the autoclave and vacuum bag. They are widely researched and can operate in harsh environments [146].
3. SHM; FOS sensors can be embedded in CFRP structures [30] and can be further optimized for in-service use, by considering their robustness and reliability [147, 148].

6.3 Experimental Design and Results

This research investigates the in-situ local monitoring of temperature and strain and relates these measurements to detecting voids and porosity problems occurring in the CFRP autoclave curing cycle. Temperature and pressure are critical variables in the process cycle and should be closely monitored [141]. Measuring any local deviations from the prescribed cycle can indicate a potential flaw and an analysis of flaws occurring may lead to a better understanding to customize or improve future cure cycles.

The following sections describe the experiments and results to evaluate fibre optic sensors as a local curing monitoring system. Therefore, optical fibres were installed in the autoclave with sensors, while connected to interrogators outside the autoclave. These experiments are summarized below:

1) Detection and localization of vacuum bag rip by pressure sensing with eFPI.
2) Monitoring temperature locally with FBGs
3) Calibrating the eFPI pressure sensors
4) Monitoring the local pressure of CFRP parts in the vacuum bag with an eFPI sensor during prescribed and deviating pressure cure cycles

6.3.a Detection and Localization of Vacuum Bag Rip

Experiment 1) was designed to test if pressure loss in a vacuum bag could be detected by eFPI sensors. The experiment was perfomred outside the autoclave in the environment of the laboratory. Figure 6.1 shows the schematic setup for experiment 1) with simulated vacuum bag rips from 1 cm incisions introduced at four locations, indicated by X_i. After each incision, the rip was repaired and the bag was brought back to vacuum pressure. For each sensor, the pressure difference was calculated based on the measurements of the four eFPI sensors. To detect the rip, it was expected that the highest pressure difference should be at the sensors closest to the rip. Pressure measurements were performed with a FISO FOP-M (-BA-C1-F1-M2-R3-ST) eFPI that has an absolute range of 0 to $1 \cdot 10^6$ Pa and an accuracy of $5.2 \cdot 10^3$ Pa and is interrogated by a FISO UMI-4 (four-channel) interrogator. A practical-sized vacuum bag was chosen to hold eight layers of 600 mm by 600 mm Delta Tech DT120 unidirectional CFRP prepreg, in a $[0/90]_4$ layup configuration. To introduce a vacuum of $2.0 \cdot 10^3$ Pa (atmospheric pressure is $1 \cdot 10^5$ Pa), standard bagging material and equipment was used [139].

a) 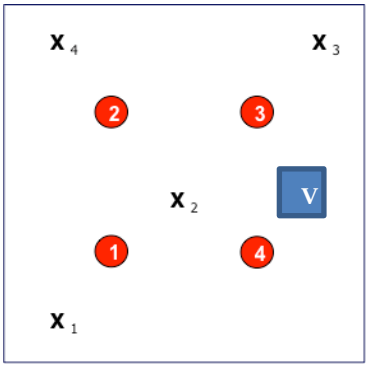

b) 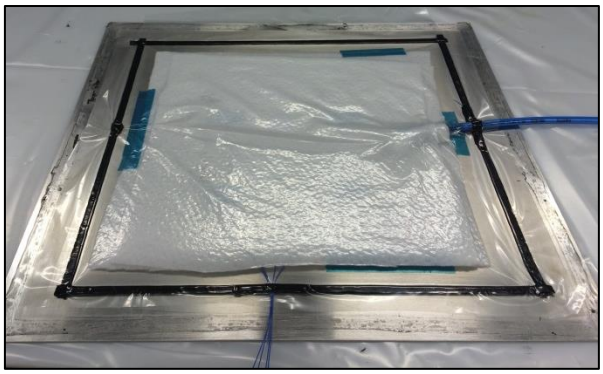

Figure 6.1 a) eFPI sensors evenly placed 20 cm from each other in a square as marked by the red circles. The vacuum bag was 600 by 600 mm. At the locations marked with X, 10 mm cuts were made to simulate a vacuum bag leak. The vacuum pump was connected at the blue square, marked V. b) Photograph of the setup.

The vacuum pump was switched on during the application of the rip.

Table 6.1 shows the results from four eFPI sensors placed in the vacuum bag. Columns 2 to 5 show the pressure difference (ΔP) at the location of each sensor for each rip (X_n) and the highest difference is indicated by bold underlined values. The vacuum pump was switched on during the application of the rip.

Table 6.1 Measurements of the pressure differences in a vacuum bag outside the autoclave. The bold underlined values show the nearest pressure sensor.

eFPI sensor	**ΔP X_1 (10^3 Pa)**	**ΔP X_2 (10^3 Pa)**	**ΔP X_3 (10^3 Pa)**	**ΔP X_4 (10^3 Pa)**
1	**<u>32.0</u>**	**<u>72.0</u>**	37.8	55.8
2	31.4	71.2	39.8	**<u>57.0</u>**
3	31.2	71.4	**<u>42.2</u>**	56.6
4	30.2	71.8	38.8	56.0

The results show the successful detection of a rip in the vacuum bag as the closest pressure sensor to the rip always detects the largest pressure deviation. However, the difference between the sensor readings is less than the specified sensor accuracy of $5.2 \cdot 10^3$ Pa.

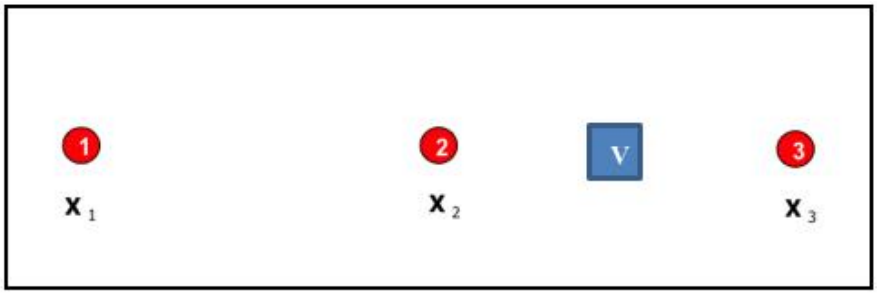

Figure 6.2 on a plate of 1850 mm three sensors where placed. Sensor 1 is placed 200 mm from the left side, sensor 2 at 950 mm and sensor 3 at 1700 mm. The vacuum nipple, marked V, was placed at 1300 mm. On the X marked locations, small 1 cm cuts were made to simulate a vacuum bag leak.

Figure 6.2 shows a similar setup, but in a larger vacuum bag (1850 mm by 600 mm) to distinguish the reaction time of each sensor compared to a vacuum bag rip. In this setup the vacuum pump was switched of during the application of the rip.

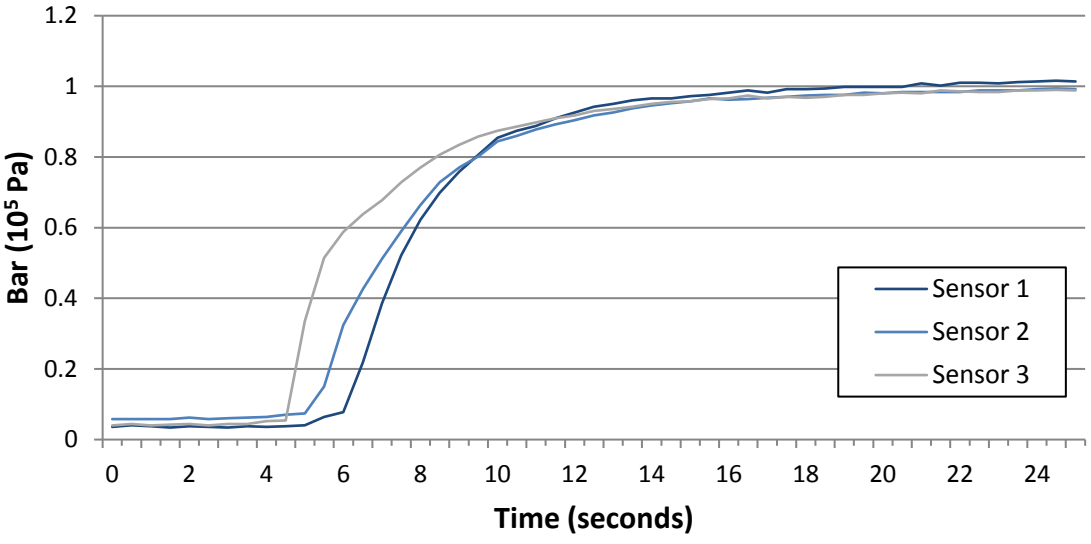

Figure 6.3 shows an example of a measurement during a simulated rip at X_3. It shows clearly that sensor 3 reacts first, followed by sensor 2 and 1.

By using the time delay in a sensor the localization of rip is possible, as example see Figure 6.3. However, a lot of variables determine the reaction time, such as

the size of the rip, volatility in the vacuum bag etc. These results do show the potential for rip localization by using the reaction time of eFPI sensors.

6.3.b Monitoring Temperature Locally with FBGs

Experiment 2) was designed to test the FBGs in the autoclave and to assess their in-situ sensing capability for temperature compared with conventional thermocouples. During this experiment, one reference CFRP part (200 mm by 200 mm) was interrogated with four K-type thermocouples to monitor a potential temperature difference. According to the manufacturer, the part should be cured within 5 °C of the prescribed temperature cycle [109]. The specimen was prepared of eight layers of 200 mm by 200 mm Delta Tech DT120 unidirectional CFRP prepreg, in a $[0/90]_4$ layup configuration and cured according to their prescribed cure cycles (see Figure 6.4, Table 6.2 and Table 6.3) in the composite manufacturing laboratory of the university.

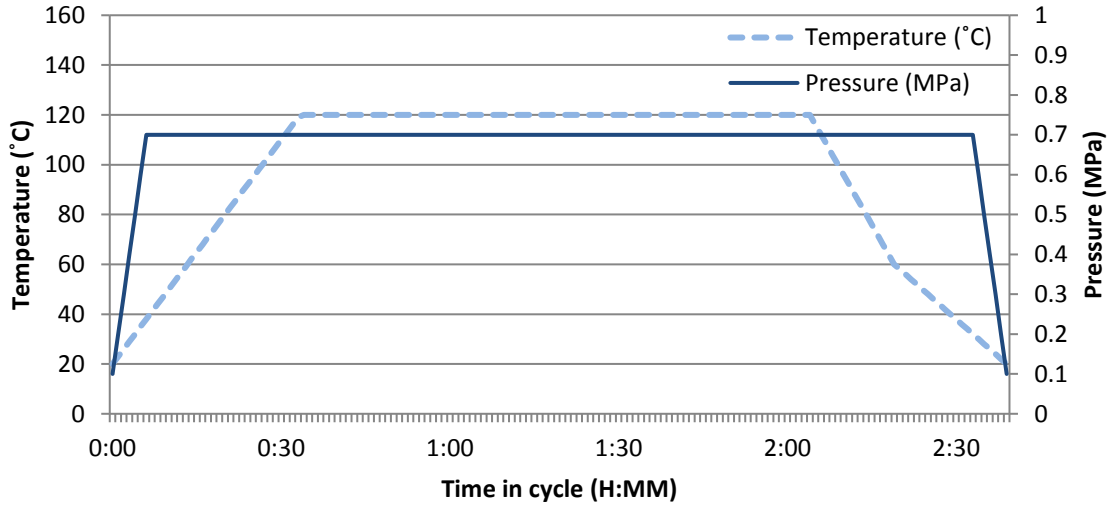

Figure 6.4 Graph of the prescribed temperature and pressure cycle in the autoclave for DT120 unidirectional CFRP prepreg [109].

Table 6.2 Temperature cycle according to the manufacturer's recommended cure cycle for DT 120 [109].

Phase	Temperature range (°C)	Rate (°C/min)	Time Period (HH:MM)	Total time (min)
Heat up	20–120	3	00:00–00:34	34
Constant temperature	120	–	00:34–02:04	90
High-rate cool down	120–60	4	02:04–02:19	15
Slow-rate cool down	60–20	2	02:19–02:39	20

Table 6.3 Pressure cycle according to the manufacturer's recommended cure cycle for DT 120 [109].

Phase	Pressure range (10^5 Pa)	Rate (10^5 Pa/min)	Time period (HH:MM)	Total time (min)
Pressurization	1–7	1	00:00–00:06	6
Constant pressure	7	–	00:06–02:33	147
Depressurization	7–1	1	02:33–02:39	6

Temperature measurements in the autoclave were performed with an unbonded FOS&S SG-01 FBG strain gauge. The temperature sensitivity of the FBG was measured as 12.3 pm/°C [149]. The FBG has a nominal wavelength of 1555 nm and an operating temperature range of –50 to +130 °C. The sensor was connected via an optical table patch cable to a National Instruments (NI) PXIe 4844 Optical Sensor Interrogator, which samples at 10 Hz with an accuracy of 1 pm. This corresponds to an accuracy of 0.08 °C. A K-type thermocouple was placed near the FBG as a reference. In addition, further thermocouples were placed in the vacuum bag to monitor the temperature locally. Two thermocouples were placed on top and two below the part to measure the temperature gradient in the part. The autoclave setup is shown in Figure 6.5.

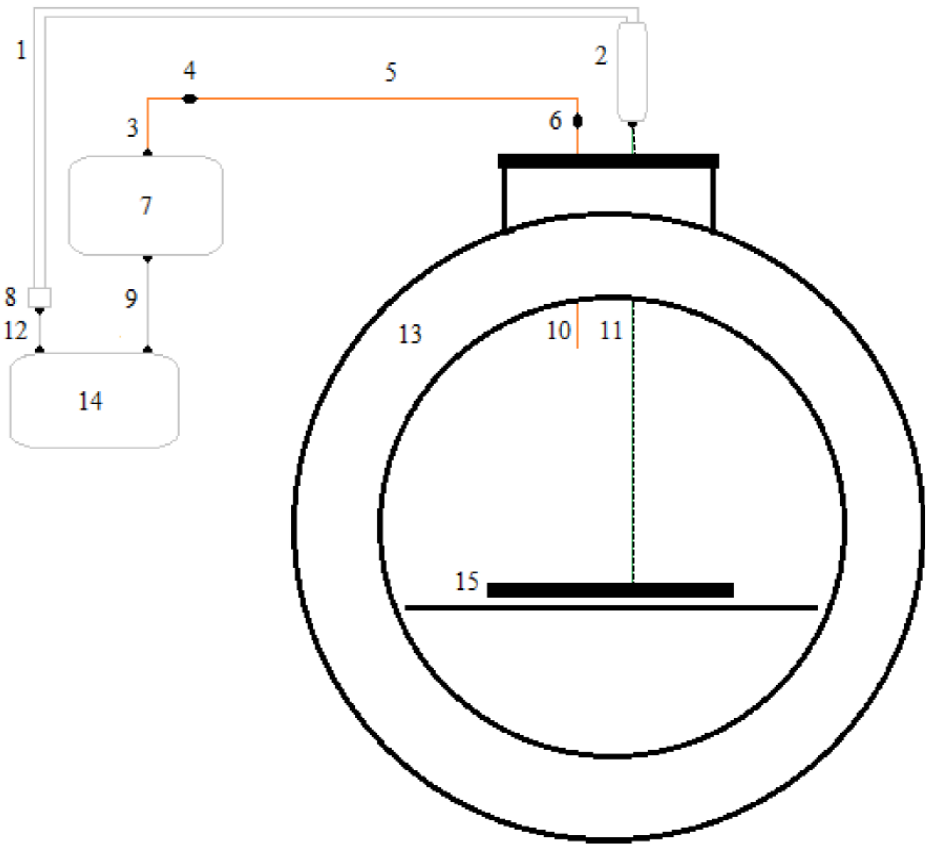

Multimode fibre 650–1000 nm

Single-mode fibre 1460–1620 nm

1. Electrical connection
2. FISO FTI-10 or UMI-eFPI interrogator
3. Optical patch cable with LC/FC connectors
4. FC to FC connector
5. Thorlabs 5 m patch cable with acrylate coating
6. FC to FC connector
7. National Instruments PXIe 4844 Fibre Optic Interrogator
8. National Instruments USB-6009 analog-to-digital converter
9. RS-232 connection
10. Unbonded FBG
11. eFPI with 5 m glass fibre connection
12. USB cable
13. Zirbus autoclave
14. Personal computer
15. Layup configuration

Figure 6.5 Schematic representation of the experimental setup.

Military specified or other high-performance connectors would be needed for the optical fibres to be connected inside the autoclave, therefore the choice was made to install a 5 metre long Teflon-coated optical fibre. This reduced the costs of the setup and signal losses due to the coupling of a multimode with single mode optical fibre, see the detailed feed trough photo in Figure 6.6. For a commercial

application, the connection of fibres with patch cords inside the autoclave would be developed further.

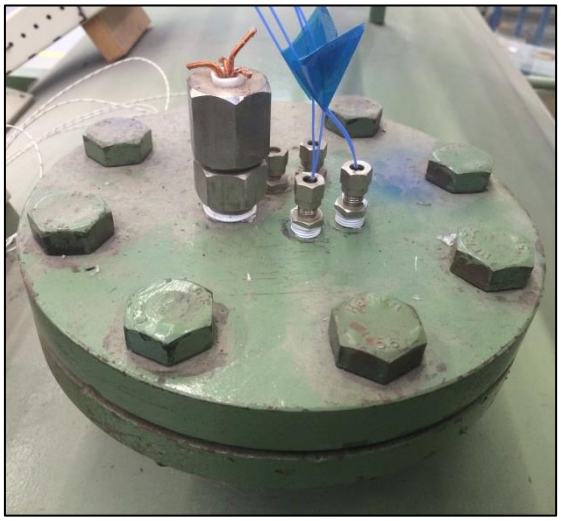

Figure 6.6 Optical fibres for FBG and eFPI sensors are installed via feed-through holes into the autoclave and the hole closed off with silica gel.

Figure 6.7 shows the temperature measurement of the cure cycle with the thermocouples and FBG. The red curve shows the difference between the thermocouple reading and the FBG sensor.

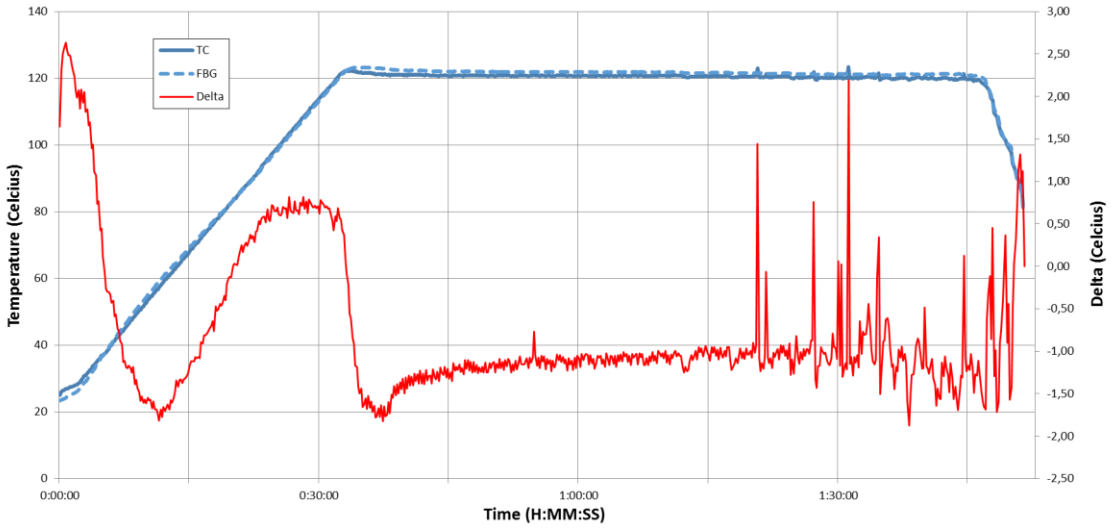

Figure 6.7 Temperature measurements of the thermocouple (TC) and FBG during the autoclave cycle. The red graph shows the difference between the TC and FBG sensors on an exaggerated scale.

The disturbances in the thermocouple, which has a faster response to temperature than FBGs, show up in the graph at the end of the constant temperature phase. The FBG has a lower temperature gradient than a thermocouple, which means a slower reaction time to temperature increase and explains the different gradient in the linear temperature increase of the cycle.

Figure 6.8 shows the absolute temperature differences between four locally placed thermocouples directly on the CFRP part during the cure cycle. The top of the part heats up more quickly and this creates a slight temperature gradient of a maximum of 1.5 °C compared to underneath the part. During cooling, the top of the part dissipates heat more quickly to create a slight temperature difference again. During the constant temperature regime, the temperature gradient is at a maximum of 0.7 °C. The measured temperature difference during the cycle stays within the composite manufacture's specified limits of ±5 °C.

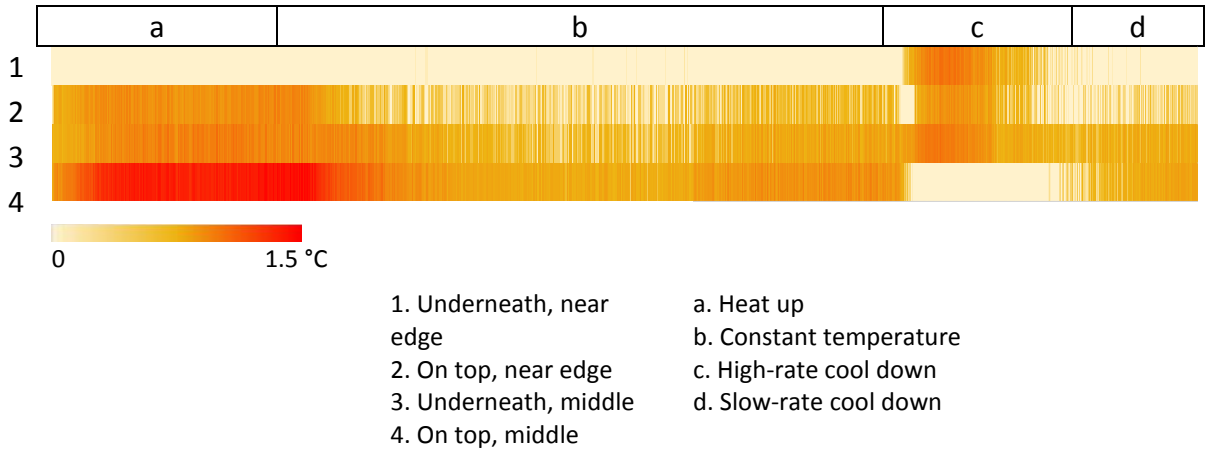

Figure 6.8 Temperature difference measured directly on a part during the cure cycle.

6.3.c Calibrating eFPI Pressure Sensors

The eFPI sensors are temperature sensitive according to theory and manufacturing specification. They will, therefore, need to be calibrated for temperatures in the autoclave using laboratory oven cycles. The calibration is performed at $1 \cdot 10^5$ Pa to investigate temperature as an independent variable. The calibration was performed using FISO FOP-M (-BA-C1-F1-M2-R3-ST) eFPI sensors and FISO UMI-4 interrogator. A 5 metre long patch cable, which is Teflon coated and can withstand temperatures up to 150 °C, was used to connect the eFPI sensor via feed-through holes to the interrogator. The first calibration cycle was tested similar to Table 6.2, while the second cycle used a heating rate of 6 °C/min. Figure 6.9 shows the raw pressure measurements during two temperature cycles in the oven for the three eFPI sensors.

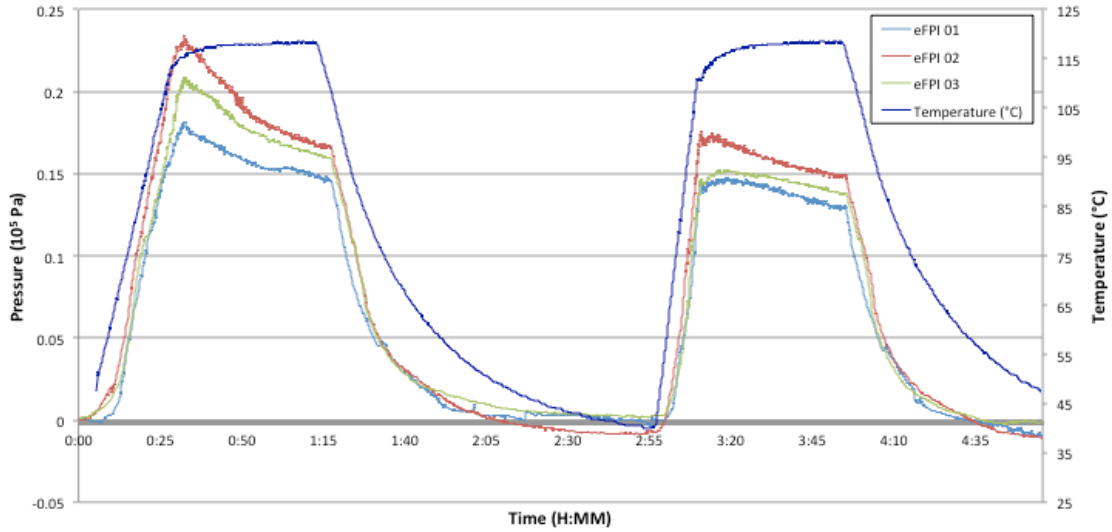

Figure 6.9 Raw pressure measurements during the oven calibration cycle of three eFPI sensors.

The eFPI sensors show a temperature dependence at constant pressure and show a delay in the heat up cycle, but also shows a clear overshoot when the stabilization temperature of 120 °C is reached. The same overshoot is also seen in the second cycle, but the peak is 26% lower. Because of this overshoot, the eFPI sensors have been calibrated on the linear increase of the heat-up phases. Equation (4) shows the calibration formula with P_1 as calibrated pressure measurement of the eFPI. P_0 is the uncalibrated pressure measurement, C_T the calculated temperature coefficient and T the temperature in the autoclave in °C.

$$P_1 = P_0 + (C_T \cdot T) \tag{4}$$

The calibrations result in the temperature coefficients shown in Table 6.4 for the eFPI sensors that are used in follow-up experiments. The linear calibrations all show an R^2 of 97% or higher.

Table 6.4 The calculated coefficients for the temperature dependence of the eFPI sensors over the temperature range of 20 °C to 120 °C. Sensor 4 was used in later experiments.

eFPI sensor	Temperature coefficient C_T (Pa/°C)	Error (Pa/°C)
1	–286	±51
2	–316	±44
3	–283	±42
4	–474	±24

6.3.d Monitoring the Local Pressure of CFRP Parts

This experiment was designed to demonstrate the capability of the system to measure in-situ pressure variations during of the cure cycle. The same setup as described in Section 6.3.b was used and the calibration values obtained in Section 6.3.c were used to correct the eFPI measurements for the temperature dependence. The pressure in the vacuum bag during the prescribed cycle should be near the vacuum set point at 2.0×10^3 Pa. Calibrated measurements of a prescribed cure cycle (see Table 6.2 and Table 6.3) are shown in Figure 6.10.

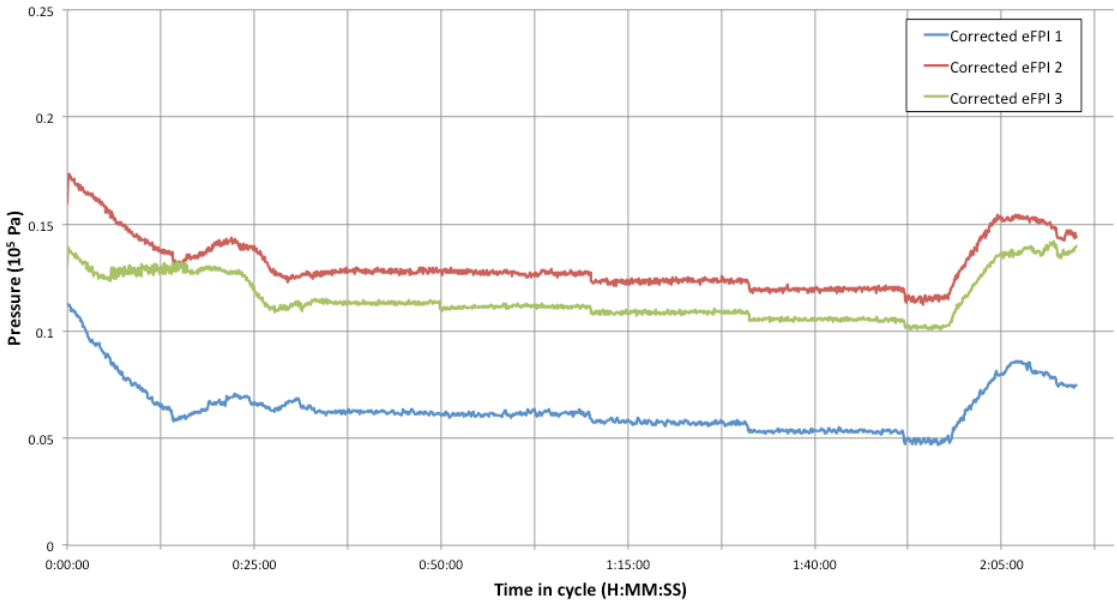

Figure 6.10 Corrected pressure data inside the vacuum bag during the autoclave cure cycle.

At constant temperature, the eFPI sensors show a discrete stepwise reduction of the pressure in the order of about $5 \cdot 10^2$ Pa. This is due to the vacuum pump slightly

correcting the pressure in the bag. On the slopes of heat up and cool down, the sensors show non-constant values due to the residuals of the temperature calibrations. This is due to the delay in the heat up and the eFPI sensor overshoot. The target pressure of $2.0 \cdot 10^3$ Pa is not reached due to pressure losses, but also slightly different pressures are measured by the different eFPI sensors as a starting point. The manufacturer provides no allowable limits for pressure deviations; however, it is expected that large pressure deviations from the specified vacuum will result in a lower quality part. In Paragraph 6.3.a, it was shown that a vacuum rip can decrease the pressure by 3×10^4 Pa or more. To detect a vacuum bag rip in-situ, the following experiments used a pressure in the vacuum bag of either $5 \cdot 10^4$ Pa or $1 \cdot 10^5$ Pa (venting), in different cycles. Figure 6.11 shows corrected pressure measurements recorded during three different cure cycles at different pressure levels.

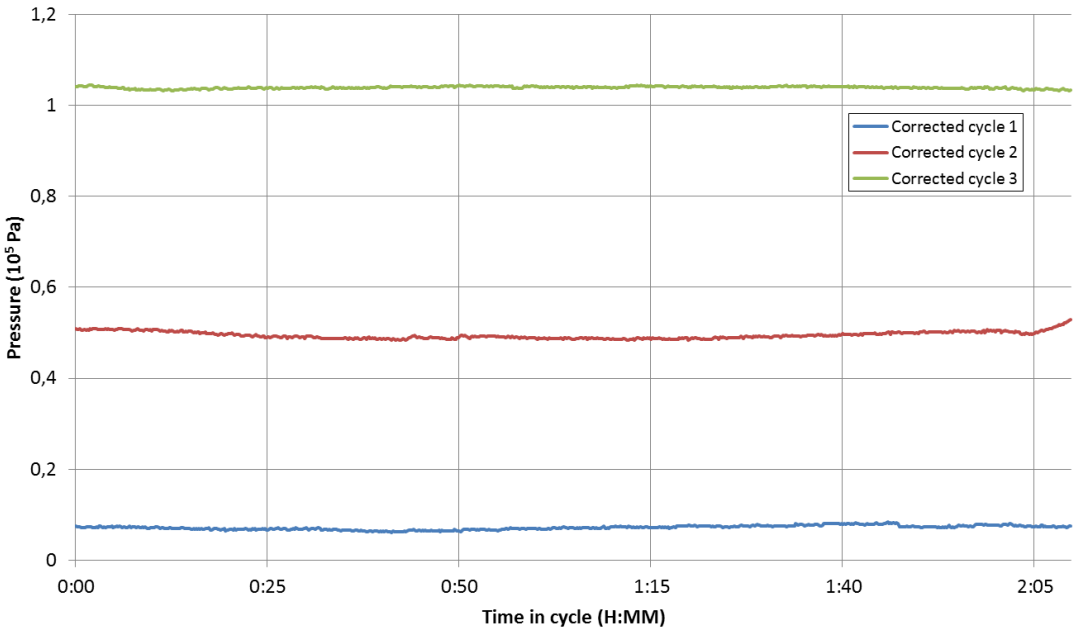

Figure 6.11 Corrected pressure measurements with eFPI sensor 4 during a prescribed cure cycle but different vacuum bag pressure levels. Cycle 1 shows the reference pressure cycle.

The eFPI sensor was used to measure a prescribed pressure cycle in the vacuum bag, and also two deviating pressure cycles. Cycle 1 shows the calibrated pressure cycle at a near vacuum of $7.0 \cdot 10^3$ Pa measured at the eFPI sensor. Cycle 2 shows the same calibrated cure cycle, but a pressure deviation is measured in-situ of

$5.1 \cdot 10^4$ Pa, where in cycle 3 an in-situ pressure deviation is measured of $1.1 \cdot 10^5$ Pa.

6.4 Discussion

The environment of the autoclave is challenging for sensors, as curing is performed at $6 \cdot 10^5$ Pa and 120 °C. The four eFPI sensors placed in the vacuum bag could detect vacuum bag rips, although precise localization of the rip was inconclusive due to the pressure sensing accuracy. In a larger vacuum bag localization would be possible to detect through the reaction time of sensors to differences (i.e rip) in the vacuum bag., according to the results shown in Figure 6.3.

Critical parameters in the autoclave cure cycle were successfully monitored by the FOS system. The assumption is that deviating pressure or temperature from the prescribed cycle can lead locally to flaws in the produced specimen. The FBG can measure the temperature profile in-situ with a sensitivity of 12.3 pm/°C. The sensitivity could be increased by several factors [79], but local temperature measurements on the parts are unnecessary as the temperature difference is lower than 1.5 °C and well within the specification of ±5 °C supplied by the CFRP manufacturer. However, if the FBG could be embedded in the structure for later SHM applications [30], it could also be utilized for cure monitoring.

Local pressure measurement with an eFPI sensor, introduced into the vacuum bag during the autoclave curing cycle was successful. The measurements provide insight into if pressure was distributed equally or if air pockets cause pressure differences that can lead to voids [139]. The eFPI sensor does show a significant temperature dependence, which can be corrected after calibration. The delay in heat up of the cure cycle and the overshoot after the heat up introduce measurement uncertainties, but these overshoots seem to decrease after more temperature cycles. These measurement uncertainties could be solved by further development of eFPI sensors with lower or no temperature dependence [69]. Due to the overshoot of the sensor valuable information may get lost and valuable time for corrective actions. The CFRP prepreg manufacturer does not specify the cure limits for pressure; however, the FOS system described in this research is able to measure with an accuracy of up to $1 \cdot 10^3$ Pa (assuming a SNR of 3). Further sensor developments to specialize the eFPI sensors for in-situ autoclave measurements would need to link with relevant research, for example, Zhu et al. [150].

Fibre optic sensor placement and instrumentation for the autoclave can be optimized for future industrial applications. EFPI sensors can be integrated into the autoclave system, similar to thermocouples, and it would be possible to apply reusable pressure sensors on any CFRP part to be cured. Because of the small size of the eFPI sensor, it could be integrated into the mould or even the vacuum nipple. However, this would require more research on how to respond when a deviation is measured and what could be an effective counter-measure to control the process. Where voids or porosity are caused by incorrect pressure levels in the vacuum bag, investigations of a corrective (second) cycle could lead to a decrease of the void content. However, the resin should not have set, otherwise the voids would be set in the material. Overall, this research is a step in the direction of the smart manufacturing concept, incorporating sensing and decision-making to improve product quality.

6.5 Conclusion

This research has focused on temperature and pressure related flaws during the curing phase of CFRP manufacturing and has successfully demonstrated in-situ autoclave cure cycle monitoring with FOS. Temperature measurements in the autoclave with conventional thermocouple sensors are currently sufficient for current process control, but eFPI sensors could be integrated to act as a process monitoring system to monitor pressure related flaws in-situ during the autoclave cure cycle. The novelty of the in-situ simultaneous measurements of temperature and pressure with FOS placed in the autoclave has been demonstrated.

7
Industrial value

Adapted from: *Financial assessment of the impact of production rework and rejection in CFRP manufacturing and the economic potential of an in-situ NDE system; Miesen, N., Sinke, J., Groves, R. M. & Benedictus, R. 2018. International Journal of Productivity and Quality Management (To be submitted for review).*

7.1 Introduction

The objective of this chapter is to identify the cost of manufacturing flaws listed in Table 1.1 during the manufacturing process of CFRP and to evaluate the economic potential of introducing in-situ NDE to reduce flaws during manufacturing.

The quality check during the NDE phase in production is critical in the manufacturing process of CFRP material. Although this process step is critical, it is an unnecessary process step if no rejection or rework is needed in the product after the cure phase.

The future state, or "holy grail", should be the detection and elimination of the flaws during the layup or cure phase. This current research focuses on the first step, which is the detection of flaws in-situ, based on Table 1.1. Within the current scope and without complete elimination of the flaws, there are already benefits:

- The laminated and cured panel has a number of known flaws, in terms of type, size and location.
- This could minimize or eliminate the quality control check. Where flaws are already known, the rework procedure can already be prepared and initiated before the panel reached the rework station.
- When a panel is evaluated to be rejected in-situ the manufacturing process, the process can be stopped to save production capacity.
- Knowing the type and occurrence of flaws the manufacturing process can be improved and adapted through root cause analysis.
- More detailed information of flaws becomes available, than for example a through transmission C-scan, which does not measure in which layer the flaw is.

Section 7.2 discusses related previous work on cost modelling, which do not show explicitly the costs of rework or rejection. Therefore, an adapted new cost model is needed and this is presented in Section 7.3, where rework and rejection are explicitly taken into the cost structure, components and assumptions. Section 7.4 presents the outcome of the cost model, using case studies in optimistic and pessimistic scenarios. The results of the case studies were validated with a Tier 1 aerospace CFRP manufacturer (1000+ employees). Section 7.5 discusses the

results, the validation, the financial impact of rework and rejection on the overall CFRP manufacturing costs and the financial potential of the implementation of an in-situ NDE process monitoring system. Section 7.6 gives the conclusions.

7.2 Related Work on Cost Modelling

This section shows related work on cost modelling in CFRP manufacturing. Several approaches for cost modelling are available. Rework and rejection are mentioned in some studies, but have never been used to estimate the costs of flaws explicitly.

Niazi et al. [151] divide the approaches for cost models into qualitative and quantitative techniques. Of the many approaches, Zhao et al. [152] give a good overview of the classifications for cost estimation methods, splitting them into:

- Estimation process
- Estimation model
- Calculation model
- Additional techniques, based on model- or method-specific techniques

Most of the methods need qualitative design information to estimate manufacturing costs. Methods with an actual reference part are more accurate [151], however, this research does not use a reference CFRP part to calculate but uses order of magnitude estimates for the financial impact of rejection and rework. Pugh [153] discusses a top-down breakdown method that can be used before any detailed design information is available. The top-down breakdown method will be used as the basis for this research, as to avoid using use specific design details to influence the actual financial impact of flaws.

Related work on cost modelling was started by Lorenzana et al. [154]. They developed an Advanced Composite Cost Estimating Manual (ACCEM) in the Northrop Grumman corporation in 1976. The composite manufacturing process was broken down using Industrial Engineering Standards. Gutowski et al. [155] developed a theoretical model to estimate processing time for human labour and machines. Summing the time for each basic step in the CFRP manufacturing process provides the total time in production. A web-based system for cost modelling was developed at Massachusetts Institute of Technology [156] and entails cost estimations for multiple CFRP manufacturing processes. Shehab et al. [157] added a cost component to estimate the cost of quality assurance, such as NDE. Rejection and rework are mentioned in some approaches, but an explicit calculation is needed to determine the financial impact of flaws.

7.3 Cost Model Methodology

The goal of this chapter is to estimate the typical cost of the rejection or the rework of flaws in a CFRP manufacturing process. Therefore, a top-down breakdown structure is chosen. No specific CFRP part is modelled and a generic cost structure was used, including realistic rejection and rework rates, to estimate the financial impact of flaws on large and small fictitious parts. The major contributing components in this model are shown schematically in Figure 7.1.

Section 7.3.a describes the cost components and Section 7.3.b lists the assumptions to analyse the cases.

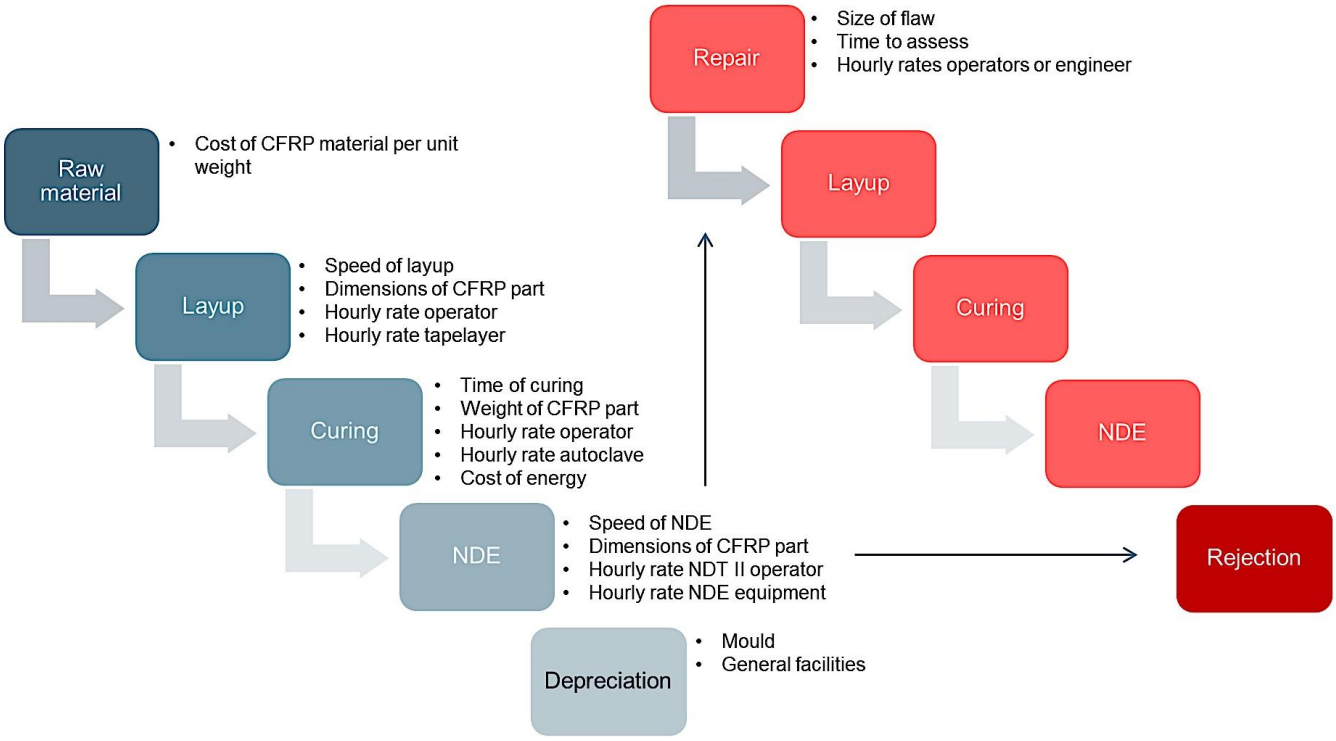

Figure 7.1 The top-down breakdown structure with the major contributors to the cost model. The blue boxes show the regular manufacturing process, while the red boxes show the additional steps needed for rework or rejection.

7.3.a Cost Components of CFRP Production

The structure of the model is schematically presented in Figure 7.1 and was validated with the Tier 1 manufacturer. The process in red in Figure 7.1 shows the additional hidden steps due to rework or rejection. Equation (7.1) shows the total sum of costs in euros of a single generic part, built up from major contributors from variable and fixed costs.

$$\begin{aligned}&\text{Variable Costs} + \text{Fixed Costs} = \text{Cost Raw materials} + \text{Cost Layup phase} + \\ &\text{Cost Curing phase} + \text{Cost NDE phase} + \text{Depreciation} + \text{Costs rework \& rejection}\end{aligned} \quad (7.1)$$

The total cost of raw materials is based on its unit price and the total weight of the part:

$$\text{Cost Raw materials} = \text{Cost CFRP (Euro/kg)} \times \text{weight specimen (kg)} \quad (7.2)$$

Total time to perform the layup is determined by the speed of layup, the total surface of the part and the total number of layers. For hand layup and automated layup, the speed of layup will be different; first, the total layup time is calculated:

$$\text{Total time layup (hrs)} = \frac{\text{Speed layup CFRP } (m^2/\text{min.}) \times \text{Surface specimen } (m^2) \times \text{Number of layers}}{60 \text{ (min/hr)}} \quad (7.3)$$

For ‘speed layup CFRP’ using automated tape layer, a conversion is calculated from the width of CFRP tape (in m) times the speed of the machine (m/min). The speed of the machine includes inefficiencies, such as setup or turning. The total costs of the layup phase are determined by the total time in layup and the hourly rate. The calculation of the layup costs is dependent on wether hand or automated layup is used:

Manual:

$$\text{Cost layup phase} = \text{Total time layup (hrs)} \times \text{Hourly rate operator (Euro/hr)}$$

Automated tapelayer: (7.4)

$$\text{Cost (tapelayer) layup phase} = \text{Total time layup (hrs)} \times \text{Hourly rate (operator + tapelayer) (Euro/hr)}$$

Total costs of the curing phase consist of the operation costs for the autoclave and the energy costs:

$$\sum \text{Costs Curing phase} = \sum \text{Costs curing (labour and machines)} + \sum \text{Energy costs} \quad (7.5)$$

Curing costs are determined by the total time in the autoclave, the hourly rate for the operator and the autoclave and the number of parts that will cure in the same autoclave cycle. This assumes equal costs for all parts in the same autoclave cycle:

$$\frac{\text{Total time curing (hrs)} \times \text{Hourly rate autoclave (Euro/hr)}}{\text{Number of parts in autoclave}} + \frac{\text{Time labour autoclave (hrs)} \times \text{Hourly rate operator (Euro/hr)}}{\text{Number of parts in autoclave}} \quad (7.6)$$

In addition, the energy costs are calculated as:

$$\text{Energy costs} = \text{Energy consumption (kWh/kg)} \times \text{Weight (kg)} \times \text{Energy price (Euro/kWh)} \quad (7.7)$$

The NDE phase is calculated through the labour and NDE equipment hourly rate, the speed of NDE and the total surface area of the part:

$$\sum \text{Cost NDE phase} = \text{Hourly rate (NDT II operator + NDE equipment) (Euro/hr)} \times \frac{\left(\text{scan speed (min/m}^2\text{)} \times \text{Surface specimen (m}^2\text{)}\right)}{\text{60 (min/hr)}} \quad (7.8)$$

Major depreciation components are taken into account: a typical mould and the NDE facility:

$$\sum \text{Depreciation (Mould, NDE facility)} \quad (7.9)$$

Summing equations (7.2) and (7.4) to (7.9) gives a gross cost estimate for the CFRP manufacturing. However, when a flaw is detected during the NDE phase, additional costs will be made, such as the costs for a Non-Conformity Report (NCR). To assess the part and the severity of the flaw, a worker needs to examine the flaw and this introduces additional costs too. A distinction is made between small and large flaws in this research. Large flaws are defined as when an engineering department needs to perform structural recalculations. Small flaws

are those that can be directly solved on the shop floor by an operator. For small flaws:

$$\sum \text{Cost rework small flaws} = \text{Cost NCR} + \text{Assessment time (hr)} \times \text{Hourly rate NDT II operator (Euro/hr)} + \text{Repair time small flaw (hr)} \times \text{Hourly rate operator (Euro/hr)} \quad (7.10)$$

For large flaws:

$$\sum \text{Cost rework large flaws} = \text{Cost NCR} + \text{Assessment time (hr)} \times \text{Hourly rate Engineer (Euro/hr)} + \text{Repair time big flaw (hr)} \times \text{Hourly rate operator (Euro/hr)} + \text{Rerun autoclave cycle (Euro)} \quad (7.11)$$

These costs for rework need to be corrected with the rework rate as not every part needs rework (or is rejected):

$$\sum \text{Cost rework} = \text{Rework rate (\%)} \times \left[\begin{array}{l} (1\text{-Ratio Big/Small flaws}) \times \text{Costs Rework small flaws (Euro)} + \\ \text{Ratio Big/Small flaws} \times \text{Costs Rework big flaws (Euro)} \end{array} \right] \quad (7.12)$$

Rejection costs are calculated as:

$$\sum \text{Cost rejection} = \text{Rejection rate (\%)} \times \text{Total Costs (Euro)} \quad (7.13)$$

The sum of equations (7.12) and (7.13) is the hidden cost of rejection and rework in CFRP manufacturing.

7.3.b Input Variables

To build up the case, cost estimates are needed as input values for the cost model. These assumptions were validated by the Tier 1 manufacturer or from other references:

Table 7.1 Overview of input variables for cost estimation for a European-based CFRP manufacturer.

Variable	Value	Unit
Cost of tape CFRP for tape layup	20	€/m^2
Cost of layer CFRP for hand layup	40	€/m^2
Density of CFRP material [a)]	0.37	kg/m^2
Hourly rate Operator/Layup worker	30	€/hr
Hourly rate NDT level II operator	35	€/hr
Hourly rate Engineer	40	€/hr
Time hand layup per layer	5	min
Speed tape layer	1.2	m/min
Hourly rate autoclave	60	€/hr
Energy rate (ec.europa.eu/eurostat)	0.20	€/kWh
Time curing for autoclave	600	min
Time labour to operate autoclave	150	min
Time NDE [b)]	11	min/m^2
Hourly NDE equipment	20	€/h
Ratio big/small flaws	1/10	
NCR	500	€/part
Time rework calculations big flaw	24	hr
Time rework calculations small flaw	2	hr
Repair procedure big flaw	2	hr
Time physical repair by operator big flaw [c)]	4.25	hr
Time physical repair by operator small flaw	0.5	hr
Depreciation mould [d)]	25	€/part
Depreciation NDE facility [e)]	43	€/part

a) *Average of CFRP unidirectional tape (297 g/m^2) and fabric (450 g/m^2).*
b) *11 minutes is the average of a regular and old C-scanner and an ultrasonic bath.*
c) *4.25 hours for the physical repair is 2 h of sanding, 2 h of layup and 15 min for reporting.*
d) *A mould costs typically €50,000 and is used about 2000 times, so this leads to €25 depreciation per CFRP part produced [157].*
e) *Depreciation of NDE facilities (e.g. C-scan) of €1,000,000, is used for 10 years, so leads to a yearly depreciation of €100,000 and operating at 66% capacity and an estimated 3500 parts per year, leads to €43 depreciation per CFRP part produced.*

In this research we assumed the following materials as provided from the Tier 1 manufacturer:

- Unidirectional tape (150mm wide and 0,18 mm thickness)
- Fabric for hand layup (per m^2 and 0,28 mm thickness)

In this research two fictitious parts are used to estimate the cost of rework and rejection:

a) Small panel of 50 cm by 1 m with 20 layers of CFRP fabricated by hand layup.
b) Large panel of 2 m by 8 m with 25 layers of CFRP fabricated by automated tape layup.

Table 7.2 Input variables for modelled CFRP parts.

	Small panel	**Large panel**
Width (m)	0.5	2
Length (m)	1	8
Layers	20	25
Surface (m^2)	0.5	16
Weight (kg)	3.7	149.4

Typical rejection rates are 2% to 5% and rework rates are 15% to 25%. This range provides input to calculate an optimistic and pessimistic estimation of the financial impact of manufacturing flaws on the total costs of a CFRP part.

Table 7.3 Optimistic and pessimistic scenarios.

	Optimistic	**Pessimistic**
Rework rate	15%	25%
Rejection rate	2%	5%

7.4 Results Case Studies

The model has been used to work out cases for a small part with high volume (order of 7000 parts) and a large part with low volume (order of 300 parts). The estimated costs are shown in Table 7.4:

Table 7.4 Estimated costs for modelled parts without rework or rejection.

	Cost
Small part	€544
Large part	€12,231

The results were validated by the Tier 1 manufacturer and give a reasonable estimation of the modelled parts. A calculation of the hidden additional costs per part due to rejection and rework are shown in Table 7.5 and 7.6. The model assumes no rework on small parts due to the relatively high costs of rework. This is mainly due to the relatively high cost of an NCR.

Table 7.5 Estimated costs for rework and rejection for small parts.

	Optimistic	Pessimistic
Rejection	€11	€27

Table 7.6 Estimated costs for rework and rejection for large parts.

	Optimistic	Pessimistic
Rework	€317	€528
Rejection	€245	€612

Figures 7.2 to 7.5 show the contributions of each step of manufacturing (see Figure 7.1) or type (e.g. labour, machine) for the modelled parts in both scenarios.

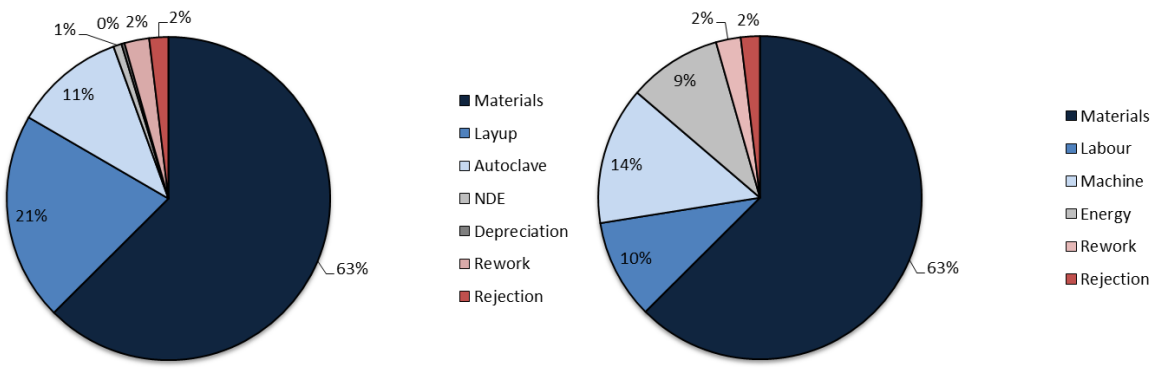

Figure 7.2 Large part manufactured in automatic tape layup in the optimistic scenario.

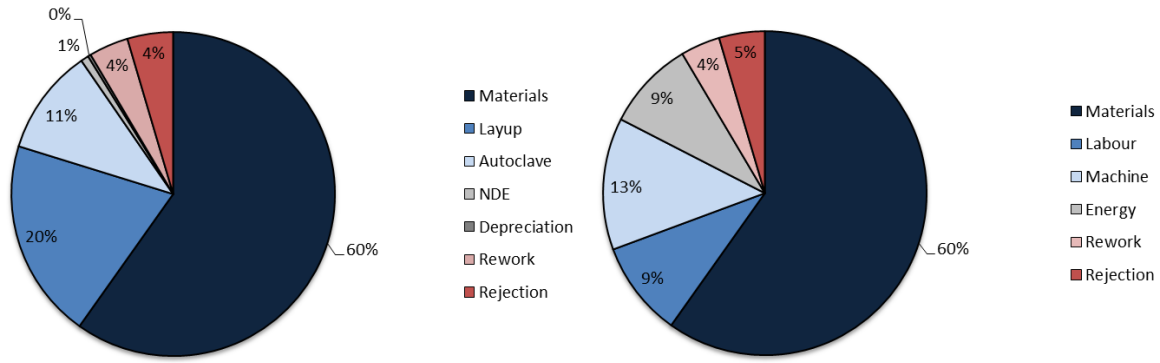

Figure 7.3 Large parts manufactured in automatic tape layup in pessimistic scenario.

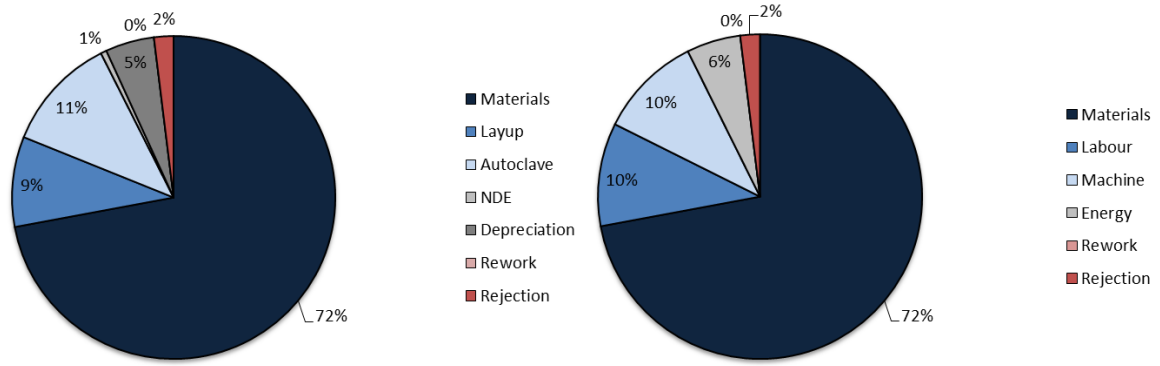

Figure 7.4 Small part manufactured in hand layup in an optimistic scenario.

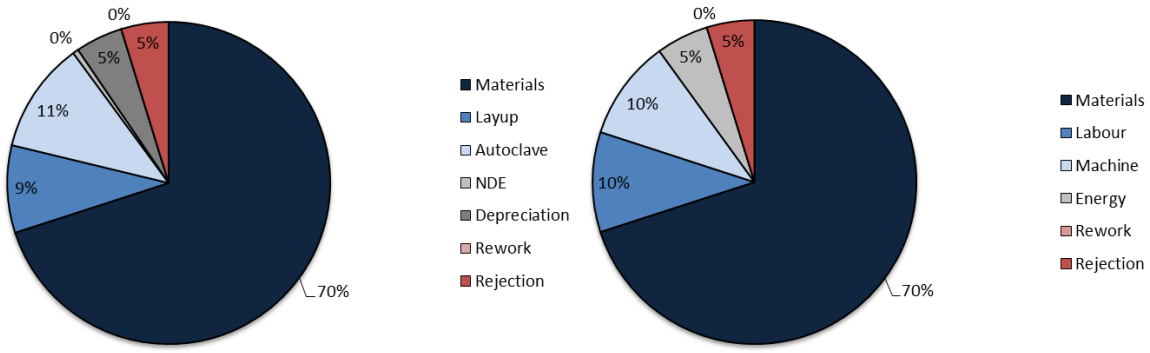

Figure 7.5 Small part manufactured in hand layup in a pessimistic scenario.

The impact of the raw material costs on the total cost is high and is in line with previous models. However, these costs are expected to change significantly over time, while other input variables are less expected to change and will have little impact. The trend in raw material CFRP costs shows a decline in costs, reaching a 50% cost reduction in raw material in 2020 [13, 14]. The impact on the cost model is shown in Table 7.7 and shows a clear decline in the costs:

Table 7.7 Recalculation of the cost of flaws with 50% raw material cost reduction.

	Cost	**Total cost reduction**
Small part	€344	(–37%)
Large part	€7595	(–38%)

Time factors in labour or energy are less likely to have a large impact on the overall costs in the near future.

7.5 Discussion

The model shows the approximate cost for the production of CFRP parts and the hidden cost of rework and rejection. A representative yearly produced volume for a Tier 1 manufacturer could be in the order of 7000 small parts (e.g. ribs) and 300 large parts (e.g. panels).

Table 7.8 Estimated yearly cost rework and rejection based on different scenarios.

	Optimistic	**Pessimistic**
Rejection—Small part	k€76.2	k€190.4
Rework—Large part	k€95.1	k€158.5
Rejection—Large part	k€73.4	k€183.5
Totals	***k€244.7***	***k€532.4***

Although the cost reduction of raw material (shown in Table 7.7) will decrease the total costs of rejection or rework, production volumes are expected to more than double by 2020 [13, 14]. Therefore, more flaws and thus more rejection and rework are expected. The total yearly costs for rejection and rework can be assumed the same as presented in Table 7.8.

Further development of an NDE process monitoring system will provide insights into developing a more efficient process, increase of quality and will increase the capacity of the manufacturing facility. The system will at least collect data on the location of the flaw during the manufacturing process; this will lead to decreased time of assessment before a possible repair and more knowledge about bottlenecks in the process. Subsequently, the removal of the flaws during the manufacturing should decrease rejection and rework. The reduction of rejection and rework in the process would also free up capacity for more production and therefore higher utilization of the production assets. True lean manufacturing would not focus on the indirect causes of the flaws but would investigate the root cause of the flaws. Currently, manufacturers do not know where the flaws actually occur in production until they are detected in the NDE phase. The proposed NDE process monitoring system will (at least) collect data on when and where a type of flaw is introduced. This will identify better where the bottlenecks of production exist and support their resolution.

The cost for the NDE system depends on the technology and the industrial implementation. Two candidates were successfully investigated as NDE technologies by the author: LDS (Chapter 5) for the layup phase and Fibre Optic Sensors (Chapter 6) for the curing phase. Major costs are expected in the development of advanced process control and manufacturing procedures. The new sensors need to be added to existing machinery and the data connected to the network and databases. To estimate the costs for further development (actual

industrialization) and the assessment of an acceptable return-on-investment, a joint development needs to be done with one or more CFRP manufacturers.

Table 7.7 showed the high impact of raw material costs and the impact of the decrease in cost for CFRP raw material. Due to the expected increase of production volumes in CFRP material, the hidden cost of rework and rejection are expected to remain high. Other aspects like human labour costs are expected to increase together with market prices, although costs could be lowered by further automation.

A decrease of 50% in labour costs would, however, lead to approximately 5% decrease in total cost. Potentially replacing the current NDE phase by in-situ NDE would not impact the direct cost structure that much, but would lead to shorter lead times, as the model assumes conventional NDE takes 180 minutes for large parts.

7.6 Conclusion

The financial model has provided insight into the cost structure of CFRP manufacturing and has given a particularly novel insight into the cost of rework and rejection. The validated model shows explicitly the high impact of rework and rejection and supports the financial feasibility of an in-situ NDE process monitoring system. It also shows the potential to bring the proof-of-concept for in-situ NDE during layup or curing to the next Technology Readiness Level and shows its applicability in an industrial environment [141, 158].

8
Conclusions

The objective of this research was to investigate the possibility of in-situ NDE process monitoring systems to detect manufacturing flaws during the fabrication process. Table 1.1 showed typical manufacturing flaws and the opportunity for an improvement in the layup and curing phases. Therefore, several technologies were evaluated (Chapter 2) and the following technologies were tested for their potential to measure critical parameters of the manufacturing process:

- Lamb waves (Chapters 3 and 4)
- Laser displacement sensors (Chapter 5)
- Fibre optic sensors (Chapter 6)

Lamb waves proved to be unsuitable for use in CFRP prepreg during the layup phase. Their attenuation is high and the reproducibility poor, which makes the technology hard to implement in an industrial environment. The novelty of this performed research was the measurement of Lamb waves in CFRP prepreg material using FBG and PZT sensors. In general, signals of Lamb waves are complex and contain lots of data; however, it is difficult to disentangle the signal and truly understand the separate components of this signal. This is even a challenge on a laboratory scale. Therefore, using this technique on an industrial scale in complex structures and with a full understanding of all separate signal components will not be possible in CFRP prepreg.

LDS has proved its potential on the laboratory scale, including for dynamic measurements. The technology was able to detect several critical flaws embedded in the layers of CFRP prepreg. The novelty of this research was the practical application of an existing technology for an opportunity in the CFRP layup process.

Fibre optic sensors gave positive results in the laboratory tests. FBG sensors were able to measure temperature during the cure cycle in the autoclave. Although these FBG sensors could measure more accurately than conventional thermocouples, the achieved level of accuracy is unnecessary to detect local temperature deviations in the specified cure cycle, as defined by the CFRP prepreg suppliers. eFPI sensors were able to detect local (in the vacuum bag) pressure deviations from design specifications in-situ of the autoclave cycle. These eFPI sensors show the highest potential of the tested optical sensor to improve the cure cycle. The novelty of these optical sensor tests was the in-situ simultaneous measurements of process variables on the CFRP prepreg part in the autoclave. Current thermocouples are sufficiently accurate to detect a local deviation of the

temperature cycle, but the addition of a eFPI sensor provides more insight on the pressure cycle.

Now that the technological feasibility has been demonstrated for several technologies, a commercial feasibility demonstration would be needed to verify the opportunity of a viable industrial process monitoring system for CFRP manufacturing. Chapter 7 demonstrated the validated potential value of the demonstrated technologies using fictitious parts. The expected return-on-investment rate for CFRP manufacturers would be sufficient for further research to be conducted to raise the TRL level.

9
Future Work

This chapter describes the future work that could be investigated as a follow-up of the presented research.

The next step in the development of the LDS system is to understand how to integrate it into the manufacturing process. Integration with a tape layer or robot arm will give the data of the sensors additional value of the location of a deviation of the actually produced part. The first step has already been performed by R. Tonnaer in the Structural Integrity & Composites Group [159]. Not only is an integration of the sensor needed, but also the path planning and a connection to the actual design (e.g. CAD design) to compare actual measurements real-time with (expected) design values to detect any deviations. The next step in the development of FOS is to integrate the eFPI sensors more fully into the autoclave system, just like the thermocouples. If the integration of FBG sensors into the CFRP parts for SHM is successful in the future, then embedded FBG sensors can be utilized during the manufacturing process. If so, another research step could be the integration of the interrogation of both FBG and eFPI sensors. The integration of fibre optical sensors in composite parts will be investigated by Dr. R.M. Groves in a follow up project

The focus of the research in this thesis was to use existing NDE techniques on CFRP prepreg, but a standalone process monitoring system cannot prevent the flaws. Future research must focus on counter-measures to remove or prevent the flaw from occurring when a deviation is measured. For example, in the layup phase, tackiness will play a role in how easy it will be to remove the top CFRP layer and to remove the inclusion. On the other hand, there is the challenge of how to pause a cure cycle if a pressure deviation is measured. Feedback from the industry states that localization (not prevention itself) already has value for the manufacturing process, as the evaluation of the parts after the cure can be shortened if flaws are already localized.

Lean manufacturing strives to have flawless manufacturing processes. As flaws still occur during the layup and cure, this shows that current manufacturing processes are not perfect yet. To eliminate all potential opportunities to introduce a flaw, an extensive process redesign would be necessary. To improve the current process, data are insufficient to understand and eliminate the causes of the flaws. Therefore, an in-situ process monitoring system is necessary. Potential sources to gain insight without the introduction of new technologies are NCRs and performing root cause analysis on the available data.

Since the time of writing of the evaluation of technologies in 2011 (Chapter 2) some other potential new advances in NDE have been developed and published. These are briefly discussed below.

To evaluate Eddy currents [104, 106] for their potential as an NDE process monitoring system, a CFRP prepreg specimen was tested by Suragus GmbH. The results are presented in Figures 9.1 to 9.3. The meaning of these measurements is explained in

Figure *9.1*. The evaluated specimen was similar to the CFRP prepreg parts measured in Chapter 5 with LDS. This was a stepwise layered CFRP prepreg of 50 mm by 200 mm, where the sixth layer has a perpendicular fibre orientation and a foil inclusion of 10 mm by 10 mm was included between layers 7 and 8. The specimen was tested for distribution of the main fibre angle, anisotropy strength layer resistance and vectors of the main angle for location on the sample.

1) Distribution of the main angles	2) Anisotropy strength of the sample
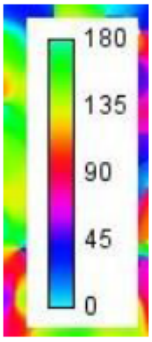 The distribution of the main angles shows the fiber orientation in colors. Warm colors indicate horizontal fiber orientation, cold colors vertical fiber orientation. **Blue = vertical fiber orientation** **Red = horizontal fiber orientation**	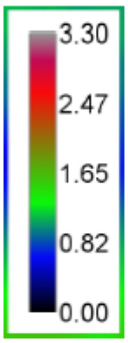 The anisotropy strength of the sample is shown as a heat map. Warmer colors mean stronger anisotropy. Note that high anisotropy at the edges of the sample is a result of the measurement process (*edge effect*) and mathematic algorithm **Blue = isotropic** (similar alignment in all direction) **Red = anisotropic** (strong orientation in one direction)
3) Fiber Areal Weight	**4) Vectors of the main angles**
This resulting image shows the average fiber areal weight. It shows more fibers with darker shades of gray (black) and less fibers with brighter shades of gray (white) **White = low FAW** **Black = high FAW**	The vector image shows a correlation between a location on the sample and the **most present fiber orientation.** The orientation and color of the vectors show the preferred direction of the fibers. **Color** (Vector) = **Anisotropy** strength **Angle** (Vector) = calculated **dominant orientation**

Figure 9.1 Explanation of the Eddy-current results by Suragus [160].

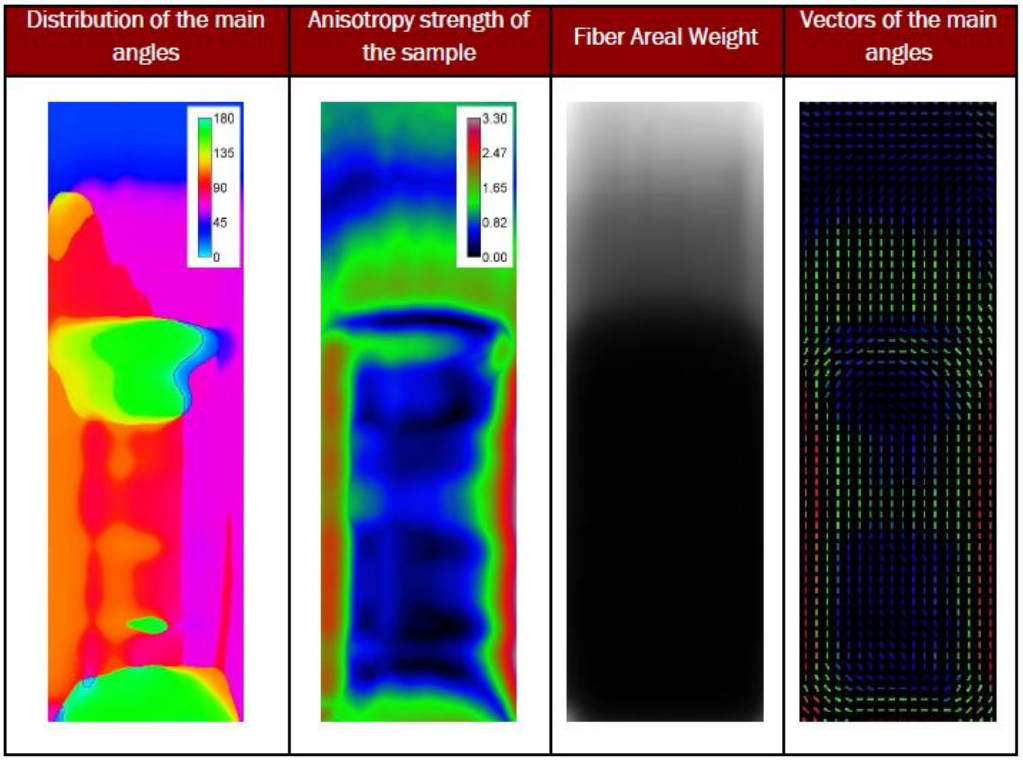

Figure 9.2 Results of the anisotropy scan by Suragus.

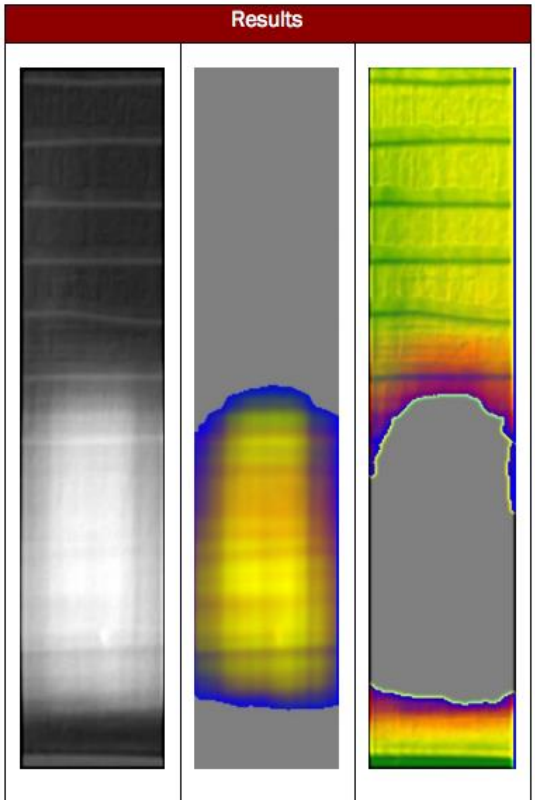

Figure 9.3 Results of the reflection scan by Suragus.

The results from Suragus show interesting results but are not sufficiently conclusive to be used immediately in an industrial environment. The number of layers can be detected through the fibre areal weight and the reflectivity scan, the perpendicular oriented fibres in layer 6 show up in the distribution of the main angle measurement and in the reflectivity scan (Figure 9.3, *right).* The foil inclusion is not detected under the top layer, as it is a non-conductive material. The Eddy-current method shows potential for an NDE process monitoring technology but needs further investigation. The system used by Suragus is not able to measure in-situ and could be developed into a more hand-held probe. Further understanding of the results from prepreg material is also needed.

The in-line ultrasonic process monitoring system [86] during the cure cycle is interesting, but this will not be able directly to detect pressure or temperature related flaws. Further development of this system could decrease additional time in the NDE phase as the manufactured part can already be tested while being cured. The developments of foil detection with thermography [92] could be followed up in parallel with LDS for process monitoring in the layup phase. This could be a complementary process monitoring system for hand layup CFRP parts. At the time of writing, no article is available on this research.

To take these and other potential technologies further could lead to the technical demonstration of a significantly decreased or even eliminated NDE phase. However, the acceptance of the industry is needed for the actual elimination and to integrate the product quality assurance during the layup and curing phases.

References

1. Womack, J.P. and D.T. Jones, *Lean thinking: banish waste and create wealth in your corporation*. 2010: Simon and Schuster.
2. Arnheiter, E.D. and J. Maleyeff, *The integration of lean management and Six Sigma.* The TQM Magazine, 2005. **17**(1): p. 5-18.
3. Näslund, D., *Lean, six sigma and lean sigma: Fads or real process improvement methods?* Business Process Management Journal, 2008. **14**(3): p. 269-287.
4. Lasi, H., P. Fettke, H.G. Kemper, T. Feld, and M. Hoffmann, *Industry 4.0.* Business and Information Systems Engineering, 2014. **6**(4): p. 239-242.
5. Lee, J., B. Bagheri, and H.A. Kao, *A Cyber-Physical Systems architecture for Industry 4.0-based manufacturing systems.* Manufacturing Letters, 2015. **3**: p. 18-23.
6. Grall, A., L. Dieulle, C. Bérenguer, and M. Roussignol, *Continuous-time predictive-maintenance scheduling for a deteriorating system.* IEEE Transactions on Reliability, 2002. **51**(2): p. 141-150.
7. Lee, J., J. Ni, D. Djurdjanovic, H. Qiu, and H. Liao, *Intelligent prognostics tools and e-maintenance.* Computers in Industry, 2006. **57**(6): p. 476-489.
8. Baker, A.A. and M.L. Scott, *Composite materials for aircraft structures*. Third ed. 2016: American Institute of Aeronautics and Astronautics.
9. Campbell, F.C., *Manufacturing processes for advanced composites*. 2004: Elsevier.
10. Rosato, D.V. and J. Murphy, *Reinforced plastics handbook*. 2004: Elsevier Advanced Technology.
11. Harris, G.Z., *Composite material and their applications in aeronautics* Ingenieur (The Hague), 1970. **82**(21): p. ll-15.
12. *Fibre reinforced plastics market: Strong growth expected by 2007.* Composites International, 2003(55): p. 30-31.
13. Heuss, R., N. Muller, W. Van Sintern, A. Starke, and A. Tschiesner, *Lightweight, heavy impact*. 2012, McKinsey&Company.
14. Infosys, *Carbon Composites are becoming competitive and cost effective*. 2015.
15. Schmitt, R., C. Mersmann, and B. Damm. *In-process 3D laser measurement to control the fiber tape-laying for composite production*. in *SPIE Photonics Europe*. 2010. Brussels: SPIE.
16. Uribe, B.E.B., E.M.S. Chiromito, A.J.F. Carvalho, and J.R. Tarpani, *Low-cost, environmentally friendly route for producing CFRP laminates with microfibrillated cellulose interphase.* Express Polymer Letters, 2017. **11**(1): p. 47-59.
17. Poodts, E., G. Minak, L. Mazzocchetti, and L. Giorgini, *Fabrication, process simulation and testing of a thick CFRP component using the*

RTM process. Composites Part B: Engineering, 2014. **56**: p. 673-680.
18. Mulligan, D.R., *Cure Monitoring for Composites And Adhesives*. 2003: iSmithers Rapra Publishing.
19. Djordjevic, B.B. *Guided wave ultrasonic characterization of advanced composites*. 2010. Seattle, WA.
20. Kundu, T., *Ultrasonic nondestructive evaluation: engineering and biological material characterization*. 2004: CRC Press.
21. Hillger, W., R. Meier, and R. Henrich, *Inspection of CFRP components by ultrasonic imaging with air-coupling.* Insight: Non-Destructive Testing and Condition Monitoring, 2004. **46**(3): p. 147-150.
22. Bastianini, F., A. Di Tommaso, and G. Pascale, *Ultrasonic non-destructive assessment of bonding defects in composite structural strengthenings.* Composite Structures, 2001. **53**(4): p. 463-467.
23. Berketis, K., D. Tzetzis, and P.J. Hogg, *Impact damage detection and degradation monitoring of wet GFRP composites using noncontact ultrasonics.* Polymer Composites, 2009. **30**(8): p. 1043-1049.
24. Imielińska, K., M. Castaings, R. Wojtyra, J. Haras, E. Le Clezio, and B. Hosten, *Air-coupled ultrasonic C-scan technique in impact response testing of carbon fibre and hybrid: Glass, carbon and Kevlar/epoxy composites.* Journal of Materials Processing Technology, 2004. **157-158**(SPEC. ISS.): p. 513-522.
25. Dubois, M. and T.E. Drake, *Evolution of industrial laser-ultrasonic systems for the inspection of composites.* Nondestructive Testing and Evaluation, 2011. **26**(3-4): p. 213-228.
26. English, L.K., *Non-destructive testing for composite quality.* Materials Engineering, 1987. **4**(9): p. 75-77.
27. Quaegebeur, N., P. Micheau, P. Masson, and M. Castaings, *Methodology for optimal configuration in structural health monitoring of composite bonded joints.* Smart Materials and Structures, 2012. **21**(10).
28. Su, Z., L. Ye, and Y. Lu, *Guided Lamb waves for identification of damage in composite structures: A review.* Journal of Sound and Vibration, 2006. **295**(3-5): p. 753-780.
29. Vellekoop, M.J., *Acoustic wave sensors and their technology.* Ultrasonics, 1998. **36**(1-5): p. 7-14.
30. Balageas, D., C.P. Fritzen, and A. Güemes, *Structural health monitoring*. 2006: ISTE.
31. Thursby, G. and B. Culshaw. *The use of fibre optic sensors to compare the internal strains and pressures produced by different*

Lamb wave modes. in *21st International Conference on Optical Fiber Sensors*. 2011. Ottawa, ON.
32. Betz, D.C., G. Thursby, B. Culshaw, and W.J. Staszewski Wieslaw J, *Structural damage location with fiber Bragg grating rosettes and Lamb waves.* Structural Health Monitoring, 2007. **6**(4): p. 299-308.
33. Thursby, G., B. Culshaw, and D.C. Betz, *Multifunctional fibre optic sensors monitoring strain and ultrasound.* Fatigue and Fracture of Engineering Materials and Structures, 2008. **31**(8): p. 660-673.
34. Okabe, Y., H. Tamaue, J. Kuwahara, and N. Takeda, *Damage detection in composites using fiber bragg grating sensors as ultrasonic receivers*, in *Composites Technologies For 2020*. 2014, Woodhead Publishing Limited. p. 987-992.
35. Amano, M., Y. Okabe, N. Takeda, and T. Ozaki, *Structural health monitoring of an advanced grid structure with embedded fiber bragg grating sensors.* Structural Health Monitoring, 2007. **6**(4): p. 309-324.
36. Holnicki-Szulc, J. and C.A.M. Soares, *Advances in Smart Technologies in Structural Engineering*. 2004: Springer.
37. Takeda, N., Y. Okabe, J. Kuwahara, S. Kojima, and T. Ogisu, *Development of smart composite structures with small-diameter fiber Bragg grating sensors for damage detection: Quantitative evaluation of delamination length in CFRP laminates using Lamb wave sensing.* Composites Science and Technology, 2005. **65**(15-16 SPEC. ISS.): p. 2575-2587.
38. Amann, M.C., T. Bosch, M. Lescure, R. Myllylä, and M. Rioux, *Laser ranging: A critical review of usual techniques for distance measurement.* Optical Engineering, 2001. **40**(1): p. 10-19.
39. Liu, X., *In situ metrology system for micro-milling machine.* Journal of Manufacturing Systems, 2012. **31**(1): p. 15-21.
40. Schmitt, R., A. Orth, and C. Niggemann. *A method for edge detection of textile preforms using a light-section sensor for the automated manufacturing of fibre-reinforced plastics*. in *SPIE Optical Measurement Systems for Industrial Inspection V*. 2007. Munich.
41. Schmitt, R., C. Niggemann, and C. Mersmann. *Contour scanning of textile preforms using a light-section sensor for the automated manufacturing of fibre-reinforced plastics*. in *SPIE Photonics Europe*. 2008. Strasbourg.
42. Schmitt, R., C. Niggemann, and C. Mersmann. *Laser light-section sensor automating the production of textile-reinforced composites*. in *SPIE Optical sensors*. 2009. Prague.
43. Faidi, W., *Wind Turbine Manufacturing Process Monitoring*. 2012, General Electric Global Research Center: Niskayuna, NY.

44. Steinchen, W. and L.X. Yang, *Digital shearography: theory and application of digital Speckle pattern shearing interferometry*. 2003: SPIE Optical Engineering Press.
45. Francis, D., R.P. Tatam, and R.M. Groves, *Shearography technology and applications: A review.* Measurement Science and Technology, 2010. **21**(10): p. 02001.
46. Chen, Y.S., Y.Y. Hung, S.P. Ng, Y.H. Huang, and L. Liu. *Review and comparison of shearography and active thermography for nondestructive testing and evaluation (NDT&E)*. 2009. Nanjing.
47. Osten, W., E. Garbusi, D. Fleischle, W. Lyda, C. Pruss, R. Reichle, and C. Falldorf. *Optical metrology - From the laboratory to the real world*. in *Speckle 2010: Optical Metrology*. 2010. Florianopolis.
48. Steinbichler. *Optical Measurement*. 2013 April 2013]; Available from: www.steinbichler.com.
49. isi-sys. *Shearography, ESPI, Image correlation and Video-Stroboscopy*. 2013 April 2013]; Available from: www.isi-sys.com.
50. Hung, Y.Y. and H.P. Ho, *Shearography: An optical measurement technique and applications.* Materials Science and Engineering R: Reports, 2005. **49**(3): p. 61-87.
51. Robinson, D.W. and G.T. Reid, *Interferogram analysis: digital fringe pattern measurement techniques*. 1993: Institute of Physics.
52. Maldague, X.P.V., *Introduction to NDT by active infrared thermography.* Materials Evaluation, 2002. **60**(9): p. 1060-1073.
53. Ley, O., M. Butera, and V. Godinez. *Inspection of composite structures using line scanning thermography*. 2012. Baltimore, MD.
54. Bates, D., G. Smith, D. Lu, and J. Hewitt, *Rapid thermal non-destructive testing of aircraft components.* Composites Part B: Engineering, 2000. **31**(3): p. 175-185.
55. Halabe, U.B., M. Roy, P. Klinkhachorn, and H.V.S. Gangarao. *Detection of air and water-filled subsurface defects in GFRP composite bridge decks using infrared thermography*. 2006. Brunswick, ME.
56. Meyendorf, N.G.H., H. Rösner, V. Kramb, and S. Sathish, *Thermo-acoustic fatigue characterization.* Ultrasonics, 2002. **40**(1-8): p. 427-434.
57. Stewart, A., G. Carman, and L. Richards, *Health monitoring technique for composite materials utilizing embedded thermal fiber optic sensors.* Journal of Composite Materials, 2005. **39**(3): p. 199-213.
58. Montesano, J., Z. Fawaz, and H. Bougherara, *Use of infrared thermography to investigate the fatigue behavior of a carbon fiber reinforced polymer composite.* Composite Structures, 2013. **97**: p. 76-83.

59. Chehura, E., A.A. Skordos, C.C. Ye, S.W. James, I.K. Partridge, and R.P. Tatam, *Strain development in curing epoxy resin and glass fibre/epoxy composites monitored by fibre Bragg grating sensors in birefringent optical fibre.* Smart Materials and Structures, 2005. **14**(2): p. 354-362.
60. Mizutani, Y. and R.M. Groves, *Multi-Functional Measurement Using a Single FBG Sensor.* Experimental Mechanics, 2011. **51**(9): p. 1489-1498.
61. Kang, H.K., D.H. Kang, H.J. Bang, C.S. Hong, and C.G. Kim, *Cure monitoring of composite laminates using fiber optic sensors.* Smart Materials and Structures, 2002. **11**(2): p. 279-287.
62. Kang, H.K., D.H. Kang, C.S. Hong, and C.G. Kim. *Monitoring of fabrication strain and temperature during composite cure using fiber optic sensor*. in *Nondestructive and Evaluation of Materials and Composites V*. 2001. Newport Beach, CA; United States: SPIE.
63. Takeda, S.I., T. Mizutani, T. Nishi, N. Uota, Y. Hirano, Y. Iwahori, Y. Nagao, and N. Takeda, *Monitoring of a CFRP-stiffened panel manufactured by VaRTM using fiber-optic sensors.* Advanced Composite Materials, 2008. **17**(2): p. 125-137.
64. Tanaka, N., Y. Okabe, and N. Takeda, *Temperature-compensated strain measurement using fiber Bragg grating sensors embedded in composite laminates.* Smart Materials and Structures, 2003. **12**(6): p. 940-946.
65. Zhang, G., Z. Zhou, G. Ding, S. Xu, C. Xie, and J. Zhang, *Cure monitoring and mechanical properties measurement of carbon fibre-reinforced plastics laminate using embedded fibre Bragg grating sensors.* Materials Research Innovations, 2015. **19**: p. S5718-S5725.
66. Pantelelis, N., G. Nedelec, Y. Amosse, M.P. Toitgans, A. Beigbeder, I. Harismendy, R. Mezzacasa, J. Zhang, and E. Bistekos. *Industrial cure monitoring and control of the RTM production of a CFRP automotive component*. in *15th European Conference on Composite Materials: Composites at Venice, ECCM 2012*. 2012. Venice, Italy: European Conference on Composite Materials, ECCM.
67. Kosaka, T., K. Osaka, S. Nakakita, and T. Fukuda. *Fiber optic strain monitoring of textile GFRP during RTM molding and fatigue tests by using embedded FBG sensors*. in *Smart Structures and Materials 2003: Smart Structures and Integrated Systems*. 2003. San Diego, CA.
68. Leng, J. and A. Asundi, *Structural health monitoring of smart composite materials by using EFPI and FBG sensors.* Sensors and Actuators, A: Physical, 2003. **103**(3): p. 330-340.
69. Wang, W., X. Jiang, and Q. Yu, *Temperature self-compensation fiber-optic pressure sensor based on fiber Bragg grating and Fabry-*

Perot interference multiplexing. Optics Communications, 2012. **285**(16): p. 3466-3470.
70. Xu, J., X. Wang, K.L. Cooper, and A. Wang, *Miniature all-silica fiber optic pressure and acoustic sensors.* Optics Letters, 2005. **30**(24): p. 3269-3271.
71. Aref, S.H., H. Latifi, M.I. Zibaii, and M. Afshari, *Fiber optic Fabry-Perot pressure sensor with low sensitivity to temperature changes for downhole application.* Optics Communications, 2007. **269**(2): p. 322-330.
72. Iannuzzi, D., S. Deladi, V.J. Gadgil, R.G.P. Sanders, H. Schreuders, and M.C. Elwenspoek, *Monolithic fiber-top sensor for critical environments and standard applications.* Applied Physics Letters, 2006. **88**(5): p. 1-3.
73. Qi, B., M. Bannister, X. Liu, A. Michie, L. Rajasekera, and B. Ashton, *Response of an embedded fibre bragg grating to thermal and mechanical loading in a composite laminate.* Materials Forum, 2004. **27**: p. 93-100.
74. Guo, M.J. and L. Liang. *A novel fiber Bragg grating pressure sensor with the smart metal structure based on the planar diaphragm*. 2010. Dalian.
75. Gifford, D.K., M.E. Froggatt, and S.T. Kreger. *High precision, high sensitivity distributed displacement and temperature measurements using OFDR-based phase tracking*. in *21st International Conference on Optical Fiber Sensors*. 2011. Ottawa, ON.
76. Zhao, W., J. Wang, A. Wang, and R.O. Claus, *Geometric analysis of optical fiber EFPI sensor performance.* Smart Materials and Structures, 1998. **7**(6): p. 907-910.
77. Liu, T., M. Wu, Y. Rao, D.A. Jackson, and G.F. Fernando, *A multiplexed optical fibre-based extrinsic Fabry-Perot sensor system for in-situ strain monitoring in composites.* Smart Materials and Structures, 1998. **7**(4): p. 550-556.
78. Othonos, A., *Fiber Bragg gratings.* Review of Scientific Instruments, 1997. **68**(12): p. 4309-4341.
79. Saidi Reddy, P., K. Srimannarayana, R.L.N.S. Sai Prasad, D. Sen Gupta, M. Sai Shankar, and P. Kishore. *Enhancing the temperature sensitivity of fiber Bragg grating sensor using bimetallic strip*. in *3rd Asia Pacific Optical Sensors Conference*. 2012. Sydney, NSW, Australia.
80. Sohn, H., J.Y. Yang, D. Dutta, M.P. DeSimio, S.E. Olson, and E.D. Swenson. *Imaging ultrasonic waves in complex structures using a scanning laser Doppler vibrometer*. in *5th International Conference on Bridge Maintenance, Safety and Management, IABMAS 2010*. 2010. Philadelphia, PA.

81. Kashyap, R., *Fiber Bragg Gratings*. 2009: Academic Press.
82. Xu, G.Q. and D.Y. Xiong, *Applications of fiber Bragg grating sensing technology in engineering.* Chinese Optics, 2013. **6**(3): p. 306-317.
83. Pant, S., J. Laliberte, M. Martinez, and B. Rocha, *In-situ characterization of isotropic and transversely isotropic elastic properties using ultrasonic wave velocities.* Materials Performance and Characterization, 2016. **5**(1): p. 164-188.
84. Ochôa, P., V. Infante, J.M. Silva, and R.M. Groves, *Detection of multiple low-energy impact damage in composite plates using Lamb wave techniques.* Composites Part B: Engineering, 2015. **80**: p. 291-298.
85. Zhao, G., H. Hu, S. Li, L. Liu, and K. Li, *Localization of impact on composite plates based on integrated wavelet transform and hybrid minimization algorithm.* Composite Structures, 2017. **176**: p. 234-243.
86. Hudson, T.B., B.W. Grimsley, and F.G. Yuan. *Development of a fully automated guided wave system for in-process cure monitoring of CFRP composite laminates*. in *Proceedings of the American Society for Composites - 31st Technical Conference, ASC 2016*. 2016.
87. Jin, L., X. Shi, H.Y. Dong, and P.J. Feng, *Study on robot automatic drilling of carbon fiber reinforced plastics (CFRP)*, in *2013 4th International Conference on Advances in Materials and Manufacturing, ICAMMP 2013*. 2014: Kunming. p. 1144-1149.
88. Tait, R., K. Harding, and C. Nafis. *Composite layup monitoring using structured light*. in *Proceedings of SPIE - The International Society for Optical Engineering*. 2015.
89. De Angelis, G., M. Meo, D.P. Almond, S.G. Pickering, and S.L. Angioni, *A new technique to detect defect size and depth in composite structures using digital shearography and unconstrained optimization.* NDT and E International, 2012. **45**(1): p. 91-96.
90. Pinto, F., F.Y. Maroun, and M. Meo, *Material enabled thermography.* NDT and E International, 2014. **67**: p. 1-9.
91. Théroux, L.D., J. Dumoulin, and X. Maladague, *Square heating applied to shearography and active infrared thermography measurements coupling: From feasibility test in laboratory to numerical study of pultruded CFRP plates glued on concrete specimen.* Strain, 2014. **50**(5): p. 404-416.
92. Baumard, T., O. De Almeida, G. Menary, Y. Le Maoult, F. Schmidt, and J. Bikard. *Determination of thermal contact conductance in vacuum-bagged thermoplastic prepreg stacks using infrared thermography*. in *AIP Conference Proceedings*. 2016.

93. Kratz, J., M. Genest, M. Preau, and P. Hubert. *Vacuum-bag-only prepreg processing of honeycomb structures: From lab-scale experiments to an aircraft demonstrator*. in *International SAMPE Technical Conference*. 2014.
94. Shepard, S.M. and M.F. Beemer. *Thermographic detection of foreign object debris in cured and uncured composite layups*. in *CAMX 2016 - Composites and Advanced Materials Expo*. 2016.
95. Lobanov, D.S., V.E. Wildemann, E.M. Spaskova, and A.I. Chikhachev, *Experimental investigation of defects influence on composites sandwich panels strength using digital image correlation and infrared thermography methods.* PNRPU Mechanics Bulletin, 2015. **2015**(4): p. 159-170.
96. Ganapathi, A.S., M. Maheshwari, S.C. Joshi, Z. Chen, A.K. Asundi, and S.C. Tjin, *In-situ measurement and numerical simulation of resin pressure during Glass/Epoxy prepreg composite manufacturing.* Measurement: Journal of the International Measurement Confederation, 2016. **94**: p. 505-514.
97. Geng, X., J. Wang, M. Jiang, Q. Sui, G. Liu, P. Li, Y. Jia, and L. Jia, *Monitoring of composite curing process based on embedded fiber Bragg grating sensors.* Fuhe Cailiao Xuebao/Acta Materiae Compositae Sinica, 2016. **33**(8): p. 1615-1620.
98. Hu, H., S. Li, J. Wang, L. Zu, D. Cao, and Y. Zhong, *Monitoring the gelation and effective chemical shrinkage of composite curing process with a novel FBG approach.* Composite Structures, 2017. **176**: p. 187-194.
99. Tian, H., J.H. Wang, Y.D. Ji, H.X. Hu, H.Y. Zhang, and Z. Xu, *The monitoring of cure-induced residual stress on different depth direction by fiber Bragg grating sensors.* Gongneng Cailiao/Journal of Functional Materials, 2012. **43**(19): p. 2671-2674.
100. Ramza, H., N. Arsad, F. Abdurrahman, L.H.S. Supian, and M.S. Ab-Rahman, *Optical fiber pressure sensor using extrinsic Fabry-Perot interferometry (EFPI); A theoretical study.* Journal of Optoelectronics and Advanced Materials, 2015. **17**(5-6): p. 545-551.
101. Xiong, L., D. Zhang, L. Li, and Y. Guo, *EFPI-FBG hybrid sensor for simultaneous measurement of high temperature and large strain.* Chinese Optics Letters, 2014. **12**(12).
102. Zhang, J., Z. Jing, A. Li, and W. Peng, *All-silica fiber EFPI high static pressure sensor in fusion with simple structure.* Zhongguo Jiguang/Chinese Journal of Lasers, 2016. **43**(10).
103. Torres, M., F. Collombet, B. Douchin, L. Crouzeix, Y.H. Grunevald, J. Lubin, and T. Camps, *Monitoring of the curing process of composite structures by tunnelling junction sensors.* Sensors and Actuators, A: Physical, 2015. **235**: p. 256-264.

104. Heuer, H., M.H. Schulze, and N. Meyendorf, *Non-destructive evaluation (NDE) of composites: Eddy current techniques*, in *Non-Destructive Evaluation (NDE) of Polymer Matrix Composites: Techniques and Applications*. 2013. p. 33-55.
105. Qiu, J., J. Cheng, C. Zhang, H. Ji, T. Takagi, and T. Uchimoto, *Novel NDT methods for composite materials in aerospace structures.* International Journal of Applied Electromagnetics and Mechanics, 2016. **52**(1-2): p. 25-33.
106. Heuer, H., M. Schulze, M. Pooch, S. Gäbler, A. Nocke, G. Bardl, C. Cherif, M. Klein, R. Kupke, R. Vetter, F. Lenz, M. Kliem, C. Bülow, J. Goyvaerts, T. Mayer, and S. Petrenz, *Review on quality assurance along the CFRP value chain - Non-destructive testing of fabrics, preforms and CFRP by HF radio wave techniques.* Composites Part B: Engineering, 2015. **77**: p. 494-501.
107. Schulze, M.H., N. Meyendorf, and H. Heuer, *Analysis techniques for eddy current imaging of carbon fiber materials.* Materialpruefung/Materials Testing, 2010. **52**(9): p. 603-609.
108. Haertling, G.H., *Ferroelectric ceramics: History and technology*. Journal of the American Ceramic Society, 1999. **82**(4): p. 797-818.
109. DeltaPreg, *Epoxy matrix system DT120* 2007.
110. Tiwari, U., K. Thyagarajan, M.R. Shenoy, and S.C. Jain, *EDF-Based edge-filter interrogation scheme for FBG sensors.* IEEE Sensors Journal, 2013. **13**(4): p. 1315-1319.
111. Jiang, W., T. Matsuda, K. Yatsui, and A. Tokuchi. *MHz pulsed power generator using MOS-FET*. in *IEEE Conference Record of Power Modulator Symposium*. 2002.
112. Kurz, J.H., C.U. Grosse, and H.-W. Reinhardt, *Strategies for reliable automatic onset time picking of acoustic emissions and of ultrasound signals in concrete.* Ultrasonics, 2005. **43**(7): p. 538-546.
113. Zhang, H., X. Sun, X. Qi, X. Liu, and D. Lu. *Ultrasonic lamb wave inspection using fiber Bragg gratings*. 2008. Shanghai.
114. Radecki, R., W.J. Staszewski, and T. Uhl, *Impact of changing temperature on lamb wave propagation for damage detection*, in *5th International Congress of Technical Diagnostics*. 2014: Krakow. p. 140-148.
115. Shevlyakov, G.L. and H. Oja, *Robust Correlation: Theory and Applications*. 2016: Wiley.
116. Su, Z. and L. Ye, *Identification of Damage Using Lamb Waves: From Fundamentals to Applications*. 2009: Springer.
117. Umchid, S. *Frequency dependent ultrasonic attenuation coefficient measurement*. in *The 3rd International Symposium on Biomedical Engineering (ISBME)*. 2008.

118. Czichos, H., T. Saito, and L.R. Smith, *Springer Handbook of Materials Measurement Methods*. 2006: Springer.
119. Swallowe, G.M., *Mechanical Properties and Testing of Polymers: An A–Z Reference*. 2013: Springer Netherlands.
120. Barroso-Romero, M., D. Barazanchy, M. Martinez, R.M. Groves, and R. Benedictus, *Time Reversal of Lamb Waves for Damage Detection in Thermoplastic Composites*, in *ICAST2013: 24th International Conference on Adaptive Structures and Technologies*. 2013: Aruba.
121. Kessler, S.S., S.M. Spearing, M.J. Atalla, C.E.S. Cesnik, and C. Soutis. *Structural health monitoring in composite materials using frequency response methods*. 2001. Newport Beach, CA.
122. Kinloch, A., *Adhesion and Adhesives: Science and Technology*. 2012: Springer Netherlands.
123. Peiponen, K.E., R. Myllylä, and A.V. Priezzhev, *Optical Measurement Techniques: Innovations for Industry and the Life Sciences*. 2010: Springer.
124. Carvalho, F.D., R. Davies, J. Dinis, C.A. Malta, A.S. Guedes, and J.F. Silva. *Laser triangulation technique for textured surface shape analysis in industrial applications*. 1994. Boston, MA, USA: Society of Photo-Optical Instrumentation Engineers.
125. Fu, G., A. Menciassi, and P. Dario, *Development of a low-cost active 3D triangulation laser scanner for indoor navigation of miniature mobile robots.* Robotics and Autonomous Systems, 2012. **60**(10): p. 1317-1326.
126. Zhang, L. and Y. Xie. *Development of automatic visual inspection sensor in robotic tailored blank welding*. 2009. Wuhan.
127. Ouyang, Q., L.Z. Zhang, L.M. Zhao, X.L. Zhang, and D.F. Chen, *Experimental study on quantitative surface defect depth detection based on laser scanning technology in continuous casting.* Ironmaking and Steelmaking, 2011. **38**(5): p. 363-368.
128. Shetty, D. and C. Campana. *Precision measurement method of misalignment, cracks, contours and gaps in aerospace industry*. 2012. San Antonio, TX.
129. Kennedy, W.P., *Basics of triangulation sensors.* Sensors (Peterborough, NH), 1998. **15**(5): p. 76, 78, 80-83.
130. Koch, T., M. Breier, and W. Li. *Heightmap generation for printed circuit boards (PCB) using laser triangulation for pre-processing optimization in industrial recycling applications*. in *2013 11th IEEE International Conference on Industrial Informatics, INDIN 2013*. 2013. Bochum.
131. KEYENCE, *LJ-V7000 series*. 2012, Keyence: Osaka, Japan.

132. Bukshtab, M., *Applied photometry, radiometry, and measurements of optical losses*. 2012. p. 1-725.
133. Goel, A., *Economics of Composite Material Manufacturing Equipment*, in *Dep. Mechanical Engineering*. 2000, Massachusetts Institute of Technology.
134. Commission, E., *G. Technology readiness levels (TRL), HORIZON 2020 – WORK PROGRAMME 2014-2015 General Annexes, Extract from Part 19 - Commission Decision C(2014)4995.* 2014.
135. Dextra. www.dextragroup.com/construction-products/cfrp-tape. 2013 August 2013].
136. Mascioni, M., N.N. Ghosh, J.M. Sands, and G.R. Palmese, *Electron beam and UV cationic polymerization of glycidyl ethers PART II: Reaction of diglycidyl ether of bisphenol A.* Journal of Applied Polymer Science, 2013. **130**(1): p. 487-495.
137. Scott, A. and M. Knott, *A cluster analysis method for grouping means in the analysis of variance.* Biometrics, 1974: p. 507-512.
138. Strong, A.B., *Fundamentals of Composites Manufacturing, Second Edition: Materials, Methods and Applications*. 2008: Society of Manufacturing Engineers.
139. Staab, G., *Laminar Composites*. 2015: Elsevier Science.
140. Baker, A.A., S. Dutton, D. Kelly, and D.W. Kelly, *Composite materials for aircraft structures*. 2004: American Institute of Aeronautics and Astronautics.
141. Miesen, N., M. Warnink, J. Sinke, R.M. Groves, and R. Benedictus, *Predictive process monitoring of CFRP manufacturing with fibre optic sensors during cure cycle* Under revision, Delft University of Technology.
142. Guo, H., G. Xiao, N. Mrad, and J. Yao, *Fiber optic sensors for structural health monitoring of air platforms.* Sensors, 2011. **11**(4): p. 3687-3705.
143. Majumder, M., T.K. Gangopadhyay, A.K. Chakraborty, K. Dasgupta, and D.K. Bhattacharya, *Fibre Bragg gratings in structural health monitoring-Present status and applications.* Sensors and Actuators, A: Physical, 2008. **147**(1): p. 150-164.
144. Hill, K.O. and G. Meltz, *Fiber Bragg grating technology fundamentals and overview.* Journal of Lightwave Technology, 1997. **15**(8): p. 1263-1276.
145. Lee, B.H., Y.H. Kim, K.S. Park, J.B. Eom, M.J. Kim, B.S. Rho, and H.Y. Choi, *Interferometric fiber optic sensors.* Sensors, 2012. **12**(3): p. 2467-2486.
146. Allwood, G., G. Wild, and S. Hinckley, *Optical Fiber Sensors in Physical Intrusion Detection Systems: A Review.* IEEE Sensors Journal, 2016. **16**(14): p. 5497-5509.

147. Di Sante, R., L. Donati, E. Troiani, and P. Proli, *Reliability and accuracy of embedded fiber Bragg grating sensors for strain monitoring in advanced composite structures.* Metals and Materials International, 2014. **20**(3): p. 537-543.
148. Liu, R., J. Xiao, D. Liang, and G. Wang, *Performance improvement method of CFRP with embedded optical fiber.* Transactions of Nanjing University of Aeronautics and Astronautics, 2015. **32**(3): p. 261-267.
149. Warnink, M., *Process monitoring during Autoclave Curing of CFRP with Fiber Optic Sensors*, in *Aerospace Non-Destructive Testing Laboratory*. 2016, Delft University of Technology: Delft.
150. Zhu, Y., K.L. Cooper, G.R. Pickrell, and A. Wang, *High-Temperature Fiber-Tip Pressure Sensor.* Journal of Lightwave Technology, 2006. **24**(2): p. 861.
151. Niazi, A., J.S. Dai, S. Balabani, and L. Seneviratne, *Product cost estimation: Technique classification and methodology review.* Journal of Manufacturing Science and Engineering, Transactions of the ASME, 2006. **128**(2): p. 563-575.
152. Zhao, X., W.J.C. Verhagen, and R. Curran, *Estimation of aircraft component production cost using knowledge based engineering techniques.* Advanced Engineering Informatics.
153. Pugh, P.G., *Working Top-Down: Cost Estimating before Development Begins.* Proceedings of the Institution of Mechanical Engineers, Part G: Journal of Aerospace Engineering, 1992. **206**(2): p. 143-151.
154. Lorenzana, J., A. Kokawa, T. Bettner, F. Timson, J. Proctor, H.J. Behrens, L. Lyle, M. Woo, and L. Bernhardt, *Advanced composite cost estimating manual.* Technical Report AFFDLTR- 76-87 Northrop Grumman Corporation, 1976.
155. Gutowski, T., D. Hoult, G. Dillon, E.T. Neoh, S. Muter, E. Kim, and M. Tse, *Development of a theoretical cost model for advanced composite fabrication.* Composites Manufacturing, 1994. **5**(4): p. 231-239.
156. Haffner, S.M., *Cost Modeling and Design for Manufacturing Guidelines for Advanced Composite Fabrication*, in *Department of Mechanical Engineering*. 2002, Massachusetts Institute of Technology (MIT)
157. Shehab, E., W. Ma, and A. Wasim, *Manufacturing Cost Modelling for Aerospace Composite Applications*, in *Concurrent Engineering Approaches for Sustainable Product Development in a Multi-Disciplinary Environment*, J. Stjepandić, G. Rock, and C. Bil, Editors. 2013, Springer London. p. 425-433.

158. Miesen, N., J. Sinke, R.M. Groves, and R. Benedictus, *Simulation and detection of flaws in pre-cured CFRP using laser displacement sensing.* International Journal of Advanced Manufacturing Technology, 2015. **82 (1-4)**: p. pp. 341-349.
159. Tonnaer, R., *On fine non-destructive evaluation in automated fibre placement*, in *Faculty of Aerospace Engineering* 2016, Delft University of Technology: Delft, The Netherlands.
160. Instruments, S.S., *Feasibility study MA17023 - TU Delft*. 2017, Suragus Sensors & Instruments.

Acknowledgements

First of all, I would like to thank the people of the faculty:

Rinze, I am very grateful that you gave me a chance for a part-time PhD research. In our few conversations, I highly appreciated your academic approach together with your practical experience in industry. Jos, I always liked our discussions, especially those that were non-technical (but of course relevant). Besides this, you may not realise how much of a positive impact you had on my career when you introduced me to lean manufacturing. Roger, your passion for science is contagious. Your drive for perfection and eye for detail got the level of my research and especially my writing to the needed level.

Gemma, the one who makes the life at the faculty a lot lighter, thanks for all your help and assistance to get things going. But especially the one who was interested in the personal lives of people and asked how things are going. Berthil, Gertjan, Victor and all the others from the ‘vliegtuighal’, thanks for your guidance, help and assistance during experiments. Mike, a special thanks to you for helping me out during your internship and your contribution to my optical sensing research. I wish you all the best in your career in aviation.

Second, I want to thank my managers who gave me the chance and time to pursue my research. Harm, thanks for giving me the opportunity to explore the possibilities of a PhD research during my time at NLR. Francois and Marco, besides providing time for my research, you gave me much more insight, understanding and especially enthusiasm for Lean manufacturing, Innovation and Industry 4.0 at AkzoNobel.

Finally, my friends, Snuutkes, colleagues, family and, of course, Fay, who showed interest and supported my research and often (impatiently) asked when the defence would take place and especially the drinks. It will be soon now!

This was the hardest thing I ever did in my life and without the people mentioned above, it would never have come to an end. But I am extremely proud to finally say: ‘Done’.

About the author

Nick Miesen was born in Maastricht on February 5, 1982. After finalizing the Gymnasium at Sint Maartenscollege Maastricht, he obtained his MSc in Physics and Astronomy at the University of Amsterdam in 2007. His first position was at the Dutch National Aerospace Laboratory (NLR) as R&D engineer, focusing on new optical technologies for aerospace applications.

During his position at the NLR, he investigated several optical technologies that are suitable for Structural Health Monitoring. After a discussion with Professor Rinze Benedictus he was able to start a PhD research part-time and after an initial investigation phase, his research focused on improvement of CFRP manufacturing. Because of his research, he became more interested in lean manufacturing.

After gaining Operational Excellence consultancy experience at Deloitte Consulting, he certified as Black Belt at AkzoNobel Industrial Chemicals and supported the Lean Six Sigma program. He is enrolled in a certification program at the Amsterdam Business School as Master Black Belt. He currently focuses on digital innovation and Industry 4.0, which can be seen as the next step for manufacturing and Lean Six Sigma. Technologies such as Advanced Analytics, Internet of Things and Robotics are implemented to increase productivity in manufacturing. He is also co-founder, together with fellow PhD colleague and friend Mayank Gupta, of an advanced analytics start-up Jugaad, founded in 2016.

He currently lives in Amsterdam and prefers to spend his free time in the city of Amsterdam, playing rugby, travelling the globe and diving.

Publications

Conferences:

Miesen, N., Mizutani, Y., Groves, R. M., Sinke, J. & Benedictus, R. *Lamb wave detection in prepreg composite materials with fibre Bragg grating sensors; 2011. In: Proceedings of SPIE–International Society for Optical Engineering. 7981, p. 1–11.*

Miesen, N., Sinke, J., Groves, R. M. & Benedictus, R. *Demonstration of novel Lamb wave detection of flaws during the layup process of composite laminate production; 2012. Proceedings of the 4th International Symposium on NDT Aerospace. Hanke, R. & Boller, C. (eds.). Berlin, Germany: DGfZP, p. 1–8.*

***Miesen, N**., Sinke, J., Groves, R. M. & Benedictus, R. Laser displacement sensor to monitor the layup process of composite laminate production; 2013. Proceedings of SPIE 8692. s.n. (ed.). San Diego, CA: SPIE, p. 1–8 (Proceedings of SPIE–International Society for Optical Engineering; vol. 8692)*

Journals:

Miesen, N., Sinke, J., Groves, R. M. & Benedictus, R. *Simulation and detection of flaws in pre-cured CFRP using laser displacement sensing; 2016. In: International Journal of Advanced Manufacturing Technology. p. 1–9*

Miesen, N., Warnink, M., Sinke, J., Groves, R. M. & Benedictus, R. *Local fibre optic pressure and temperature sensing for autoclave monitoring in CFRP manufacturing; 2018: International Journal of Advanced Manufacturing Technology (To be submitted for review).*

Miesen, N., Sinke, J., Groves, R. M. & Benedictus, R. *Financial assessment of the impact of production rework and rejection in CFRP manufacturing and the economic potential of an in-situ NDE system; 2018. International Journal of Productivity and Quality Management (To be submitted for review).*